# Active Tremor Control of Human Motion Disorder

by

Gary Ellis Hall

B.S., Mechanical Engineering
University of Rochester, May 1998

Submitted to the Department of Mechanical Engineering
in partial fulfillment of the requirements for the degree of

Master of Science in Mechanical Engineering

at the

MASSACHUSETTS INSTITUTE OF TECHNOLOGY

June 2001



Author .....
Department of Mechanical Engineering
May 22, 2001

Certified by .....
Kenneth W. Kaiser
Senior Technical Staff
The Charles Stark Draper Laboratory, Inc.
Thesis Supervisor

Certified by .....
Mandayam A. Srinivasan
Principal Research Scientist & Lecturer
Department of Mechanical Engineering
Thesis Supervisor

Accepted by .....
Ain A. Sonin
Chairman, Committee on Graduate Studies
Department of Mechanical Engineering

This page intentionally left blank.

# Active Tremor Control of Human Motion Disorder

by

Gary Ellis Hall

Submitted to the Department of Mechanical Engineering
on May 22, 2001, in partial fulfillment of the
requirements for the degree of
Master of Science in Mechanical Engineering

## Abstract

All humans are subject to a physiological phenomenon known as tremor, which introduces unintended, relatively high-frequency movements into various parts of the body. These unintended movements serve to limit human motor performance with respect to normal human performance (for cases in which tremor is severe), and with respect to tasks that require "superhuman" performance (for cases in which not even normal tremor is tolerable). For example, the elderly often experience reduced motor control to the point where they can not eat. Similarly, surgeons performing eye surgery must have very little tremor to enable them to operate on the small anatomy of the eyes. In both cases, a motion disorder known as *essential tremor* can be the cause of the insufficient level of human motor performance.

Current treatments for tremor disorders such as essential tremor include a small set of extremes (brain surgery versus doing nothing), with very little "middle ground." A device that could easily be placed onto the body and removed when not needed could fill this niche nicely. Due to the potential for high performance and portability, a new type of tremor stabilizer is proposed that uses a proof mass actuation scheme. This prototype device intended to attenuate human essential tremor along two translational axes was designed, constructed, and tested. Mechanical design, dynamics, and control systems modeling were performed, and the end device built to specifications.

A shaker and experimental mount were constructed to artificially simulate tremor, and all data were gathered using this setup. The prototype demonstrated a 4:1 reduction in simulated tremor acceleration power from open- to closed-loop operation, as well as a 2:1 reduction in simulated tremor amplitude from open- to closed-loop operation. Medical personnel at Massachusetts General Hospital have suggested that this level of tremor attenuation would be helpful for their patients.

Results were limited to vibrations along one of the two translational axes. Limitations of the prototype are discussed, as well as design strategies to improve performance in future work.

Thesis Supervisor: Kenneth W. Kaiser
Title: Senior Technical Staff
The Charles Stark Draper Laboratory, Inc.

Thesis Supervisor: Mandayam A. Srinivasan
Title: Principal Research Scientist & Lecturer
Department of Mechanical Engineering

This page intentionally left blank.

## Acknowledgments

I don't know where to begin when it comes to writing the acknowledgements of this thesis. So many people and entities have assisted me along the path to completion of this work that I feel as if I am really completing *our* thesis. The largest group project in which I have taken part. I'll do the best I can to include everyone.

I would like to thank Professor Mandayam A. Srinivasan, for agreeing to take a slice of his already busy schedule and devote this time to me. I look forward to hearing of future discoveries in the Touch Lab at MIT.

To Draper Laboratory, I would like to extend thanks. As a graduate student, I was well provided-for within Draper, both in terms of material assistance, and access to expert personnel. Numerous people within Draper deserve my regards. To Mitch Hansberry, I would like to extended my gratitude for the excellent work he did in preparing drawings and designs for this thesis. Mitch dispatched all of the bizarre design requests I sent his way quickly and professionally. A special thank you goes out to Tony Emberly and Bob Visser, who tolerated the introduction of a petty thief disguised as a graduate student into their lab. I promise I'll return all of your equipment. Thanks to Bob Faiz, who introduced many useful ideas that were incorporated into the later design revisions of the prototype. Jay Courturier, of Draper Media Services, took nearly all of the photographs seen in this thesis. Thank you, Jay, for you fast and excellent work.

Kenneth Kaiser deserves my greatest thanks. Ken has guided me through this work, found funding for my project, patiently pointed out that my prototypes were not working because wires were reversed or something important was left ungrounded, and survived the wave of thesis drafts I have thrown his way. At the same time, he also provided me with help in all of the classes I've taken. In our frequent discussions, he has also taught me a lot about life, and I will take his perspectives on many issues with me when I leave. I look forward to learning of Ken's progress in future tremor control projects.

I feel a special need to thank Donna Jean Kaiser. She selflessly provided a wonderful source of support at a crucial time in my life. I also learned a great deal from her, both technically and about life, and continue to look to her life and accomplishments as a source of inspiration. Also, Donna has eased the life of this graduate student with frequent trips to Cambridge for food.

Last, but not least, I would like to thank my family. My parents and brother have always loved and supported me, and I'm fortunate to be able to crash at my grandmother's house (with all of

my laundry) every time I head home for a break. It is easy to look at this thesis and see the pages, the equations, the plots. It is slightly more difficult to see the effort that went into the creation of these things. It is nearly impossible to know that the existence of this thesis is due to the influences of these special people.

This thesis was prepared at The Charles Stark Draper Laboratory, Inc., under Internal Company Sponsored Research Project 13058, Tremor Control.



(author's signature)

This thesis is dedicated in memory of

Gardner Avery Cross

This page intentionally left blank.

# Contents

# List of Figures

This page intentionally left blank.

# List of Tables

This page intentionally left blank.

# Definition of Symbols

| Symbol | Units | Description |
|---|---|---|
| $A$ | length | Amplitude of oscillations at the wrist. |
| $x_1$ | length | Position of wrist/hand. |
| $x_2$ | length | Position of proof mass. |
| $x$ | length | Distance between wrist and proof mass, $x = x_2 - x_1$. |
| $m_1$ | mass | Observed inertia of entire forearm and hand as experienced at wrist. |
| $m_2$ | mass | Inertia of proof mass. |
| $I$ | mass·length$^2$ | Rotational inertia of forearm about the elbow. |
| $l$ | length | Length of forearm from elbow to wrist. |
| $k_1$ | force/length | Spring constant of coupling between the body and wrist. |
| $k_2$ | force/length | Spring constant of coupling between wrist and proof mass. |
| $b_1$ | mass/time | Damping constant of coupling between the body and wrist. |
| $b_2$ | mass/time | Damping constant of coupling between the wrist and proof mass. |
| $K_{AP}$ | Volt/Volt | Proportional feedback gain of accelerometer loop. |
| $K_{AD}$ | (Volt·time)/Volt | Derivative feedback gain of accelerometer loop. |
| $K_{AI}$ | Volt/(Volt·time) | Integral feedback gain of accelerometer loop. |
| $K_{LP}$ | Volt/Volt | Proportional feedback gain of LVDT loop. |
| $K_{LD}$ | (Volt·time)/Volt | Derivative feedback gain of LVDT loop. |
| $K_{LI}$ | Volt/(Volt·time) | Integral feedback gain of LVDT loop. |
| $K_{GP}$ | Volt/Volt | Proportional feedback gain of the Galil DMC–2040. |
| $K_{GD}$ | (Volt·time)/Volt | Derivative feedback gain of the Galil DMC–2040. |
| $G_{P1}$ | time$^2$/mass | Transfer function of $m_1$. |
| $G_{P2}$ | time$^2$/mass | Transfer function of $m_2$. |
| $G_L$ | – | Transfer function of LVDT control loop. |
| $G_A$ | – | Transfer function of accelerometer loop. |
| $G_D$ | – | Transfer function of plant acted on by disturbance. |
| $\zeta$ | – | Damping coefficient of system. |
| $\gamma$ | – | $\sqrt{1 + m_2/m_1}/\sqrt{1 + K_{AP}}$ |
| $S_A$ | – | Attenuation sensitivity function. |
| $\omega$ | time$^{-1}$ | Natural frequency. |

Table 1: Variables used in this thesis, the variable units, and a description of the variable.

This page intentionally left blank.

# Chapter 1

# Introduction

## 1.1 Overview

Tremor is a physiological phenomenon found in all human beings. It is typified by relatively low amplitude, relatively high frequency (in the 4–12 Hertz range), unintended movements of various parts of the body. All people deal with at least some tremor in their day to day lives with few consequences. For example, the beating of an individual's heart produces what are deemed *cardioballistic* disturbances in the motion of the individual. We are all subject to these disturbances, yet almost none of us suffer any ill effects [10]. In certain cases, particularly in those people with neurological disorders, tremor can be a debilitating condition that erodes quality of life. An effective means of tremor attenuation could therefore improve the lives of those adversely affected by tremor.

The medical community views tremor as both a symptom of other ailments and as an ailment in itself. Physical tasks, such as eating, drinking, reading, walking, and proper personal care are made more difficult (and sometimes impossible) by the interference of tremor. In fact, tests used within the medical community to gauge the severity of tremor often assess the ability of a patient to accomplish these simple tasks [7, 16, 17, 25]. The majority of the medical literature deals with analysis and modeling of the hands, fingers, and lower forearms of those with tremor, since unwanted motion within these body parts contributes largely to the decrease in quality of life. Thus, it would seem as though stabilization of the hands and/or fingers would provide one of the biggest benefits to those affected by pathological tremor.

In addition to having negative medical consequences, human tremor limits the attainable performance of a wide variety of man-machine systems. Effects of these limitations range from annoying, as in the case of those suffering from drug-induced tremor attempting to perform precision mechan-

ical work, to potentially life-threatening, as in the case of surgeons with tremor. As society becomes more and more technologically advanced, it is common for the devices with which humans interact to become capable of higher accuracy than the people interacting with them. For this reason, the unintended motion introduced by tremor is becoming a limiting factor in the performance of many modern systems.

Attempts at controlling human tremor have begun to appear in the marketplace. Binoculars and camcorders that actively attenuate tremor of the operator are currently commercialized. While these systems work well in controlling tremor, the modality of tremor control is of limited utility. These systems are concerned primarily with the removal of tremor noise from optical data. As such, means to remove tremor *information* are all that are required. Thus, while the camcorder or binoculars are still moving due to the tremor of their operators, the active systems inside are *virtually* removing tremor from the imagery captured by the device. In the application studied in this thesis, the physical object (which would be attached to an individual) must not be physically moving for a real benefit to exist.

Many attempts to control tremor using passive technologies have been undertaken, with limited results [23]. This thesis was motivated by a desire by the experimenters to implement current off-the-shelf (COTS) technology to actively control tremor. Some classic works on the subject of active versus passive control of oscillating systems have clearly demonstrated the superiority of actively controlled systems to passively controlled systems [9]. Den Hartog demonstrated that a pair of small hydroplanes on the hull of a ship could much more efficiently stabilize the vessel in rough waters than a variety of passive technologies. It is the author's belief that a similar active system, constructed with many of the same design philosophies as the oscillating ship example in Reference [9], will yield a similar payoff in terms of tremor attenuation per unit mass of, power input to, and size of the device.

Discussions between the experimenters and Drs. Alice Flaherty and David Standaert at the Massachusetts General Hospital Department of Neurology indicated that efforts at controlling tremor would be best directed at a motion disorder known as *essential tremor*. Essential tremor (ET) is a condition typified by an uncharacteristically large tremor in otherwise healthy patients that is controlled by a "central oscillator" within the patient's central nervous system [13]. Unlike Parkinsonian tremor, which is attenuated as the patient concentrates on the task at hand, essential tremor is *always* present. A system designed to control the characteristics of Parkinsonian tremor would therefore achieve little more than a cosmetic fix when the stabilized limb was not in use. A cosmetic

fix is indeed very important, but the author is more concerned with the impairment suffered by those with debilitating tremors. A system designed to control essential tremor would help those otherwise disabled by tremor perform normal tasks.

## 1.2 Previous Work

The medical literature regarding tremor is well developed and provides a good background of the various characteristics of tremor [13]. Attempts to understand and model tremor have taken the form of a wide range of activities, from one- and two-degree of freedom lumped parameter mechanical models to more detailed models that describe complex neurological systems and processes [10, 11, 13, 18]. Unfortunately, experts in the field of tremor admit that there exists almost no knowledge of the physiological systems that cause tremor [10]. As such, medical treatments for tremor range from nothing in the case of mild or weak tremors that do not interfere with everyday activities, to deep brain implants and other brain surgeries for the most severe cases of tremor. It would seem as though a mechanical treatment to suppress tremor could help "fill the gap" between these extremes in treatment. Such a mechanical treatment could help individuals who don't have tremors severe enough to warrant surgical procedures, but who do have tremors severe enough to interfere with routine activities. Medications to control tremor are frequently used, but are not particularly effective and are plagued with side effects. In any event, it is likely that some form of simple mechanical stabilization is superior to the added cost and potential side effects found with prescribing medication for the patient. Fortunately, this thesis can proceed knowing only the mechanical characteristics of tremor.

Previous attempts at mechanical tremor reduction have relied heavily on passive technologies. Viscous damping, added inertia, and gyroscopic stabilization have all been attempted [12, 23]. Only limited success has been obtained largely due to the fact that these methods seek to attenuate *all* motion, rather than just unintended motion. In other words, it is not very useful to a tremor patient to have a steady hand that has severely limited mobility, which would be the case for these other mechanical stabilization schemes. Other problems encountered with passive technologies have included the increased muscle strength created with extended use of the dissipating element, and fatigue associated with constantly "fighting" the passive device [23]. A well-designed tremor reduction system should counteract only *unintended* motions, thereby going almost unnoticed by the user.

Data regarding the amplitude, velocity, acceleration, and dominant frequencies of tremor are sought by the author. Luckily, these data are readily available in a number of resources [10, 11, 20]. In particular, a characterization of tremor as it appears within movement disorders such as essential tremor is sought. The body of literature detailing tremor generally agrees that the prominent frequencies of the tremor motions are in the range of 4–12 Hertz, depending on a wide range of variables (i.e., the physiological cause of the tremor, the location of the tremor within the body, the age of the patient, the recent activity level of the patient, medications taken by the patient, etc.). Typical tremor characteristics for the hands and fingers are in the range of 8–12 Hertz, with maximum amplitudes for severe tremor in the range of 40 mm (1.57 inches) [11].

As mentioned previously, some commercial stabilization systems have found their way to the marketplace. For example, Canon USA, Inc. manufactures and markets an entire product line of image stabilizing components. The components include binoculars, telescopes, and telephoto lenses for cameras. Again, these technologies do not perform a *physical* stabilization of the system. The imagery the device is designed to capture is the only entity that benefits from tremor removal [3]. These systems, therefore, are not well-suited to situations in which the physical vibrations from a complete man-machine system must be removed.

Some experimental work has been undertaken at the Carnegie Mellon University Robotics Institute in an effort to perform a physical stabilization of a scalpel blade used in eye surgery [21, 22]. This work utilized closed-loop control of piezoceramic actuators to remove tremor motion from the blade of the instrument. Work such as this is pertinent to this thesis, but the system later proposed aims to be more versatile. This thesis also proposes the use of a proof mass stabilizer, as opposed to direct movement of the object to be stabilized. While the preliminary results from the tremor-controlled scalpel look promising, this is but one application of vibration control technology to a wide range of existing problems. It is possible that the scalpel could be adapted into a wide range of other tremor-controlled objects (such as a spoon, knife, fork, or pen), but each of these devices would need to be independently designed, constructed and purchased. This would no doubt increase the costs associated with tremor control for the patients. It is hypothesized that building a tremor controller for the entire hand would allow the other objects to be used with only one system. This versatile system could, it is hoped, allow a tremor patient to buy one device that could be used in conjunction with other handheld objects. The cost of stabilization would be driven by just one object rather than several.

Some interesting work has also been performed by Ken Kaiser of Charles Stark Draper Labo-

ratory, Inc.[1] in the area of active stabilization of small arms for the United States military. Sniper rifle design and manufacturing practices have brought these weapons to a point at which they are capable of higher accuracy than their human operators [6]. Sniper rifles are capable of higher performance than their human operators under optimal shooting conditions, and performance of the man-machine sniper and rifle system is only degraded once soldiers are exposed to the rigors of field conditions (i.e., cold temperatures, anxiety, malnutrition, sleep deprivation, etc.). The Defense Advanced Research Projects Agency[2] (DARPA) has therefore funded research to actively reduce the effects of human tremor on the accuracy of sniper rifles. This research has been developed to the successful demonstration of an alpha prototype, and research into the technology is continuing. Again, though, this application of tremor control aims to attenuate one type of motion in one type of system. This thesis aims for a more generic solution to tremor.

Some studies also appear to examine the relationship between tremor and excitations to a limb with tremor [11, 18]. In these studies, a torque motor was utilized in order to try to influence the phase of the tremor. Results demonstrated that the phase of some forms of tremor could be "reset" through mechanical influence. While these studies seem to hint at the subject of influencing tremor using mechanical actuation, closed-loop tremor reduction is never introduced. Also, these studies focused more on the modification of the tremor phase rather than the tremor amplitude. A change to the tremor phase is of little practical use in this thesis.

## 1.3 Proposed Active Tremor Control System Description

This thesis will serve as the first investigation into an active control system intended to perform tremor attenuation from a human hand and wrist. More specifically, this thesis details the study of a "wrist cuff" stabilizer intended to remove translational tremor along two axes from an individual with essential tremor.

The subsections that follow will develop the concept of a proof mass stabilization system, as well as its particular application in this thesis. The theory of operation of a proof mass stabilizer is often misunderstood, and for this reason great care is taken to describe the system that will be developed in this thesis. Subsection 1.3.1 begins the explanation with a description of how a proof mass stabilizer applies correcting forces. Subsection 1.3.2 continues the development with an

[1] 555 Technology Square, Cambridge, MA 02139.
[2] 3701 North Fairfax Drive, Arlington, VA 22203-1714

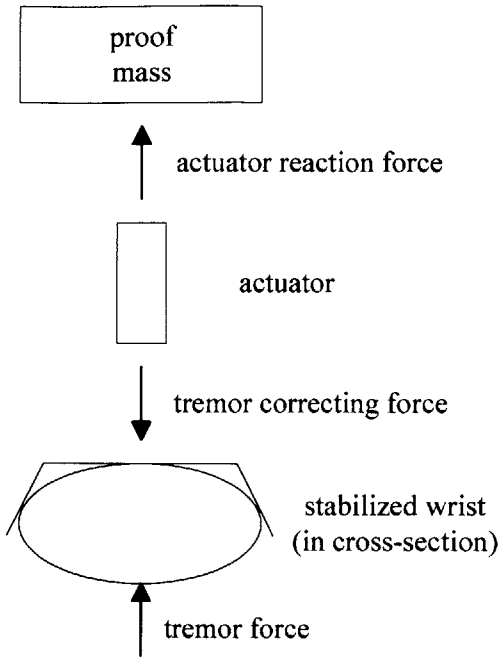


Figure 1-1: Free body diagram of single axis proof mass stabilizer.

explanation of the specification of correcting forces using acceleration feedback. Subsection 1.3.3 adds a description of the tuned damper. Lastly, Subsection 1.3.4 outlines the concept of using one shared proof mass for two axes of operation.

### 1.3.1 Concept of Correcting Forces

The operational paradigm of the proposed system is the application of correcting forces to a moving wrist via a proof mass actuation scheme, as shown in the free body diagram of Figure 1-1. A proof mass stabilizer is generally used in situations in which the system that needs stabilization must be freely moving, and therefore cannot be attached to a rigid structure capable of exerting reaction forces. The system therefore receives correcting forces by reacting against a proof mass, or an inertia, rather than a rigid reaction surface. A reaction mass is attached to an actuator, and when the actuator exerts a tremor correcting force, the actuator reaction force is exerted on the proof mass. The end goal of a proof mass stabilization scheme is to remove oscillations of the system one wishes to stabilize by applying forces between the system and the proof mass. The inertia of the proof mass limits the acceleration of the proof mass (if the system is properly designed), and the system requiring stabilization receives correcting forces to counteract the oscillations. This concept is illustrated in Figure 1-1.

A proof mass actuation scheme is used on orbital satellites. In order for a satellite to be useful,

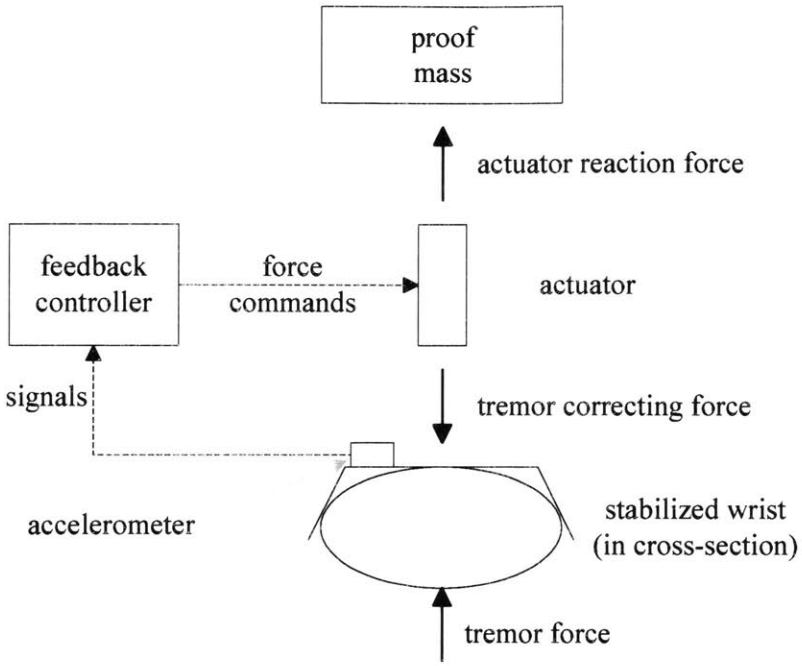


Figure 1-2: Free body diagram of single axis proof mass stabilizer with acceleration feedback.

it must be able to communicate with other systems on Earth, which requires pointing the antenna of the satellite in the proper direction. A satellite in orbit does not have any structure against which to push so that it can turn itself. Instead, the satellite carries reaction wheels mounted on motors, and it is these massive reaction wheels that are spun, which results in equal and opposite torque application to the satellite.

Figure 1-1 does not tell the whole story, however. Two questions remaining are, "How does the system know when to apply a tremor correcting force, and how large should the tremor correcting force be?" Subsection 1.3.2 develops the answers to these questions.

### 1.3.2 Concept of Acceleration Feedback

Figure 1-2 is identical to Figure 1-1, except for the addition of controller electronics and an accelerometer. Section 1.3.1 makes mention of the fact that the tremor forces in Figures 1-1 and 1-2 are not constant. In fact, tremor forces are time-varying forces that approximate sinusoids, but can have a wide range of frequencies and magnitudes. Thus, a means to determine *when* to apply a tremor correction force is needed, as is a means to determine *how large* a tremor correction force to apply.

Both of these questions can be answered through the use of acceleration feedback. A tremor

force acting on a wrist will lead to an acceleration of the wrist via Newton's 2nd Law

$$F = ma, \tag{1.1}$$

in which $F$ is the force acting on the mass $m$, producing an acceleration $a$ [14]. If an accelerometer were attached to the accelerating wrist, as in Figure 1-2, then the acceleration resulting from the action of the tremor force on the wrist could be sensed. The signal from the accelerometer can now be used to answer the questions of when to apply tremor correcting forces and how much tremor correcting force to apply.

To answer these two questions, we pass the signal from the accelerometer to controller electronics, as shown in Figure 1-2. These electronics will receive acceleration signals from the accelerometer, and then send commands to the actuators that will produce tremor correction forces. If the accelerometers sense no acceleration, the controller electronics will send no commands to the actuators. If the accelerometers sense a moderately-sized, positive (upward) acceleration caused by a positive (upward) acting tremor force, the controller electronics will respond by instructing the actuators to produce a moderately-sized, negative (downward-acting) tremor correcting force. Conversely, if the accelerometers sense a large, negative (downward) acceleration, the controller electronics will respond by instructing the actuators to produce a large, positive (upward) tremor correcting force. Thus, the addition of accelerometers and controller electronics allow the system to become stabilized.

### 1.3.3 Concept of Tuned Damping

Subsection 1.3.2 provided an explanation of reducing tremor vibrations using an accelerometer and controller electronics. A second sensor can be added to the system to provide even better performance. A sensor that measures distance, in this case a linear voltage displacement transducer (LVDT) can also be added to the system to measure distance between the proof mass and the wrist. Addition of an LVDT is shown in Figure 1-3.

The LVDT is added to the system for the purposes of centering the proof mass against the ever-present forces of gravity. The actuators are limited in how far they can move the proof mass by their stroke lengths. As such, some means to instruct the actuators to hold the proof mass in a centered position is needed, so that the proof mass will be able to move up or down in response to the application of tremor correcting force by the actuator. In other words, if the proof mass

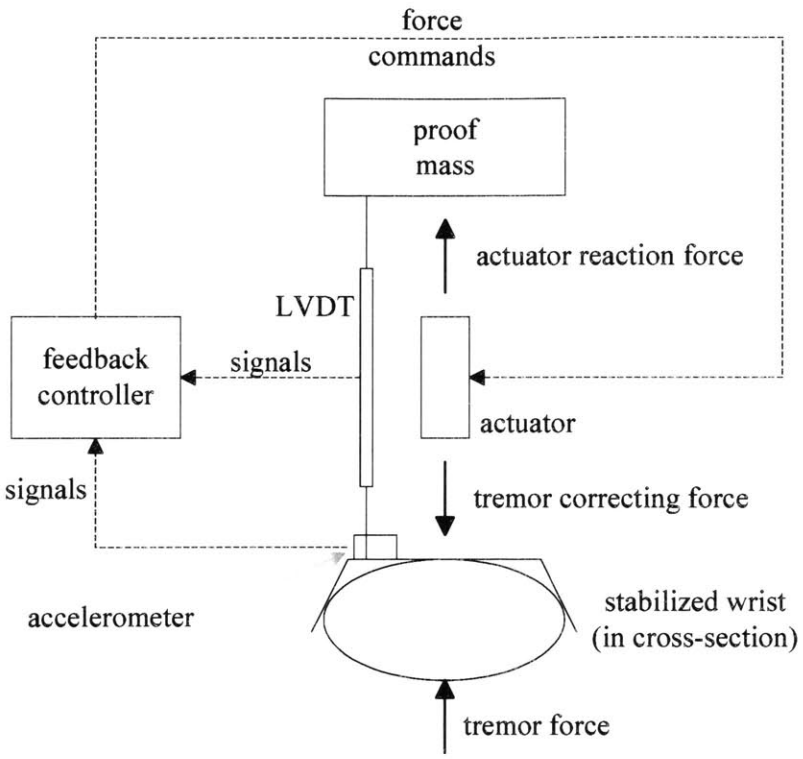


Figure 1-3: Proof mass stabilizer with acceleration feedback and tuned damping.

were not centered and ended up resting against the wrist, a command to apply an upward tremor correcting force would result in a downward actuator reacting force, which would not accelerate the proof mass since it is already in its "full down" position. Thus, an LVDT is added to the system to maintain an approximately centered position for the proof mass.

A side benefit of the presence of the LVDT is that the signals from the LVDT and the controller electronics can be used to create a tuned vibration absorber for the system. Tuned vibration absorbers function by addition of a spring-mass system to a vibrating system, such that the characteristics of the spring-mass system absorb energy from the vibrating system. The end result is that the added spring-mass system vibrates, leaving the system vibrating due to tremor with less energy, and a lower vibration amplitude. The theory of vibration absorbers is mature and well developed, as for example in [9].

Thus, the main components of a vibration absorber are a mass and a spring, and sometimes a damper. The spring provides a force in response to a *displacement*. So, if the spring is stretched, it attempts to contract to its original length. If the spring is compressed, it attempts to extend to its original length. The proof mass system mentioned so far already has a vibrating system (the wrist), a mass (the proof mass), and now it has a spring. The LVDT signals sense displacement,

and so can be utilized with the controller electronics to create an *electronic spring.* In other words, if the LVDT senses a "stretch" in the distance between the wrist and the proof mass, the controller electronics send a force command to the actuator to try to "unstretch" the electronic spring. In this way, an electronic spring can be made to link the wrist and proof mass.

A damper acts by providing a force in response to a *velocity.* In other words, the damper provides reaction forces when the ends of the damper are displaced with respect to one another in some time-varying manner. Again, the LVDT signals can be differentiated with respect to time to provide information regarding the velocity of the proof mass with respect to the wrist. The effect of this is to create an electronic damper, analogous to the previously detailed electronic spring.

Specification of appropriate controller feedback values will create an electronic spring and damper with the correct physical sizes. Details of selecting the actual feedback values will be presented later in this thesis.

### 1.3.4 Concept of Shared Proof Mass

The benefit of using a proof mass actuation scheme in an application like tremor control is that the system can be unconstrained in space. The proof mass actuation scheme does not require attachment to a wall or other structure, and so would allow the user unrestrained motion. Thus, the author envisions the device as one which could be worn by a user much as a wristwatch or a pair of eyeglasses, that function to enhance the life of the wearer while being as unobtrusive as possible. Unfortunately, the unconstrained nature of the device means that the individual wearing the device will have to support the entire weight of the device. There is an incentive to make the device as light as possible, while maintaining effectiveness of the proof mass stabilization system.

Figure 1-4 shows the system of Figure 1-3 extended to act in two directions. The device is now capable of counteracting tremor forces acting both vertically and horizontally. Along with this increased capability comes the need for a second proof mass. As previously mentioned, though, the goal is to make the system as light as possible. Thus, it would be beneficial to find a way to efficiently use the mass of the device.

One way to do this is to have both actuators share a common proof mass. In other words, the proof mass is free to move along two axes, vertical and horizontal. The benefit of this approach is that the system mass is effectively halved. The disadvantage is increased mechanical complexity from the mechanism needed to allow the actuators the flexibility to share the proof mass. Mechanical design of the prototype will encompass a number of innovative design features. In addition to

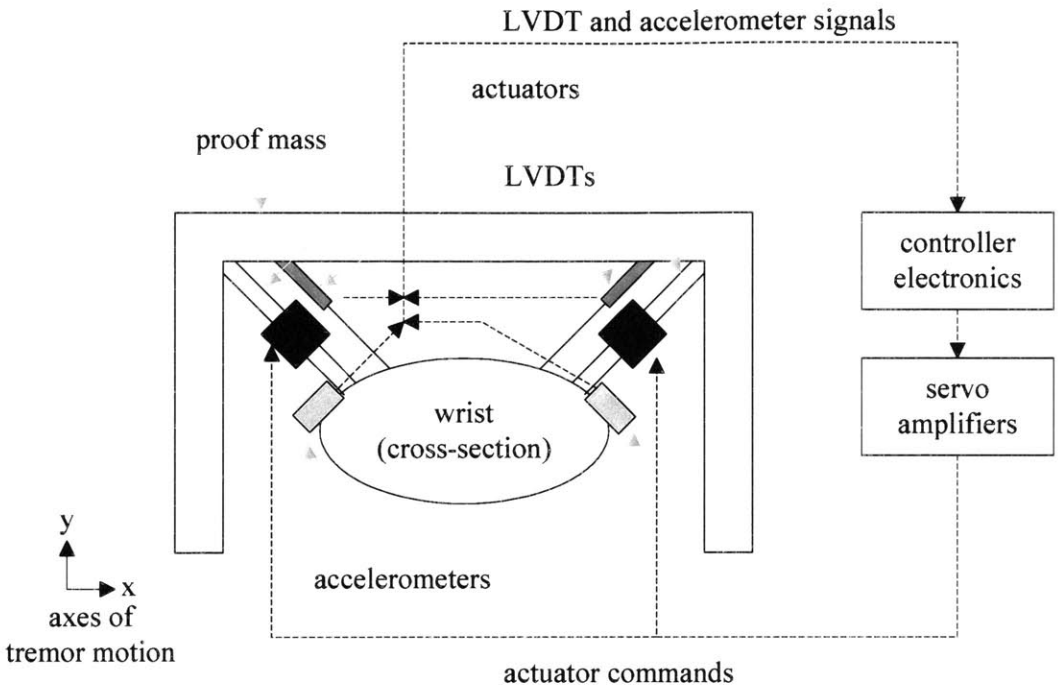


Figure 1-4: Diagram of proposed active tremor control system.

the sharing of the proof mass, the proof mass will be designed such that the center of mass of the device is very close to the center of the wrist. The details of the mechanical design will become apparent in Chapter 3.

## 1.4 Thesis Scope

This thesis proposes to model, design, construct, and test a system to physically remove two axes of translational tremor from the wrist/hand of an individual with essential tremor. As mentioned before, it is the author's belief that the greatest utility could be extracted by stabilizing the hands of those afflicted with severe tremor so that normal activities involving the hands can be performed. Stabilization of a hand can, in theory, allow the individual to properly eat, drink, and perform other manual tasks such as dialing telephones, without the assistance of caretakers or relatives. Thus, the design and construction of a prototype "wrist cuff" stabilizer is undertaken in this thesis.

Using information available in the literature, I hope to obtain the required specifications for sensors and actuators to attain the thesis goals. Once these specifications are obtained, a lumped-parameter system model will be constructed, and its performance analyzed. This will allow proper control system design to take place. Mechanical and electrical design of the modeled system will

follow, and the thesis will conclude with a qualitative and quantitative evaluation of the performance of the constructed system.

# Chapter 2

# Preliminary Analysis and Modeling

## 2.1 Overview

This chapter details the initial engineering study aimed at determining the feasibility of constructing a wrist-stabilizing tremor controller. An engineering study was performed in order to determine what types of tremors could be attenuated, what the system operation paradigm would be, and what types of sensors and actuators would be required.

It was decided that a proof mass stabilization scheme would best meet the engineering requirements. Such a stabilization system would sense tremor motions, and then activate an actuator between the wrist and a proof mass. A correcting force would act on the wrist, with the inertia of the proof mass acting as the inertia against which the actuator would apply force. See Figure 1-3 for a schematic representation of the architecture of such a system.

## 2.2 Analysis Guidelines from Literature

In order to expedite the design and construction of the device, specification of the major components was begun as soon as possible. For example, the linear actuators could have had a lead time of up to four months if custom actuators were required or if a production actuator model were out of stock. Also, it was known that silicon micromachined accelerometers were only in development within Draper Laboratory, but were in production at Analog Devices. If custom accelerometers were needed, this would have also created a long lead time. Faced with delays such as these, the design of the device was begun in earnest. It was decided that the most critical components to specify would be those that absolutely had to be obtained from sources outside of Draper Laboratory. The

only parts for the prototype that had to be procured from outside sources were the sensors and actuators. Thus, the preliminary analysis presented in this chapter is that used to specify sensors and actuators for the thesis.

The design of the tremor suppression device had to have some starting point determined by the type of behavior we expected the system to exhibit. Since the thrust of this application was the modification of mechanical behavior, a logical starting point was a characterization of the mechanical behavior we wished to modify. Preliminary design studies were performed using tremor characteristics available from the literature. Assuming a very simple model of tremor motion, the displacement of the wrist/hand associated with tremor, $x_1$, was approximated by the sinusoid

$$x_1(t) = A\sin(2\pi\omega t + \phi), \tag{2.1}$$

in which $A$ is the amplitude of the tremor displacement, $\omega$ is the frequency of the tremor in Hertz, $t$ is time in seconds, and $\phi$ is the phase angle [9]. Indeed, data displaying essential tremor often appear to be sinusoidal in shape, so this model may not be as simplistic as it seems [11]. Furthermore, Elble and Findley define tremor as *any involuntary, approximately rhythmic, and roughly* sinusoidal *movement* [10]. Thus, it would appear as though the model of hand tremor presented in Equation 2.1 was a respectable starting point. Taking the first and second derivatives of Equation 2.1 resulted in similar expressions for velocity and acceleration, respectively.

$$\dot{x}_1(t) = 2A\pi\omega\cos(2\pi\omega t + \phi) \tag{2.2}$$

and

$$\ddot{x}_1(t) = -4A\pi^2\omega^2\sin(2\pi\omega t + \phi). \tag{2.3}$$

Hence, from Equation 2.3, the maximum acceleration experienced by the limb could be calculated knowing only the frequency and amplitude of tremor; the coefficient $4A\pi^2\omega^2$ corresponds to the maximum acceleration. The importance of computing the maximum acceleration experienced by the limb will become apparent in Section 2.3.

An excellent quantification of tremor amplitudes at various frequencies was here applied with Equation 2.3 to help estimate the accelerations with which we would be dealing [11]. Elble's goal is to show the strong negative correlation between tremor frequency and amplitude, and he presents Figure 3 on page 56 of Reference [11] in order to do so. The data are curve fit in this figure, and an

| Frequency [Hz] | Worst-Case Tremor Amplitude [inches] | Worst-Case Tremor Acceleration [g] |
|---|---|---|
| 4 | 0.787 | 1.29 |
| 5 | 0.386 | 0.985 |
| 6 | 0.189 | 0.695 |
| 7 | 0.0925 | 0.463 |
| 8 | 0.0453 | 0.296 |
| 9 | 0.0222 | 0.184 |
| 10 | 0.0109 | 0.111 |
| 11 | 0.00532 | 0.0658 |
| 12 | 0.00261 | 0.0384 |

Table 2.1: Worst-case tremor amplitudes and accelerations at various frequencies computed using Equation 2.4.

equation describing the curve fit is presented. By shifting the y-intercept of this plot to 20 mm, it was possible to come up with a conveniently placed line that bounded nearly all of the data. The equation that resulted from this shift was

$$logA = -0.31\omega + 2.541. \tag{2.4}$$

Evaluation of Equations 2.3 and 2.4 over the full range of frequencies revealed that the maximum acceleration occurred at the minimum frequency of 4 Hertz, and had a value of 1.25 $g$'s. Therefore, the sensors, mounting structures, and control system dynamics should be capable of supporting wrist accelerations of at least this magnitude and frequency.

Realistically, the tremors experienced by a device resulting from this thesis will be of lower magnitude. The tremor frequencies specified in the literature were obtained in cases for which the limb of interest was either unloaded or minimally loaded. In other words, the experimenters made extensive efforts to ensure that the lightest possible sensors were used so that the presence of instrumentation did not alter the dynamics inherent to the limb. This application will, no doubt, add considerable mass to the steadied limb. This mass, which will act as added inertia, will certainly lower the natural frequency of the system according to an equation such as

$$\omega_n = \sqrt{\frac{k_{eff}}{m_{eff}}}, \tag{2.5}$$

in which $k_{eff}$ is the effective stiffness of the system, $m_{eff}$ is the effective inertia of the system, and

$\omega_n$ is the natural frequency of the system [9]. For example, referring to Figure 2-4 on page 41, if $m_1$ were fixed, the resonant frequency of the $m_2$, $k_2$ system would be $\omega_2 = \sqrt{\frac{k_2}{m_2}}$. A decrease in the natural frequency of a loaded limb as compared to the unloaded condition is shown frequently in the literature, and the relationship used to describe the behavior is often Equation 2.5 [11, 13]. Referring to Equation 2.3, it is apparent that even a small change in the frequency of motion can have a big impact on the acceleration experienced by the system, since $\omega$ is squared in this relationship.

Many sources in the literature attempt to incorporate a simplified spring-mass model into the analyses they undertake. Results from these sources indicate that tremors in the forearms exhibit characteristics of both a mechanical resonance that adheres to Equation 2.5, and tremors that appear to be caused by resonant conditions within the nervous system. The former type of tremor is generally referred to as a "mechanical reflex tremor." This thesis will attempt to attenuate both mechanically and neurologically effected tremors using mechanical means, but it should be noted that significantly different systems can be used in order to attenuate tremors arising as a result of varying excitation sources. In other words, if it were assumed that the amplitude of tremor oscillations was a result of a force driving inertia in a non-resonant fashion, then it would be easy to determine the driving force responsible for the tremor. However, if it is assumed that the amplitude of tremor oscillations is a result of driving a mass-spring system at its resonant frequency (described by Equation 2.5), then the driving force would be of markedly different amplitude. Namely, the force required to drive the resonant case for the same amplitude as the non-resonant case would be much lower. It will be seen in Section 2.4 that the magnitude of the driving force is a major consideration in actuator selection. Traditionally, vibration theory assumes that a system with a given set of characteristics, i.e., a certain value for effective mass and stiffness, will exhibit resonant motion at the frequency $\omega_n$ when excited by a force with something close to that frequency [9]. An equation such as Equation 2.5 would apply to such a system. The result is that a small excitation force of the proper frequency causes large-displacement behavior because the system "wants" to vibrate at that frequency.

The literature further state that, at least in forearm and hand tremor, the lower frequency tremors in the range 4–8 Hertz are mechanically effected, and the higher frequency tremors 8–12 Hertz are neurologically affected [10, 11]. Details of the mechanical modeling of the system appear in Section 2.4. It is interesting to note, though, that the largest-amplitude tremors—those occurring at lower frequencies—are those that are caused by mechanically resonant conditions [10, 11]. Thus,

it may be that the most problematic tremors can be easily dealt with by capitalizing on the fact that they are caused by mechanical resonance. This assumption will be a key premise in the controller design of this thesis. In other words, the system will be designed to attenuate tremors as if they are caused by forces acting in non-resonant conditions. However, tremors caused by resonant conditions would require less actuator force to correct. Thus, the resultant system will be able to attenuate tremors caused by "worst case" conditions, and those caused by conditions that we would expect to see causing real-world tremors.

Often a relationship as simple as Equation 2.5 is easily studied. Unfortunately, in biological systems, this is not the case. The mass of a forearm varies wildly from one individual to the next, as does the forearm stiffness. In addition, an individual can change the stiffness of a limb by flexing or relaxing his/her muscles. Joints within the human body are lubricated using fluids, and become more difficult to move with decreases in temperature due to increasing fluid viscosity. Also, the stiffness of a limb varies greatly depending simply on what *position* the limb is in. For example, if the portion of an arm below the elbow is positioned so that it is orthogonal to the portion of the arm above the elbow, the arm will have a given set of stiffness characteristics. If this same arm is then extended so that it is straight it will have a high stiffness to further extension as the elbow resists this motion, and a much lower stiffness to flexion of the joint. In short, it is very difficult to arrive at a general relationship for the effective impedance of a biological appendage, and the effective mass of an appendage will vary wildly from one individual to the next.

This thesis aimed to circumvent the need to know the exact mass and/or stiffness of the forearm by attenuating worst-case predicted tremor over a frequency range of 4–12 Hertz. This approach was implemented by sizing actuators and proof masses such that the lower frequency, higher amplitude tremors could be attenuated by assuming they were caused by resonant conditions, and by designing the tremor controller such that it could attenuate lower amplitude, higher frequency tremors not caused by resonance. Such an approach should make the tremor controller appealing to a wider range of the population and effective in reducing most tremors plaguing the population.

Design of the prototype was made more daunting by the plan to use proof mass actuators in the construction of the stabilizer. A simpler design paradigm could include mounting the stabilizing system to a rigid structure, such as a table or wall. With the structure present to support the weight of the stabilizer, it would be easier to utilize very powerful actuators in the design, and yield a very effective system. Unfortunately, though, this approach would limit the utility of the device since the user must always be in a predetermined spot to use it. The use of proof mass

actuators implies that the stabilizer will *not* be attached to any rigid structure, and the greatest utility is achieved by this approach. However, the individual using the device must support the entire system including proof masses and actuators. Thus, it is far more important to make the masses and actuators as light as possible in the latter approach. With such difficulty in determining what the actuator needed to actuate (in terms of the physical characteristics of and excitation forces within the appendage), one must proceed cautiously.

## 2.3 Sensor Selection

For the detection of tremor, it was decided to use accelerometers in order to sense tremor accelerations. This decision was based on a number of assumptions regarding the planned behavior of the tremor suppression device. First, there was the assumption that the stabilizer would *not* aim to remove intended motions of the limb to which it was attached. Intended movements would take the form of constant velocity motions, and low-frequency displacements and/or accelerations, none of which it would do any good to sense. Furthermore, the author knew of no displacement transducers that could function inertially, i.e., with no external reference, which would be necessary in order to design a freely moving system utilizing proof mass actuators. Secondly, Elble and Findley make an interesting argument for the case of acceleration sensing of tremor based on the frequencies of the detected motions [10]. Since tremors are higher in frequency than intended motions, and acceleration amplitudes of sinusoidal movements change as the frequency squared (as shown in Equation 2.3), tremors are more easily distinguished from lower frequency, intended motions, by the use of acceleration sensing [10]. Lastly, since this thesis wishes to use a proof mass actuation scheme, no integrations will be necessary in the control loop algorithms if accelerations are sensed directly. Proof mass actuation provides controlling forces to the system by accelerating a mass, thereby following Newton's $2^{nd}$ equation, which appeared as Equation 1.1 [14]. If displacement or velocity sensors were utilized, additional signal processing would need to be performed (Fast Fourier Transforms, differentiations, etc.) in order to determine when and how to activate the control system. Acceleration sensing provides the most straightforward and appropriate means of sensing tremor for this application.

The sensor selection can be performed using the analysis performed in Section 2.2. We sought an acceleration sensor with the proper resolution, range, and size to allow unobtrusive mounting and monitoring of tremor acceleration. A good candidate for this application proved to be the PCB

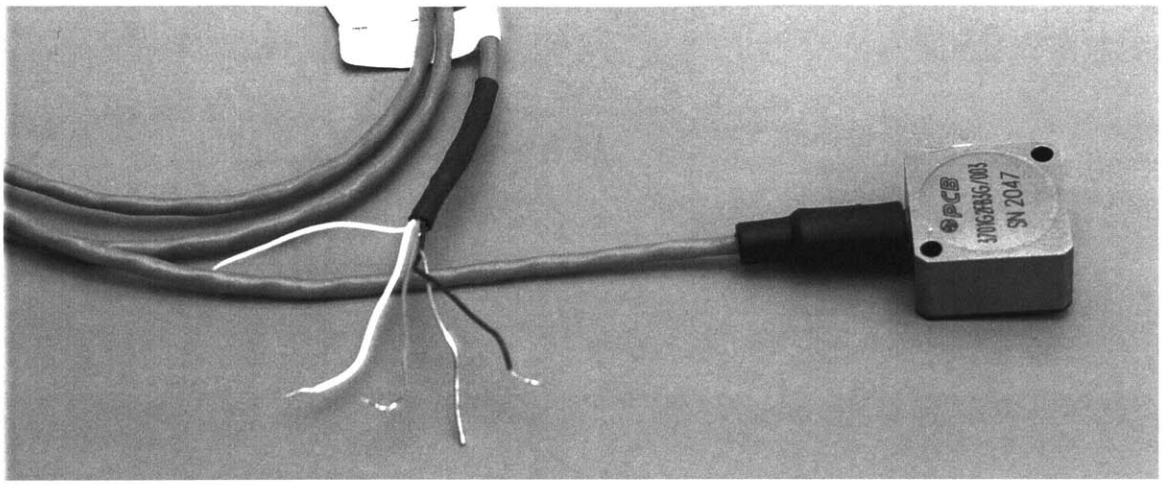


Figure 2-1: Photograph of the PCB Piezotronics 3701 accelerometers.

Piezotronics[1] model 3701G2FB3G accelerometer, shown in Figure 2-1. It provided a compact case, measuring 0.85 by 0.85 by 0.45 inches. The range of the PCB accelerometer was $\pm 3$ $g$, which was perfect for this application. An accelerometer for this application would likely sense 2.3 $g$ at most, computed by adding the normal 1 $g$ of Earth's gravity to the worst-case acceleration of 1.3 $g$ from Table 2.1. In addition, the model 3701 had a scale factor of 1 V/$g$, which was very compatible with the inputs for the control electronics, providing a high-level signal in response to the accelerations that were expected. Lastly, a very high resolution of 30 $\mu g$ ensured the ability to sense the slightest tremors and excellent noise performance. As noted from Table 2.1, the lowest acceleration value expected would be approximately 40 milli$g$.

The PCB accelerometers were packaged in titanium casings with integrated wiring for easy mounting to the tremor controller structure and wiring into the controller electronics. All that was required was to supply the device with low-current (7 milliAmperes) power at 15 Volts; the devices did not require the charge amplifiers and signal conditioners typically required of more conventional accelerometers [5]. Product literature for these accelerometers also revealed that there was no phase lag over the 8–12 Hertz range of interest [5]. This ensured that the control system would be reacting to real accelerations, rather than the artifact of an acceleration that was occuring faster than the instrument could accurately sense. Thus, a wide range of options within this line of accelerometers was available to the experimenters for integration into the control system.

Another good candidate for this application was one of the *i*MEMS silicon micro-machined

[1] 3425 Walden Avenue, Depew, NY 14043

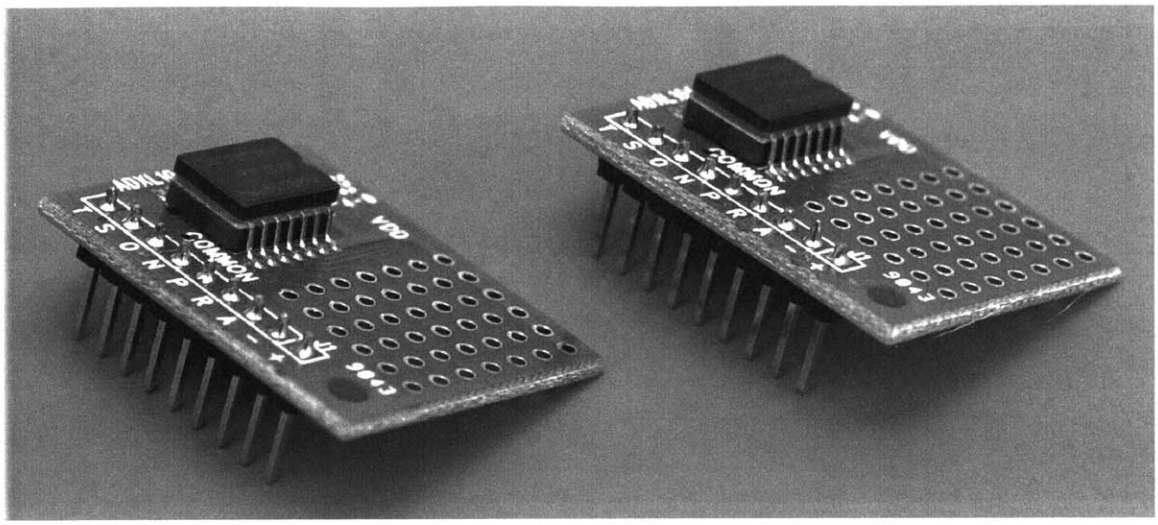

Figure 2-2: Photograph of the Analog Devices ADXL105 accelerometers.

accelerometers manufactured by Analog Devices, Inc.[2] These accelerometers have the ability to sense ranges of $\pm 2$ $g$, $\pm 5$ $g$, $\pm 20$ $g$, $\pm 50$ $g$, $\pm 100$ $g$, they can output an analog signal for easy integration into analog control-loop electronics, and they weigh less than 2 grams. The *i*MEMS accelerometers quote a typical noise floor of 225 $\mu g/\sqrt{\text{Hertz}}$ [1]. Assuming the accelerometer is sensing motion at 12 Hertz, this noise floor would be at approximately 779 $\mu g$. Over a worst-case frequency of 12 Hertz, Equation 2.3 would (theoretically) allow the control loop to stabilize the motion of the afflicted limb to an amplitude of approximately 0.712 $\mu$m. Thus, one of these accelerometer models, sized to sense the appropriate range of values, should be capable of sensing the required accelerations. The Analog Devices model ADXL105 accelerometer, capable of sensing $\pm 5$ $g$ accelerations, is shown in Figure 2-2.

A particularly interesting sensor choice for this thesis would be the Analog Devices, Inc. $\pm 2$ $g$ *i*MEMS accelerometers (model ADXL202). These units went into volume production as of August 2000, and as such were not incorporated into the original prototype design. These units are particularly attractive because they should be able to sense the entire range of interesting accelerations with the highest resolution possible. Since we expect the worst-case acceleration the prototype will face will be approximately 1.25 $g$, and gravity can contribute up to a maximum of 1 $g$, the unit is very nearly able to sense the entire worst-case range. Also, this unit is the first of the *i*MEMS product line to incorporate *two* input axes into one chip. This could pose a significant advantage if a wrist tremor controller were ever put into volume production, since only one accelerometer chip

[2]One Technology Way, P.O. Box 9106, Norwood, MA 02062-9106, U.S.A.

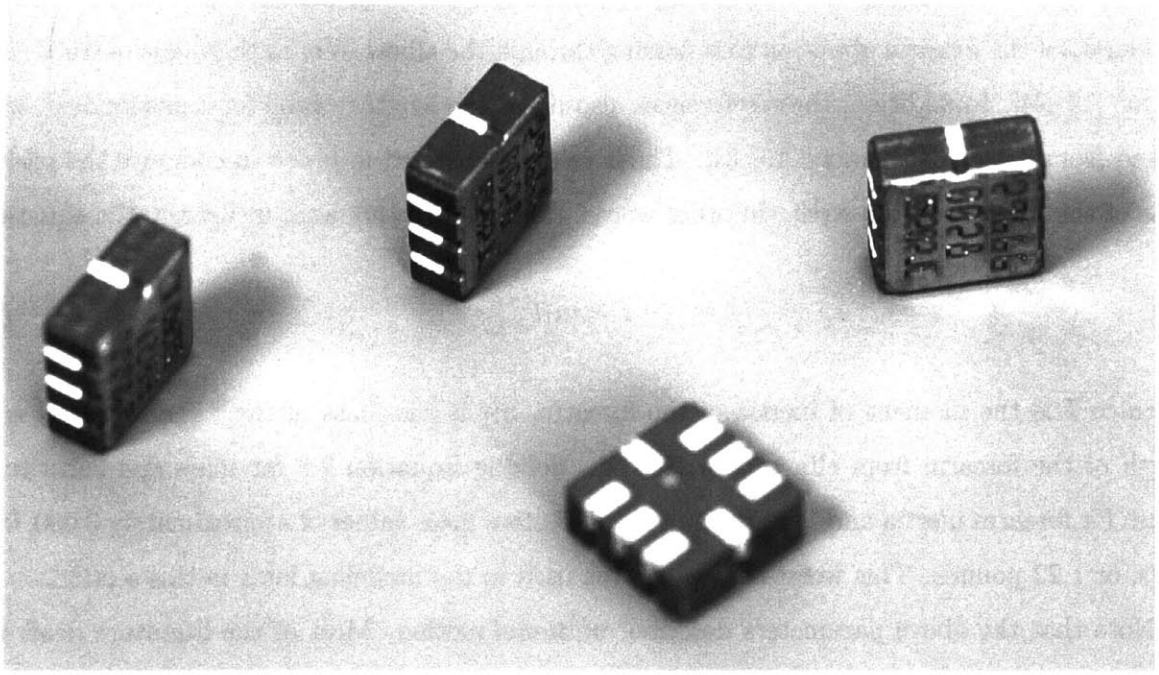

Figure 2-3: Photograph of the Analog Devices ADXL202 accelerometers.

could satisfy all of the acceleration sensing needs of the device. Also, the $\pm 2$ $g$ unit is the first to come with both digital and analog outputs. A volume production wrist tremor controller would no doubt incorporate the entire control electronics onto a digital application specific integrated circuit (ASIC) of some sort. An accelerometer with digital outputs would be ideal for such a configuration. Lastly, the model ADXL202 accelerometers were shrunk even further from the ADXL105 model, providing an incredibly small package with more sensing capabilities. Although the tremor controller was designed around the PCB accelerometers, several $\pm 2$ $g$ samples were procured on evaluation boards for experimentation purposes. The ADXL202 accelerometers are shown in Figure 2-3.

## 2.4 Actuator Selection

The most challenging part of the analysis phase was actuator selection. Since the system needed to be as light as possible, great care was taken in order to ensure that the actuators were no heavier than absolutely necessary. On the other hand, heavier actuators could supply more force, and the actuators had to be able to provide enough force to adequately stabilize the wrist. Some literature supplies inertial properties of the human forearm, presenting an opportunity for preliminary analyses to be undertaken. The literature obtained reported a wide range of inertial values for the

human forearm, depending on the sex, height, and body type of the individual. Nominal values for the inertia of the forearm about an axis passing through the elbow were in the range of 0.030–0.090 $\text{kg} \cdot \text{m}^2$ [19, 24]. In addition, these references also listed the lengths of the forearms studied, which ranged from 0.33–0.385 meters [19, 24]. These values were used in order to compute the effective mass of the forearm at the wrist. In other words, these parameters were utilized in the equation

$$I = m_1 l^2 \tag{2.6}$$

in which $I$ is the moment of inertia of the forearm, $m_1$ is the mass of the forearm, and $l$ is the length of the forearm from elbow to wrist [14]. Solving Equation 2.6 for mass and substituting values for forearm inertia and length resulted in effective mass values of approximately 0.030–0.038 slugs, or 1.22 pounds. This worst-case value was used in the modeling later in this section.

Note that the above parameters describe *rotational* motion. Most of the literature dealt with the rotational motion of the forearm, which one would expect on examination of the limb. For the purposes of this study, though, the location of the wrist was treated as a variable in terms of translational motion. The main reason for making this simplification was that tremor of the hands most often exhibits motion that is predominantly linear [10]. Keeping all of this in mind, a simple two-degree of freedom translational model was proposed to aid in actuator design. See Figure 2-4 for a lumped parameter representation of this model. The variables in the figure correspond to the following physical entities. Mass $m_1$ is the effective mass of the hand/forearm as observed at the wrist of an individual, and is the mass that needs stabilization. The proof mass is $m_2$, which is moved in order to stabilize the hand. The distance $x_1$ is the motion of the hand, and the distance $x_2$ is the motion of the proof mass, both with respect to inertial space. Although not defined in Figure 2-4, the quantity $x$ is defined as

$$x = (x_2 - x_1) \tag{2.7}$$

which conveniently expresses the stroke length of the actuator. This quantity will be a topic of intense study later in this section, since actuator travel corresponds to actuator stroke length, and stroke length is a key selection criterion for linear actuators. Continuing, the quantity $F_c$ is the actuation force that acts on both the proof mass $m_2$ and the wrist $m_1$. The quantity $F_D$ is a model of the disturbance force acting on the limb to cause the tremulous motion.

Note that there was no resonance in this model of the creation of the tremor, as introduced in

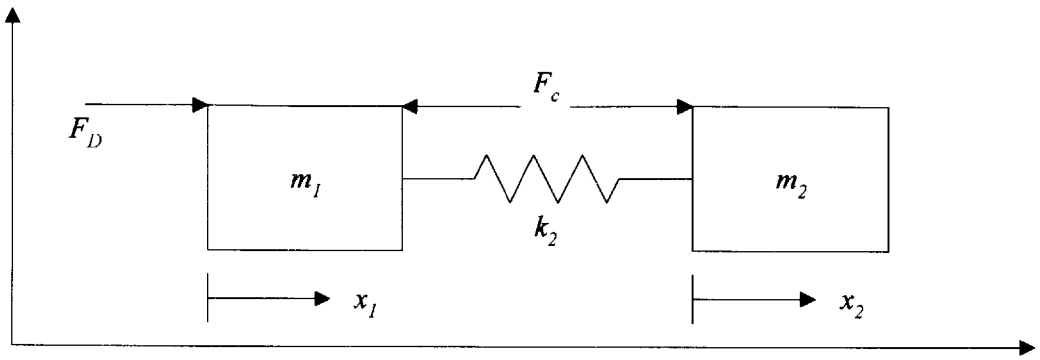


Figure 2-4: A 2 degree of freedom model to aid in actuator specification.

Section 2.3. Although using a resonant mass-spring lumped parameter model would have recreated the same tremor amplitude using lower amplitude excitation forces, the emphasis at this point was on designing a system that was capable of handling *worst-case* scenarios. In other words, a system able to attenuate tremors caused by non-resonant conditions would certainly be powerful enough to attenuate tremors caused by resonant conditions.

The equations of motion of this system were easily derived using any of a variety of methods. The Lagrangian method was used for consistency, as it will be used later in this thesis [8]. The kinetic coenergy of the system, $T^*$, is given by

$$T^* = \frac{1}{2}m_1\dot{x}_1^2 + \frac{1}{2}m_2\dot{x}_2^2. \tag{2.8}$$

The potential energy of the system is given by

$$V = \frac{1}{2}k(x_2 - x_1)^2. \tag{2.9}$$

The Lagrangian of the system is given by

$$L = T^* - V. \tag{2.10}$$

We take the derivatives of the Lagrangian with respect to the variational coordinates, including the generalized forces, according to the equations

$$\frac{d}{dt}\left(\frac{\partial L}{\partial \dot{x}_1}\right) - \frac{\partial L}{\partial x_1} = -F_c + F_D \tag{2.11}$$

and

$$\frac{d}{dt}\left(\frac{\partial L}{\partial \dot{x}_2}\right) - \frac{\partial L}{\partial x_2} = F_c. \tag{2.12}$$

The results of applying Equations 2.11 and 2.12 to Equation 2.10 are the equations of motion for the system,

$$\begin{aligned} m_1\ddot{x}_1 - k\left(x_2 - x_1\right) &= -F_c + F_D \\ m_2\ddot{x}_2 + k\left(x_2 - x_1\right) &= F_c. \end{aligned} \tag{2.13}$$

The controller used in this model was also very simple. It consisted of a simple proportional feedback on the acceleration $\ddot{x}_1$. In other words,

$$F_c = K_{AP}\ddot{x}_1, \tag{2.14}$$

in which $K_{AP}$ is the proportional gain of the accelerometer feedback. Simple time lags for the accelerometer and the controller electronics were included with low time constants denoted by $\tau_1$ and $\tau_2$, respectively. The disturbance force was

$$F_D = F_{AMP}\sin\left(2\pi\omega t\right), \tag{2.15}$$

in which $F_{AMP}$ was the amplitude of the disturbance force.

While this model was an extraordinarily simple one, it allowed a significant amount of analysis to be performed. Equations 2.13, 2.14, and 2.15 were used in order to construct a Simulink block diagram model of the system. See Figure 2-5 for a block diagram of the model analyzed in Simulink. Casting the model as above allowed a variety of system models to be examined utilizing the linear time invariant (LTI) analysis tools available within The Mathworks, Inc.[3] Simulink and Matlab. The LTI tools conveniently gave transfer functions, which were extensively analyzed using the Bode plot functions in Matlab. By taking transfer functions from one point of interest in the model to another point of interest in the model, the characteristics of the system's performance over a wide range of frequencies was easily quantified. The process taken in this thesis was the following.

1. Using Equation 2.4, and an open-loop version of the Simulink model in Figure 2-5, the disturbance forces required to produce the amplitudes specified by Equation 2.4 at frequencies between 4 and 12 Hertz were determined. These values were computed for the case in which

[3] 3 Apple Hill Drive, Natick, MA 01760-2098

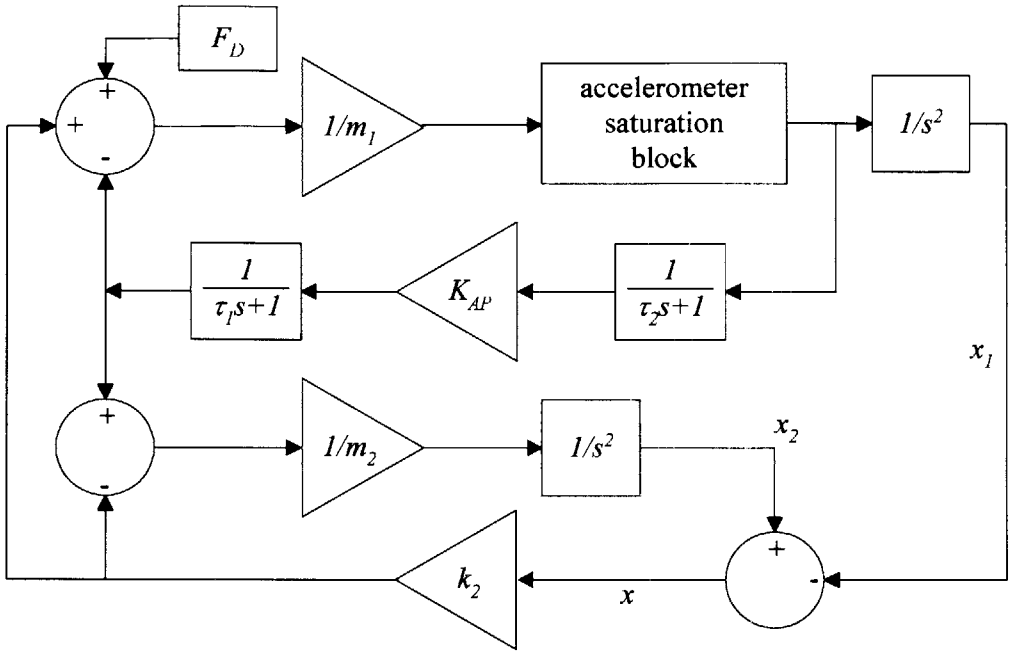


Figure 2-5: Block diagram of the 2 degree of freedom model analyzed on Simulink.

$m_2 = m_1$, and it was assumed that the very weak spring coupling the two masses ($k_2 =$ 0.5 lb/ft) would minimize the interaction between $m_1$ and $m_2$. The spring was incorporated into the model for numerical tractability within Matlab. Matlab gave the best results when the numerical integrators were given a physically realizable initial condition for the two masses. The weak spring allowed a numerically definable initial position of one mass with respect to the other to be entered into Matlab. The values discovered for disturbance forces were tabulated according to frequency, as shown in Table 2.2. For comparison purposes, the values computed using only Equation 2.3 and Newton's 2$^{nd}$ equation are displayed in Table 2.2. Note the excellent agreement between the two sets of results to three significant figures, lending confidence to the assumption that the weak spring minimizes interactions between the masses.

2. With these disturbance forces known, the system was analyzed using various values of the feedback gain $K_{AP}$ from Equation 2.14 and the proof mass $m_2$ to determine the stroke of actuation $x$ required for tremor attenuation. The LTI tools within Matlab were used to accomplish this step; the output point monitored $x$ while the input point monitored $F_D$. This scheme allowed the transfer function to be studied, and $x$ quantified, subject to the forces $F_D$ that caused the tremors corresponding to those bounded by Equation 2.4. Gain levels taken from the Bode plot of the resulting transfer function were utilized in the relation

| **Frequency [Hz]** | $F_D$ **[lbs]** $(F = ma)$ | $F_D$ **(Simulink Model)** |
|---|---|---|
| 4 | 1.57 | 1.56 |
| 5 | 1.21 | 1.21 |
| 6 | 0.850 | 0.853 |
| 7 | 0.567 | 0.584 |
| 8 | 0.363 | 0.361 |
| 9 | 0.225 | 0.227 |
| 10 | 0.136 | 0.137 |
| 11 | 0.0805 | 0.0806 |
| 12 | 0.0469 | 0.0474 |

Table 2.2: Disturbance force values to create tremor amplitudes seen in Equation 2.4 computed using two different methods.

[15]

$$\text{gain [db]} = 20 \log_{10}\left(\frac{\text{output}}{\text{input}}\right). \tag{2.16}$$

See Figure 2-6 for a graphical view of the $m_2$ versus stroke results.

3. The output point of the LTI viewer was moved to provide values for the transfer function from the disturbance force $F_D$ to the movement of the hand $x_1$. This analysis afforded the opportunity to determine how well different combinations of feedback gain and proof mass were able to suppress tremor. The feedback gain was changed until the amplitude of $x_1$ was approximately 2 orders of magnitude of its open loop value.

4. An analysis of the transfer function from disturbance force $F_D$ to actuator force $F_c$ was examined, in order to determine the required force output of the actuator. Interestingly, the maximum actuator force encountered in the modeling always closely matched the disturbance force found at that particular frequency, even for very high values of feedback gain $K_{AP}$. This provided an excellent rule of thumb method of actuator selection.

The above solution process proved to be very powerful, allowing the author to evaluate the behavior of hundreds of different system configurations very quickly and easily using Matlab. A great deal of conclusions were drawn regarding system performance across a spectrum of system parameters. For example, guidlines for feedback gains were developed, as well as theoretical limits for best-case tremor attenuation. The end result of this modeling was the selection of voice coil linear actuators from BEI Sensors & Systems Corporation, Kimco Magnetics Division[4]. BEI model

[4]804-A Rancheros Drive, P.O. Box 1626, San Marcos, CA 92069

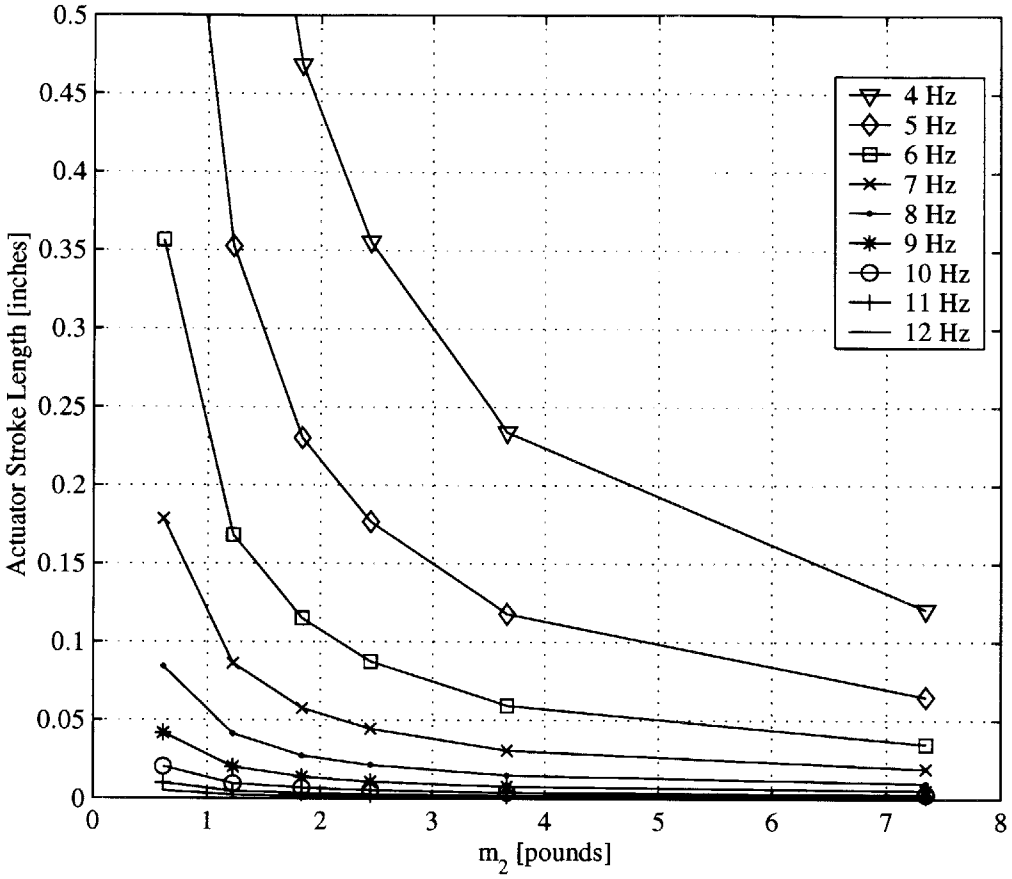


Figure 2-6: Plot of actuator stroke $x$ versus $m_2$ for a variety of frequencies.

| Frequency [Hz] | Mean Mass-Stroke Product | Standard Deviation |
|---|---|---|
| 4 | 0.880 | 0.0206 |
| 5 | 0.440 | 0.0195 |
| 6 | 0.221 | 0.0179 |
| 7 | 0.114 | 0.0133 |
| 8 | 0.0554 | 0.00846 |
| 9 | 0.0282 | 0.00538 |
| 10 | 0.0141 | 0.00324 |
| 11 | 0.00703 | 0.00186 |
| 12 | 0.00357 | 0.00106 |

Table 2.3: Mass-stroke product for the data points in Figure 2-6.

number LA10–12–027A linear actuators provided ±0.180 inches of stroke and 3 pounds of force in a compact, lightweight (3.2 ounce) package [2]. At a relatively inexpensive price of US$300, they proved to be well-suited to the task. See Chapter 3 for more detail on the design and use of these actuators. Figure 2-7 is a photograph of the BEI actuators. The two pieces on the left are an individual coil and field end. An assembly of the two components in shown on the right of Figure 2-7.

Although the BEI LA–10–12–027A actuators had an officially quoted stroke length of ±0.180 inches, it should be noted that this stroke length was merely the range of *linear* behavior of the actuator [2]. It was assumed that the actuators could be made to move further, and as such they were mounted on ball slides having a stroke length of ±0.25 inches. As can be seen in Figure 2-7, the two halves of an actuator did not have any rigid mechanical coupling limiting their travel, and they could be freely disassembled. Referring to Figure 2-6, one notices that a stroke length of ±0.25 inches places a very large number of data points within the realm of the tremor control prototype's performance capabilities. As a starting point, the author chose to use a proof mass weight of approximately 1 pound. Such a weight was high enough to include all but the lowest frequency data points on Figure 2-6, yet low enough to be practical for a prospective patient to wear for some time. According to the analysis that went into creating Figure 2-6, a data point corresponded to a 2-order of magnitude reduction in tremor amplitude. That is, the controller gains in the mathematical model were increased until the closed loop tremor amplitude was 2 orders of magnitude less than the open loop tremor amplitude. The required stroke length then became a data point on Figure 2-6. Choosing a lighter proof mass value simply meant that attaining such a high level of tremor reduction would not be possible. Some effects would be noted, though.

Selecting a proof mass weight of 1 pound also had practical causes, most notably the capability of the actuators. If the tremor control device were rotated such that one actuator were to provide all of the centering force, it would require 1 pound of force from the actuator. Referring to Table 2.2, the maximum disturbance force we would expect to see would be approximately 1.6 pounds. Thus, an actuator supporting the full weight of the proof mass and attenuating a maximum disturbance force would be required to produce approximately 2.6 pounds of force. The LA10–12–027A actuators fit very nicely in this niche in terms of their size, performance capabilities, and stroke length.

Also of interest is the appearance of the curves in Figure 2-6. It seems as though the curves of individual frequencies were hyperbolic in shape, suggesting that the product of $m_2$ and $x$ was a constant. Indeed, computing the *mass-stroke product* lead to the results displayed in Table 2.3.

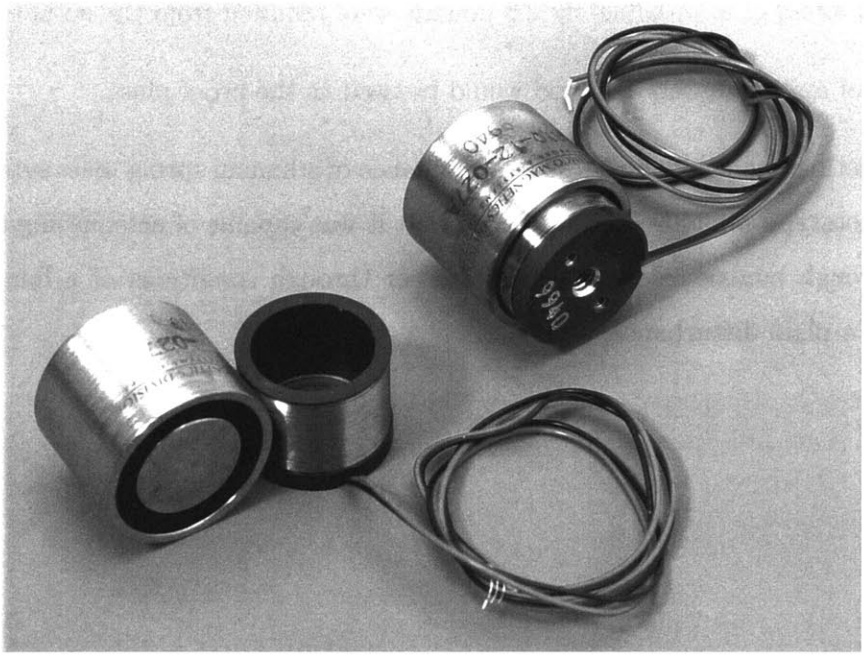

Figure 2-7: Photograph of BEI LA10–12–027A voice coil assembly, single core assembly, and single coil assembly.

Standard deviation computations show that the means are relatively tightly distributed, suggesting a true hyperbolic relationship to the curves. Worse agreement (in the form of higher standard deviations as a percentage of mean) is noted for higher frequencies, in which cases the full range of interest of the mass-stroke parameter space was not explored. On the other hand, very low standard deviations are noted for lower frequencies, for which a good portion of the hyperbolic curve was reconstructed. The existance of this mass-stroke product constant greatly simplified the process of selecting actuators and proof mass weights.

## 2.5 Summary of Analysis and Modeling

The analyses undertaken in the preceding sections of this chapter served as the basis of the design of the physical components and specification of the control system used in the prototype constructed in this thesis. Chapters 3 and 4 describe the design of the prototype and its control system in great detail, but the guidelines developed in this chapter served as the foundation for the design chapters that follow. The main assumptions that will be carried throughout this thesis are listed below.

1. The largest acceleration the system was expected to experience will be approximately 1.25 $g$'s.

2. Maximum forces of approximately 2.6 pounds were required from the actuators.

3. A weight of approximately 1 pound would be used as the proof mass.

4. Tremor motions were created through a resonance of a human spring mass sytem. The tremor control prototype would be designed such that it was capable of attenuating tremors created either through human resonance conditions or through conditions of a human mass being driven by a plain disturbance.

# Chapter 3

# Mechanical Design

## 3.1 Overview

Mechanical design of the tremor suppressing wrist cuff was one of the most important and challenging tasks undertaken in this thesis. Not only did the system have to be compact and lightweight to increase user acceptance, but the design also had to be compatible with all of the control systems embedded within the prosthesis.

It was recognized from the very beginning that, in order to make the device practical for use by tremor patients, the mass of the device would have to be kept to an absolute minimum. Unfortunately, the use of a proof mass actuation scheme entailed the addition of mass to the system. According to analyses undertaken in Section 2.4, additional proof mass would lead to a higher performance system (one better able to attenuate tremor) that utilized a smaller amount of the actuator travel. The positive correlation between proof mass weight and system performance is expected, since the proof mass is the mass against which the actuators act. A proof mass of greater inertia will accelerate less when acted on by a given force, resulting in the actuators being able to exert higher forces (being better able to attenuate tremor) on the larger mass while moving very little (requiring a shorter stroke length).

The end result of these realizations was that the system had two conflicting goals with regard to the addition of mass. On the one hand, additional proof mass enhanced system performance. On the other, a heavy system degraded user acceptance. In order to try to optimize the system, every step was taken to ensure that mass added to the system could be moved as part of the proof mass. An innovative system was devised to allow the *actuators and accelerometers themselves* to become proof masses for the system. The resultant design increased complexity, but yielded a

highly efficient system with regard to the allocation of moving mass.

The basic design paradigm required the creation of a device that could accomplish a number of tasks. These tasks included:

1. Mounting of the system onto a human wrist, with the ability to sense accelerations of the wrist and transmit correcting forces via a proof mass actuation scheme.

2. The ability to center the actuators, both longitudinally and radially. The actuators were provided from BEI as separate coil and field parts, with no system to provide centering of the actuator. As such, a custom designed and built configuration was required.

3. The protection of the user from moving parts and pinch points in the system. Also, protection of the user from electrical currents and heat generated by the actuators.

4. Imposition of as little additional mass to the wrist as possible. A heavy system would do little other than provide passive attenuation of tremor motion and tire the user.

The design detailed in this chapter accomplishes the above tasks through the use of clever packaging and a special system devised to enable both actuators to share the same proof mass. The packaging allowed nonintrusive mounting of the sensors and components necessary for proper function of the device. The ability of both actuators to share the same proof mass dramatically reduced the overall weight of the device.

The design features of the device are detailed in the following sections. Section 3.2 describes the polymer part used to mount the entire assembly to the wrist. Later sections describe the configuration of the device from this mount outward. The linear bearings are described in Section 3.3. The design and construction of the proof mass structure are detailed in Section 3.4. The design of the sensor systems embedded into the device is detailed in Section 3.5. Sections 3.2 through 3.5 give a general overview of the major parts and subsystems of this thesis. Section 3.6 is a summary of the mass of the device and the costs associated with its construction. Section 4.4 details the packaging of the various supporting electronics. The interested reader can turn to Appendix A for a compilation of the mechanical drawings and assembly details of the parts used in the construction of the tremor control prototype.

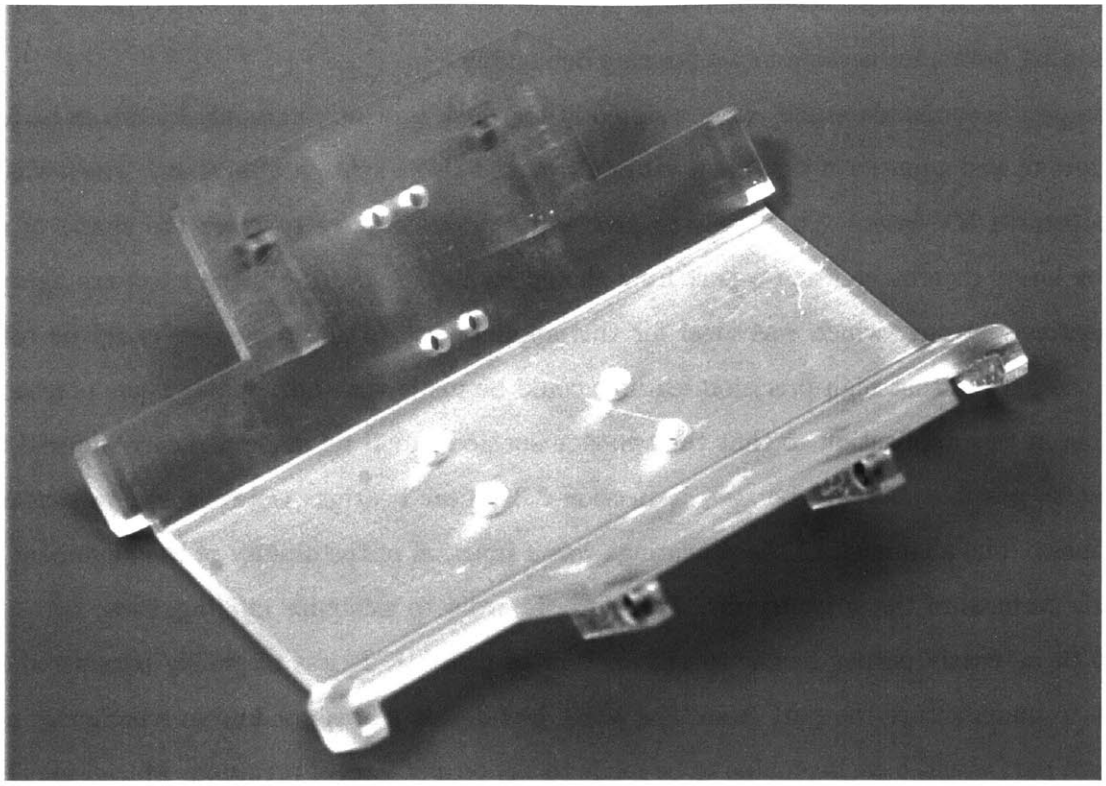

Figure 3-1: Photograph of the wrist/actuator mount of the tremor controller.

## 3.2 Wrist/Actuator Mount

A key part of the tremor controller was the piece that served as the interface between the wrist and the moving proof mass structure. The design of this part was very important, due to the fact that it performed so many functions. First, the part had to transmit the forces from the actuators to the forearm as effectively and comfortably as possible. The part also had to be light weight so as to add as little unmoving mass as possible, and the mount had to have provision for providing a stable point of attachment for both the accelerometers and LVDTs that would be part of the device. The resulting part is displayed in Figure 3-1.

This relatively simple design fulfilled all of the goals. First, the three-planed surface was able to transmit the forces to the bones of the forearm quite nicely. The side flat surfaces made excellent contact with the two bones in the forearm, and were fashioned such that they were normal to the axes along which the actuator forces acted. Flat surfaces spread the force out over some finite area, which greatly enhanced the comfort of the device. In addition, it was easy to place self-adhesive felt between the mount and the wrist to provide some cushioning between the device and the wrist.

The central, broad surface was a mounting point for the LVDTs, while the side surfaces also acted as mounting points for accelerometers during debugging.

The part was manufactured using a stereo lithography process commonly known as SLA. This procedure moved a platform through a vat of ultraviolet (UV) light-curable epoxy, which was cured by a steerable UV laser. The resulting process allowed the laser to trace the shape of a part layer by layer, thereby creating a part from the epoxy in the vat. Resulting parts are lightweight and relatively strong, which was ideal for this application. In addition, care could be taken to orient the part so that high-precision features could be made within the part. Some precision was desirable in this application so that the two side surfaces could be made as nearly normal to one another as possible. As will be seen in Section 3.3, linear bearings were utilized to support the proof mass. The alignment of these bearings was a function of the quality of the alignment of the two side surfaces of the wrist mount. Therefore, in order to minimize binding, these two surfaces had to be as nearly perpendicular to one another as possible. It was originally considered by the author to manufacture the part from bent sheet metal, but it was not known whether or not the resultant part would have been able to be made to the proper level of precision. Machining the part would have been expensive and would have also resulted in much wasted material. In addition, it was considered by the author that this part would likely be modified as the progress of the thesis continued. This would not be unlikely, given that the part was the interface between the device and person (and feedback would result in design improvements), and due to the fact that it performed so many functions. A new SLA part revision could be made cheaply in under 24 hours.

Both the LVDTs and additional accelerometers used on the device were also mounted to the wrist mount. Small flanges were built into the SLA part, and Emhart Fastening Technologies, Inc.[1] Heli-Coil inserts were added so that ADXL105 accelerometers could be firmly screwed to the base. The LVDT tubes were also mounted to the base via machined ABS mounts that were screwed to the SLA wrist mount. Additional details regarding these mounting procedures will be presented in Section 3.5.

[1] 510 River Road, Shelton, CT 06484.

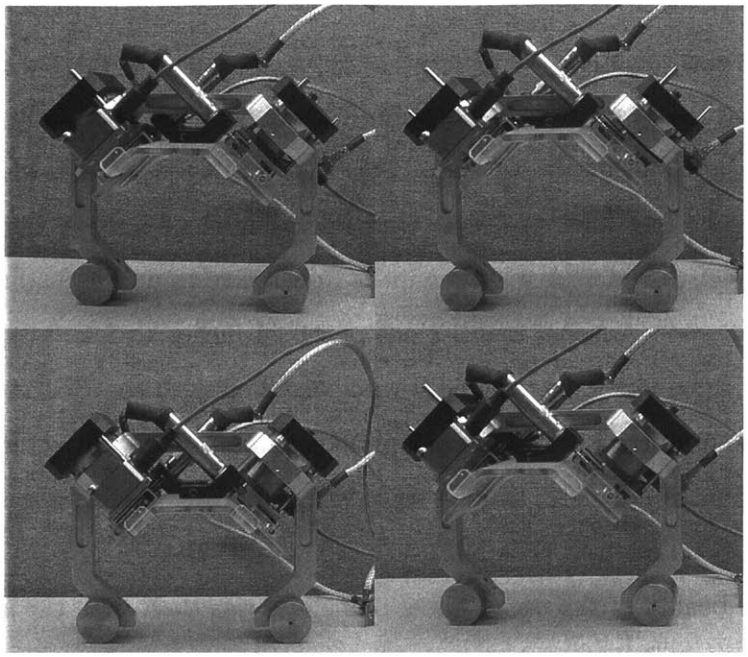

Figure 3-2: Photograph of the tremor control prototype in four different stages of articulation.

## 3.3 Linear Bearings

As alluded to in Section 3.2, the actuators were mounted on Del-Tron[2] model D–1 linear ball slides that allowed the actuators to translate $\pm 0.25$ inches orthogonally to their axis of actuation. The ball slides were screwed directly to the SLA wrist mount in order to keep the profile of the device as low as possible. Ball slides were used due to the fact that the BEI actuators had a stroke length of $\pm 0.180$ inches, while there existed only $\pm 0.015$ inches of clearance between the coil and field portions of the actuator. Were one actuator to translate the proof mass past $\pm 0.015$ inches it would bind the actuator of the other axis, which would be attached to the same proof mass through the proof-mass sharing scheme. Obviously, this could not be allowed to happen. Mounting the actuator on a linear ball slide allowed free lateral translation, thereby preventing binding problems due to motion of the opposing actuator. When one actuator moved past $\pm 0.015$ inches, the other actuator simply translated along its ball slide mount, thereby eliminating any binding problems. See Figure 3-3 for a photograph of the ball slides used.

Figure 3-2 shows the tremor control prototype in four different stages of articulation. The position of the SLA wrist mount with respect to the proof mass frame can be determined by examining how much of the guide pins is protruding beyond the tops of the actuators, and also by

[2]5 Trowbridge Drive, Bethel, CT 06801. 800-245-5013

the amount of the actuator coil visible (right axis only). The top left image shows the prototype with both of its axes approximately centered. The top right image shows the prototype with both of its axes in a full up position, while the bottom left image shows both of its axes in a full down position. Lastly, the bottom right image shows the device with the left axis in the full up position, and the right axis in the full down position. Understanding the ability of the device to move the proof mass with respect to the SLA wrist mount is imperative to understanding its operation.

The Del-Tron ball slides allowed translations of $\pm 0.25$ inches to take place, and were able to support 4 pounds of force [4]. This capability coincided well with the BEI actuators, which were specified to be able to produce a maximum of 3 pounds of force [2]. Additionally, the units weighed approximately 0.30 ounces per slide, making them nearly perfect for this application [4]. The cost was approximately US$60 per ball slide [4].

Another inherent beauty of the use of linear ball slides was that, with the actuators themselves moving *they became part of the proof mass for the opposing degree of freedom.* In other words, if the $x$ actuator pushed against the proof mass, it would move the proof mass *and the actuator for the $y$ axis* as a system. Thus, the actuators themselves "paid" for their own mass by becoming part of the proof mass for the opposing axis. In addition, the actuators were mounted such that the moving half of the actuator—the permanent magnet—was part of the proof mass. Such design features reduced the added mass to the system immensely. See Section 3.6 for a mass breakdown of the resulting system.

To further prevent binding of the actuators, each of the BEI actuators were guided along their axis of force application by a slider bearing. Steel posts were press fit into 303-series non-magnetic stainless steel adapter plates, and these adapter plates were in turn placed between the Del-Tron ball slides and the field ends of the BEI actuators. Teflon bushings were press fit into the proof mass structure frame (see Section 3.4 for additional details), and then reamed to make sure that the bushing, after insertion, had the proper inner diameter for the application. The steel posts press fit into the stainless steel adapter plates were then inserted into the bushings. The end result of this arrangement was that the proof mass structure slid along the steel posts, and the actuators themselves did not have to provide forces orthogonal to their axes of operation.

The resulting linear bearing exhibited excellent characteristics when finally assembled. Side to side play was minimal, and the proof mass slid freely along the steel posts. More friction was present than was anticipated, but this was beneficial to the operation of the device. The friction in the sliders provided at least *some* damping to the movement of the proof mass, which lead to greater

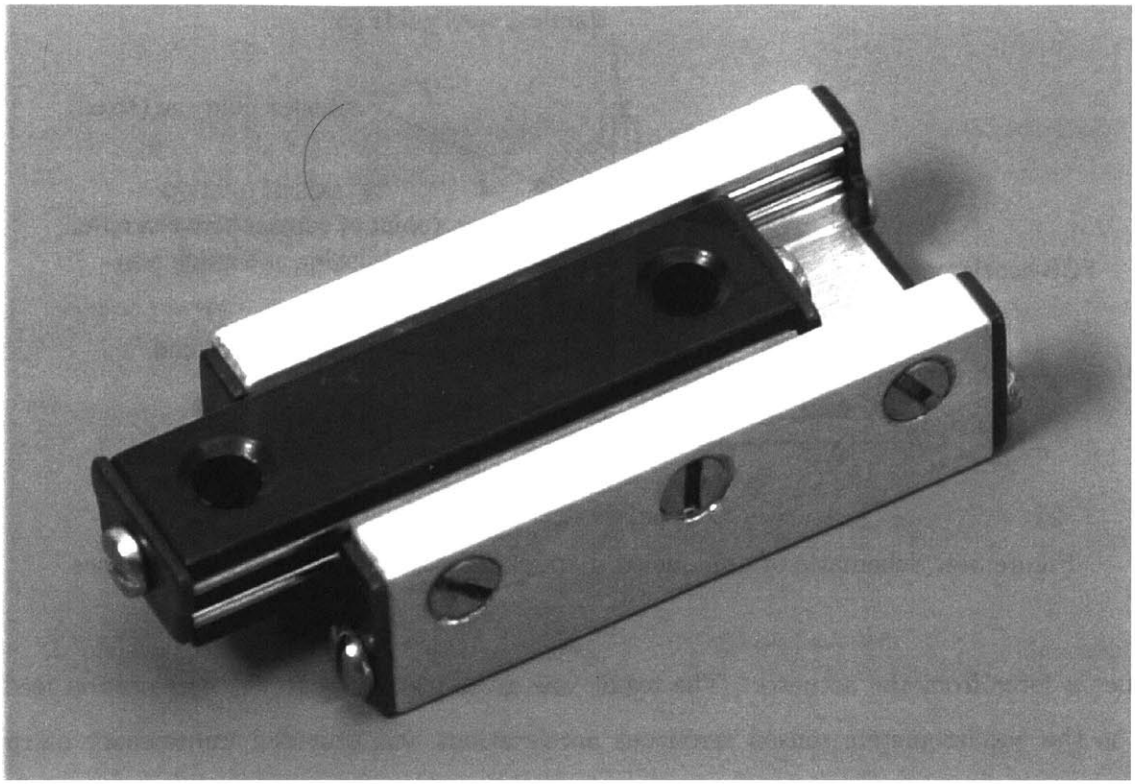

Figure 3-3: Photograph of Del-Tron model D–1 ball slide used in the fabrication of the prototype.

control system stability. Stainless steel posts that were long enough to avoid moving beneath the top surface of the Teflon bushings were installed. Making the steel posts this long prevented them from gouging the inner surface of the soft Teflon bushing, which created binding conditions in early tests. Also, the Teflon to stainless steel interface was lubricated with thin machine oil, further reducing friction between the two surfaces.

Unfortunately, testing revealed that the Teflon-on-guide pin bearing was not stiff enough to properly constrain the proof mass with respect to the ball slides. Figure 3-4 shows a schematic representation of the actuator halves, the stainless steel adapter plate, guide pin, and stainless steel guide pin. In Figure 3-4, consider the actuator field end fixed, and visualize the assembly consisting of the actuator coil end, PCB accelerometer, and stainless steel guide pin *unfixed*. That is, this assembly would be free to rotate about the axis of rotation resulting from the flexibility in the interface between the stainless steel guide pin and Teflon bushing (the Teflon bushing is not shown). It is easily seen that this resonance would allow the assembly to pivot about the rotation axis, resulting in an acceleration of the PCB accelerometer. The rotated configuration is represented by dashed lines in Figure 3-4. This acceleration would be sensed by the controller electronics and

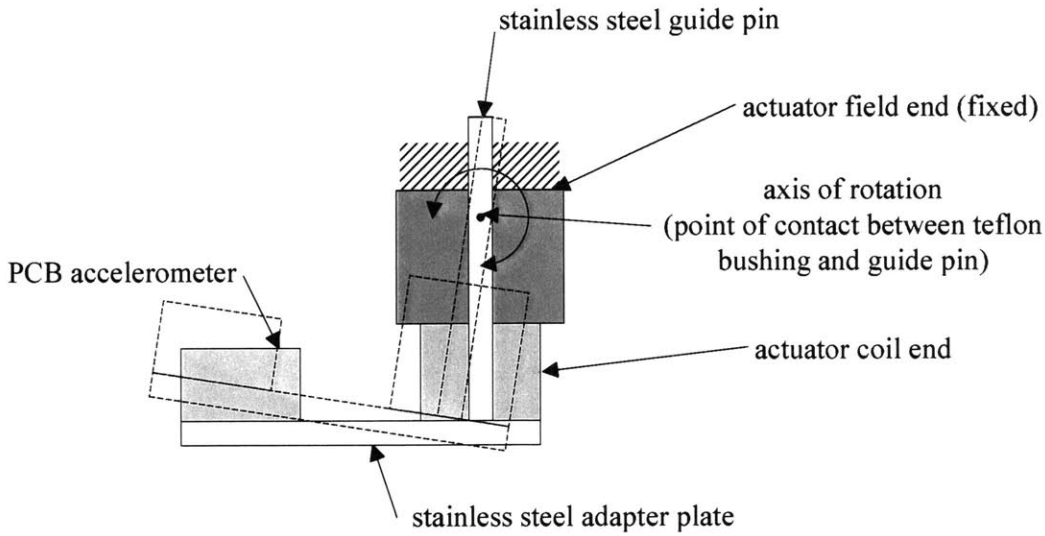


Figure 3-4: Schematic of unmodeled dynamic that lead to structural resonance.

produce a force from the actuator. The result was gross instability in the acceleration feedback loop as the accelerometers sensed erroneous accelerations and provided unnecessary correcting forces through the actuators.

To remedy this resonance problem, additional guide pins and ABS plastic guide blocks were added to the system. Figure 3-5 shows a schematic of these additional parts, while Figure 3-6 shows a photograph of the additional parts. The additional guide pin screwed through the PCB accelerometer, and into the stainless steel adapter plate. The ABS plastic guide block screwed to the top of the actuator field end, and had holes for the existing guide pin and the newly added guide pin that screwed through the accelerometer. The result of this fix was a much stiffer system than before, for two reasons. The first reason is that the existing guide pin passed through the Teflon bushing and the ABS guide block, which helped stabilize rotations of the adapter plate. The second reason is that the "new" guide pin slid into the guide block, and restrained the system from rotating. A rotation about the former axis of rotation would lead to a lateral force at the interface between the new guide pin and the guide block, to which the coupling of the new guide pin and guide block would be rigid.

The fix for the structural resonance produced mixed results. On the one hand, the accelerometer feedback loop gain was able to be nearly tripled as a result of this fix. Chapter 4 will detail the gain levels achieved, but it should be mentioned here that this controller gain increase was imperative to good system performance. On the other hand, the interface between the guide pins and the guide block proved to have too much friction for good system performance. ABS was used rather than

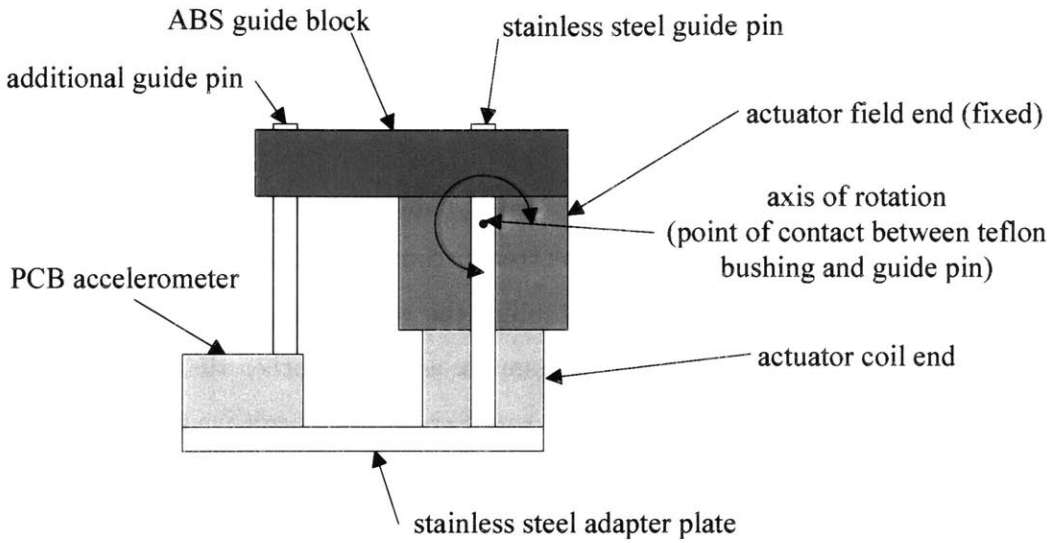


Figure 3-5: Schematic of parts added to eliminate structural resonance.

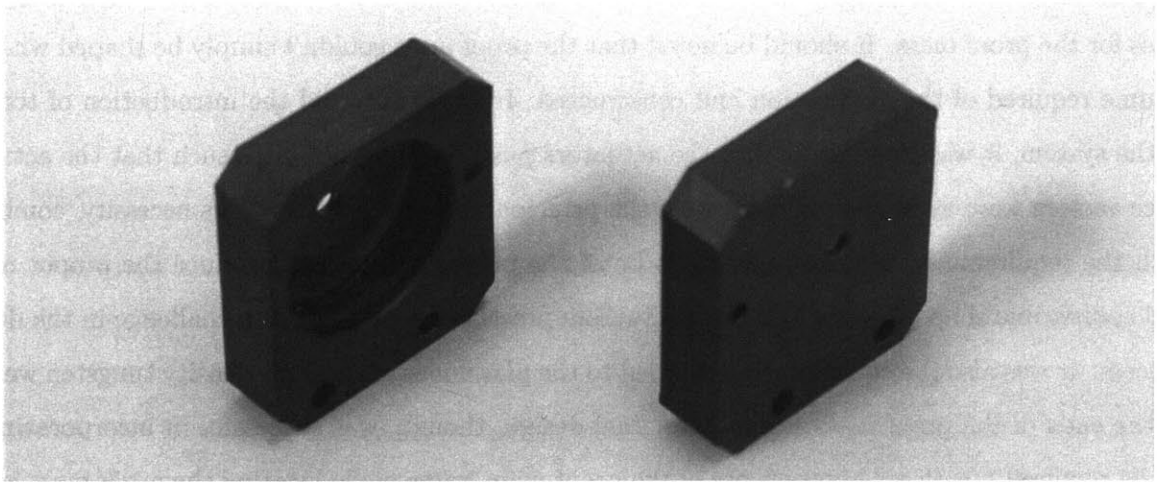

Figure 3-6: Photograph of parts added to eliminate structural resonance.

Teflon because ABS is able to be machined to much higher tolerances than Teflon. The tradeoff comes in the form of a higher coefficient of friction for ABS over Teflon. Chapter 5 will detail how this additional friction was dealt with.

## 3.4 Proof Mass Structure

The final major mechanical component of the tremor controller was the proof mass. This part served as one of the most important pieces of the tremor controller. The proof mass was the inertia against which the actuators exerted force to stabilize the wrist. The proof mass was also a very interesting part due to the fact that it was a complex assembly rather than a single part. The proof mass was composed of an aluminum frame, tungsten weights, both the field and coil portions of the actuators, adapter plates, Teflon inserts, the cores and extension rods of the LVDTs, the accelerometers, and part of the Del-Tron ball slides. It was this composite nature of the proof mass—the fact that it contained so many parts that were part of the prototype—that contributed to the excellent overall efficiency of the design in allocating moving versus non-moving mass.

The proof mass frame was machined from aluminum and shaped to encompass the wrist. This design allowed both actuators to easily attach to the proof mass, and allowed the design to be "tweaked" so that the inertial properties of the proof mass were acceptable. The ends of the proof mass frame served as attachment points for tungsten weights that were added to boost the inertia of the proof mass. These weights could be easily changed, or removed entirely, to arrive at the optimal mass for the proof mass. It should be noted that the proof mass couldn't simply be shaped with the volume required of the application and constructed. In order to avoid the introduction of torques to the system, it was imperative that the actuators push on the proof mass such that the actuator force vectors were as nearly collinear with the principal axes as possible. This necessity, combined with the requirement that the proof mass be of the proper volume (to produce the proper mass) and compatible shape to attach to both actuators presented something of a challenge in the design process. It was also the consideration that led to the placement of the high-density tungsten weights at the ends of the proof mass frame. The final design, though, was successful in incorporating all of the required functional components of the proof mass frame while locating the proof mass center of mass within 0.125 inches from the axes of actuation of the actuators. Placing the proof mass center of mass in this location also meant that the actuators could act on the proof mass while the forces would act through both the center of mass of the proof mass and the center of the wrist of

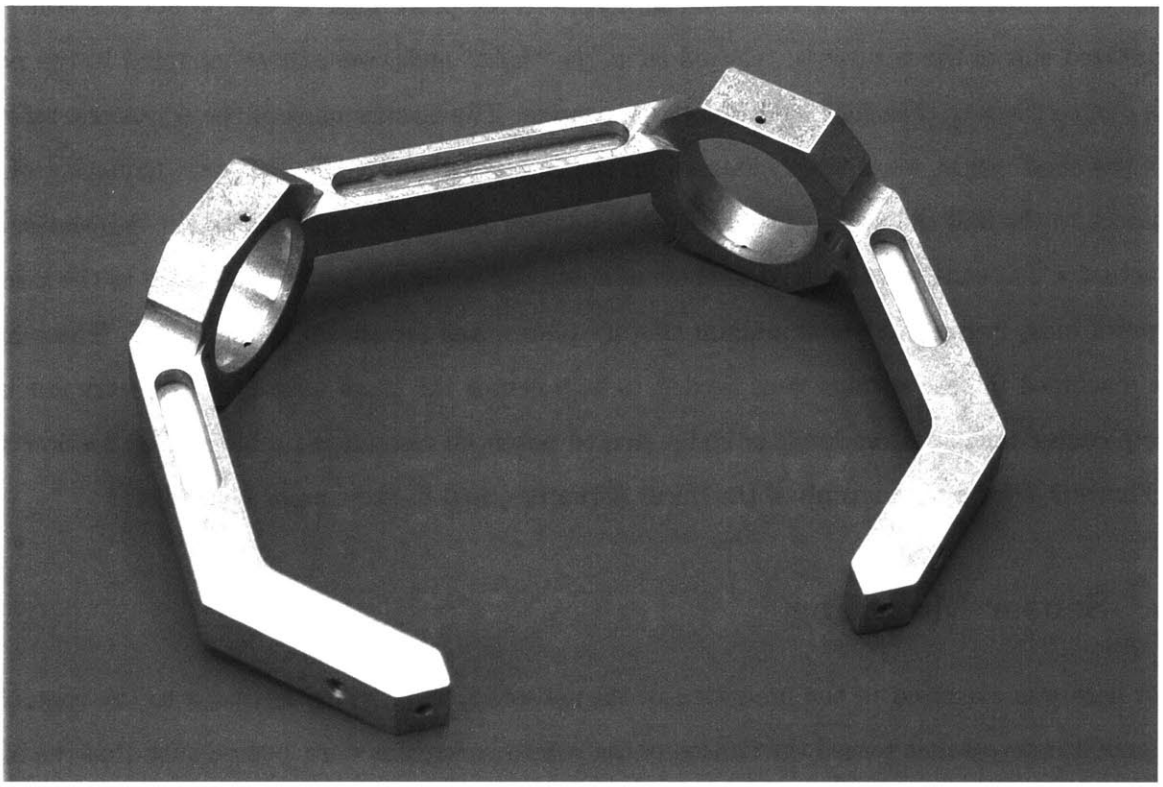

Figure 3-7: Photograph of the proof mass frame.

the individual wearing the device. Having the force pass through the center of mass of the proof mass meant that the correcting forces would not impart torques to the system. This could happen if a large enough moment arm were present between the axis of force actuation and the center of the proof mass. Similarly, ensuring that the axes of force application acted through the center of mass of the wrist kept the system from transmitting torques to the wrist rather than correcting forces. See Figure 3-7 for a photograph of the proof mass frame.

In addition, threaded holes were machined in the ends of the proof mass frame in the event that resonance problems were found in the "tuning fork" shape resulting in the design process[3]. The C-shaped proof mass frame, with the heavy tungsten weights mounted on each end, could have easily resonated in the 4–12 Hertz range the tremor apparatus was supposed to function within. The availability of extra mounting holes meant that a strap or bar could be added to stiffen the structure, thereby changing its natural frequency.

Actuators were mounted in the proof mass structure, as alluded to previously in this section.

[3]I would like to extend a special thanks to Mitchell Hansberry for this suggestion.

Epoxy was utilized in order to secure the actuators to the proof mass at the proper position. The magnetized end of the actuators, referred to as the "field" ends, were those mounted to the proof mass due to the fact that they were the most massive. The electric ends of the actuators, referred to as the "coil" ends, were those mounted on the linear ball slides. To facilitate mounting of the actuators to the ball slides, small stainless steel adapter plates were screwed to the ball slides, and the actuator coil ends were screwed to these adapter plates. Small holes were drilled in the sides of the proof mass frame and the aluminum adapter plates, and are shown in Figure 3-7. These holes were machined in case springs were needed to help center the proof mass. Springs were not used to help center the actuators longitudinally, due to potential resonance problems (see Section 3.5). See Figure 2-7 for a photograph of the linear actuators used in the tremor controller.

## 3.5 Sensor Mounting

Great care was exercised in the mounting of the sensors that provided feedback to the controller. The accelerometers that sensed the motion of the wrist in each axis were located such that the input axis of each accelerometer was parallel with the force axis of the corresponding actuator. The wide, flat guards molded integrally with the wrist/actuator mount were used as mounting surfaces for the accclerometers. Mounting the accelerometers in this position allowed the elimination of any offset between the input axis of the accelerometer and the output axis of the actuators. The sensitivity of the accelerometers to torques imparted by the actuators, or other external influences, was limited by this approach.

As mentioned in Section 3.1, the design of the tremor controller also had to have provision for longitudinal centering of the actuators. This necessity was driven by the fact that the actuators could not be allowed to rest at one end or the other of their travel and then be expected to successfully move in an approximate sine wave shape. If the actuators were to rest against one of their stops, and then be required to move further in the same direction (against the stop), the stabilization would be completely ineffective. Centering the actuators would allow them to start motion from the middle of their range of motion, and successfully move in a sinusoidal fashion. The most straightforward way to accomplish this centering would have been the addition of springs between the proof mass structure and the wrist mount, as alluded to in Section 3.4. The addition of springs would have created a problem because springs of the appropriate stiffness would have created a resonant system. Sizing springs such that the stiffness of the springs would have maintained the

proof mass position to within ±0.10 inches of center would have resulted in a spring-mass system whose resonant frequency, according to Equation 2.5, would have been in the 4–12 Hertz range of interest of the tremor suppression device. Therefore, tremors of the proper resonant frequency could have excited resonant oscillations between the wrist mount and proof mass structure.

Perhaps the next most straightforward way to accomplish centering was to add a position control loop for the actuator position. LVDTs were a logical choice for the sensors of this control loop due to their relatively small size, completely electrical operation, and low mass. Lucas-Schaevitz[4] Model 250–MHR LVDTs were procured for use in this capacity. The 250–MHR LVDTs provided precise measurement of a ±0.25 inch range, which was perfect for this application. In addition, Lucas-Schaevitz model LVM–110 signal conditioning modules were procured for use with the 250–MHR LVDTs. The LVM–110 modules accepted ±15 Volts of external power and provided the 10 kilohertz excitation frequencies required for proper operation of the 250–MHR LVDTs. These modules also performed the necessary signal conditioning to return the high frequency signals returned from the 250–MHR's to direct current (DC) signals easily integrated into control electronics.

Mounting of the LVDT sensors was another design issue to be considered. The LVDTs were mounted by attaching the coils of the LVDTs to the wrist/actuator mount while the movable cores of the LVDTs were mounted to the stainless steel adapter plate of the opposing axis. See Figure 3-8 for a photograph of the LVDTs, an LVDT core, and an LVDT mount. The LVDT mounts were machined from ABS plastic, and Heli-Coil inserts were added to the mounts so that they could be screwed to the wrist mount. A thin extension rod was threaded into the stainless steel adapter plates located between the ball slides and actuators, and the LVDT core so that the core was in the proper location for position sensing. This resulted in the LVDT being able to measure the distance between the wrist mount and the aluminum adapter plates, which was an indication of the position of one actuator half with respect to the other. See Figures 3-9 through 3-12 for photographs of the LVDTs mounted in the completed assembly.

## 3.6 Resultant Prototype Characteristics

The resulting system, when designed and assembled, had a mass of approximately 0.640 kilograms, or a weight of approximately 1.41 pounds. Largely through the use of clever design strategies, such as incorporating the actuators into the proof mass, the tremor suppression device was greater

[4]1000 Lucas Way, Hampton, VA 23666. 757-766-1500

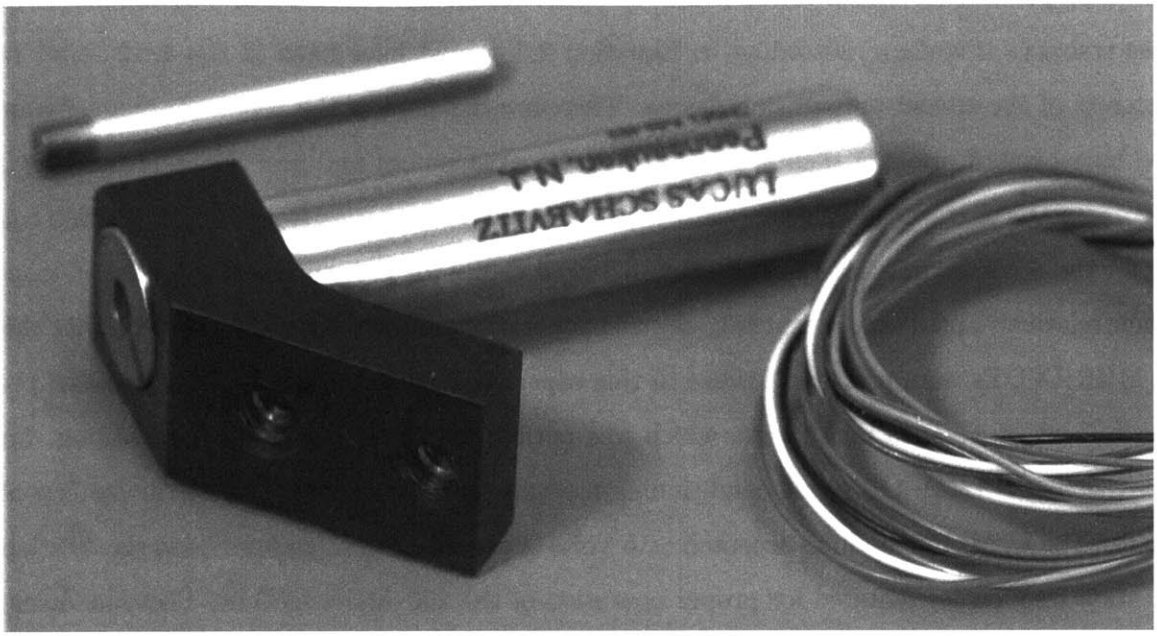


Figure 3-8: Photograph of a Schaevitz 250–MHR LVDT sensor inserted into an ABS mounts with core in the background.

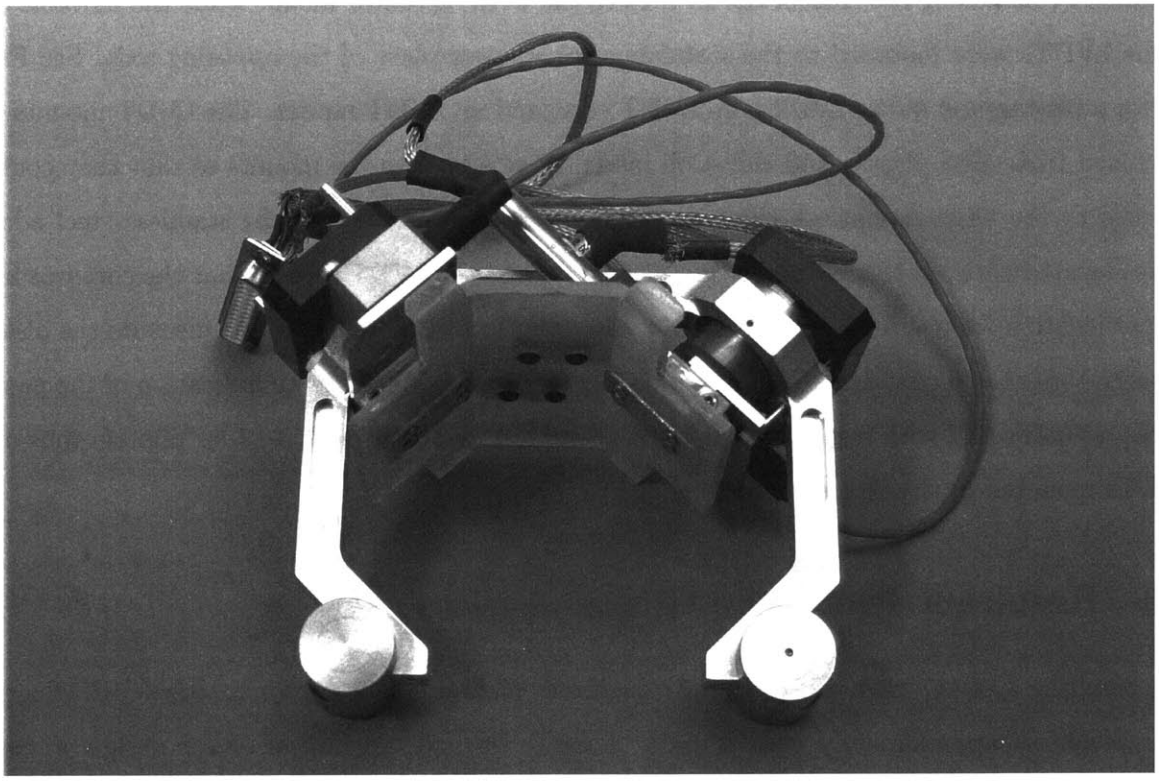

Figure 3-9: Photograph of completed assembly, front view.

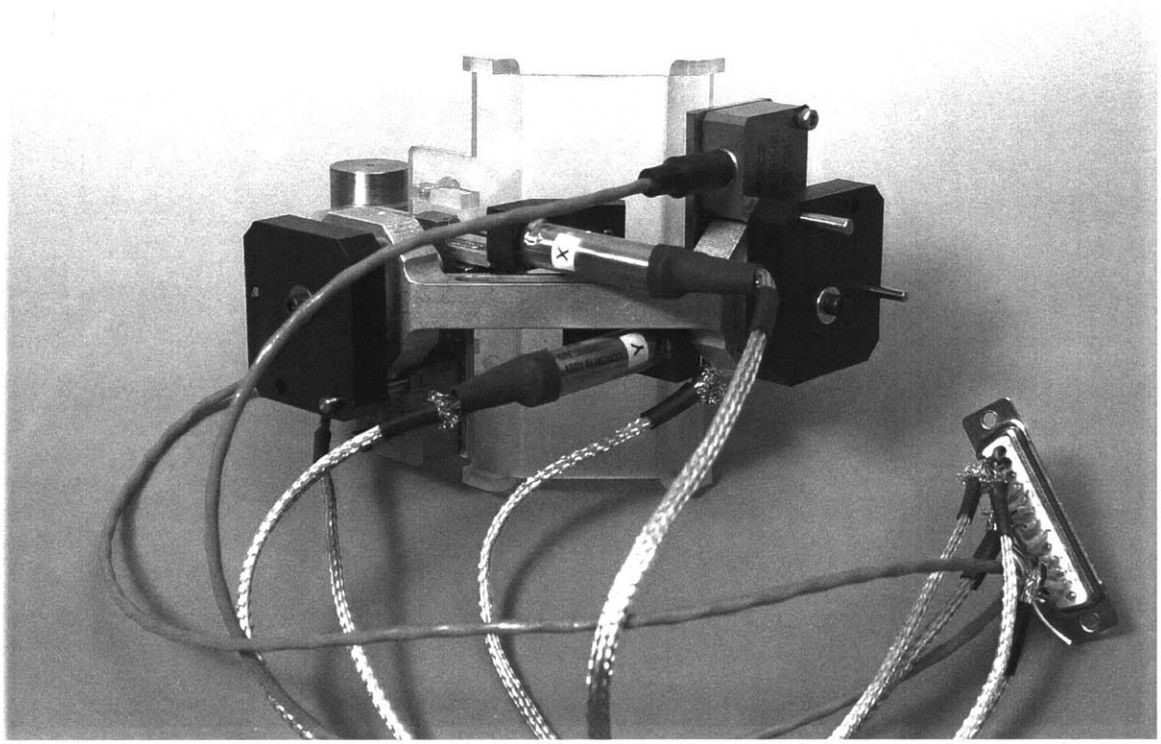

Figure 3-10: Photograph of completed assembly, top view.

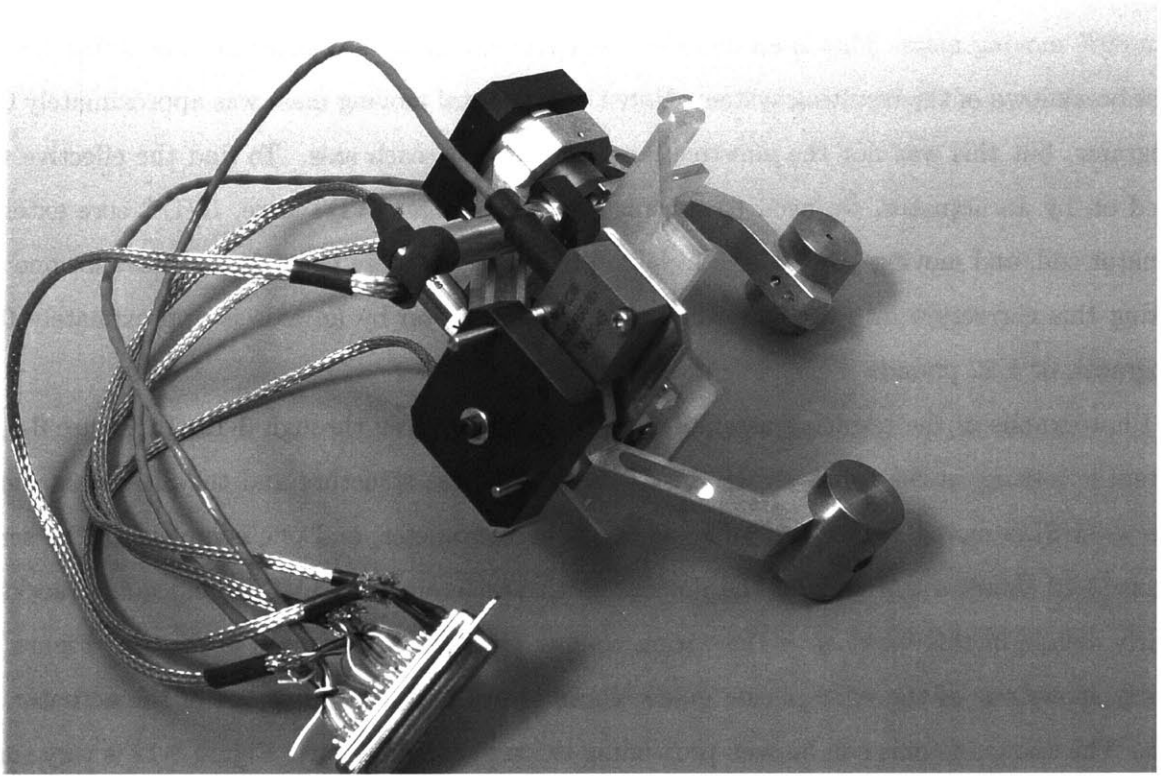

Figure 3-11: Photograph of completed assembly, left view.

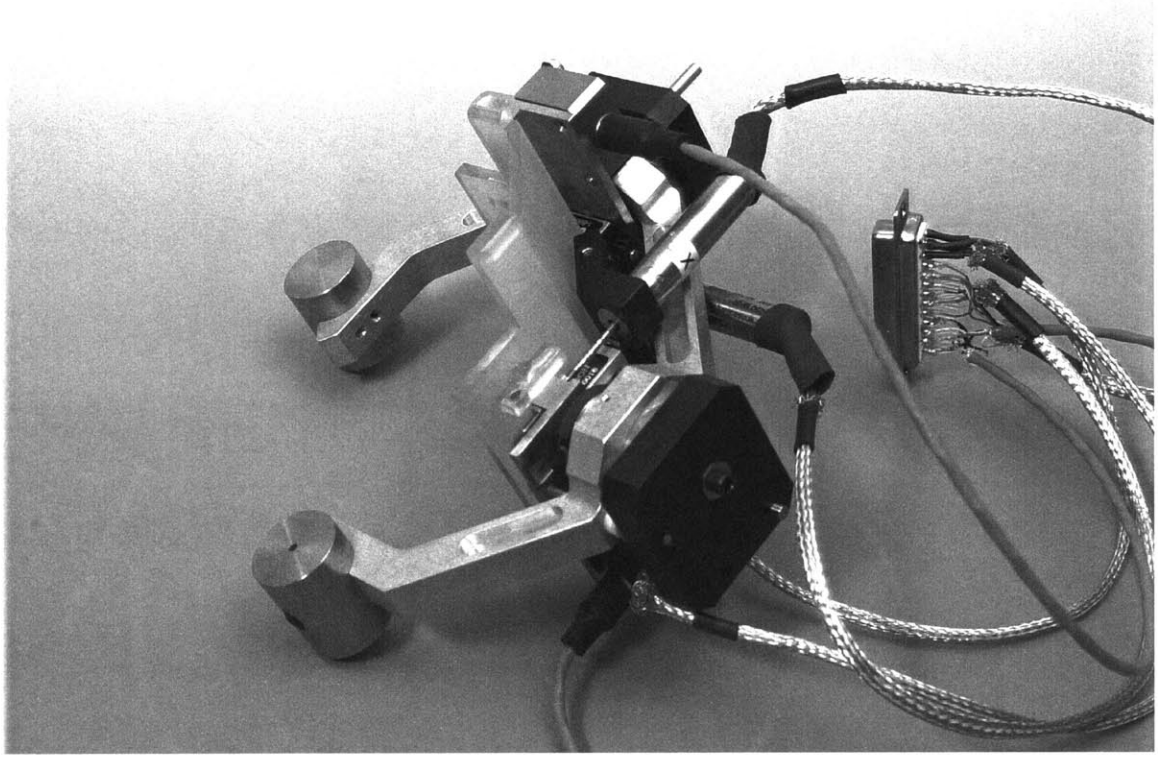

Figure 3-12: Photograph of completed assembly, right view.

than 89% moving mass! This is an incredibly efficient design by any measure. See Table 3.1 for a mass breakdown of the resulting system. Note that the total moving mass was approximately 0.572 kilograms, but this was not the effective mass acted on by each axis. To find the effective mass acted on by an actuator, we need to subtract the mass of an LVDT core, LVDT core extender, actuator coil, and moving portion of a Del-Tron ball slide, as these parts do not move for one axis. Taking this correction into account, the proof mass acted on by an axis is approximately 0.553 kilograms, or 1.22 pounds

Photographs of the resulting assembly appear in Figures 3-9 through 3-12. In Figure 3-9, the system is resting on the tungsten weights of the proof mass structure and the SLA wrist mount. The wrist SLA mount is clearly visible, as is one accelerometer, and one complete LVDT sensor. Figure 3-10 shows a top view of the device. Both accelerometers, LVDTs and guide blocks are clearly visible in this view, as is the wiring coming from the sensors and actuators. Figure 3-11 clearly shows one of the ABS plastic guide blocks screwed to the top of one of the actuator field ends. The two guide pins can be seen protruding through the ABS part. Figure 3-12 is very similar to Figure 3-11, except that the actuator is in its full up position in Figure 3-11, while the other

| Component | Mass [g] | Quantity | Total Component Mass [g] | % Total Mass |
|---|---|---|---|---|
| Tungsten Weight | 117.5 | 2 | 235 | 36.7 |
| Actuator Core | 55 | 2 | 110 | 170.2 |
| Proof Mass Frame | 66 | 1 | 66 | 10.3 |
| Adapter Plates with Guides | 29.5 | 2 | 59 | 9.22 |
| PCB accelerometers | 15 | 2 | 30 | 4.69 |
| Actuator Field | 14 | 2 | 28 | 4.38 |
| ABS Guide Blocks | 10 | 2 | 20 | 3.13 |
| New Guide Pins | 5 | 2 | 10 | 1.56 |
| Ball Slide (moving part) | 3 | 2 | 6 | 0.938 |
| Screws for Tungsten | 1.5 | 2 | 3 | 0.469 |
| LVDT core | 1 | 2 | 2 | 0.313 |
| LVDT core extensions | 1 | 2 | 2 | 0.313 |
| Teflon Bushing | 0.5 | 2 | 1 | 0.156 |
| **Total Moving Mass** | – | **25** | **572** | **89.4** |
| Wrist SLA mount | 30 | 1 | 30 | 4.69 |
| LVDT Field | 11 | 2 | 22 | 3.44 |
| Ball Slide (stationary part) | 5.5 | 2 | 11 | 1.72 |
| LVDT mount | 2.5 | 2 | 5 | 0.781 |
| **Total Stationary Mass** | – | **7** | **68** | **10.6** |

Table 3.1: Mass breakdown of parts of the tremor controller assembly.

actuator is in the full down position in Figure 3-12. This can be determined by the length of the guide pins extending above the ABS guide block.

Notice the very compact design of the completed structure. The wrist is inserted under the SLA mount, and the aluminum proof mass frame encircles the wrist and forearm. Also notice the wiring and shielding emanating from the device. Unfortunately, the servo amplifier used to drive the voice coil actuators was a pulse width modulated (PWM) unit that utilized a 33 kilohertz switching frequency. Since the LVDTs used relatively low-level 10 kilohertz excitation and return signals, copious amounts of shielding were added to the LVDT wires to eliminate erroneous readings from the actuators. More details regarding the electrical configuration of the device will be presented in Chapter 4. In addition, it seems worthwhile to examine the costs of the device. A table of the parts used in the construction of the prototype appears as Table 3.2.

| Component | Quantity | Unit Cost [US$] | Component Cost [US$] |
|---|---|---|---|
| DMC–2040 controller | 1 | 2995 | 2995 |
| PCB 3701 accelerometer | 2 | 670 | 1340 |
| MSA–12–80 amplifier | 2 | 325 | 650 |
| BEI LA10–12–027A actuator | 2 | 300 | 600 |
| HP 3630A Power Supply | 1 | 525 | 525 |
| LVM–110 LVDT signal conditioner | 2 | 250 | 500 |
| 250–MHR LVDT | 2 | 250 | 500 |
| ICM–2900 breakout box | 1 | 295 | 295 |
| PCS–12–24 power supply | 1 | 250 | 250 |
| Pelican Case 1620 | 1 | 200 | 200 |
| WSDK Servo Software | 1 | 195 | 195 |
| Analog Devices ADXL105 | 2 | 80 | 160 |
| 4 meter, 100 pin cable | 1 | 150 | 150 |
| Del-Tron D–1 Ball Slides | 2 | 55 | 110 |
| **Total** | – | – | **8470** |

Table 3.2: Cost breakdown of parts of the tremor controller prototype.

# Chapter 4

# Control System Design

## 4.1 Overview

Design of the tremor reducing control system was the foundation of this thesis. Using analysis guidelines developed in Sections 2.3 and 2.4, a linear time invariant (LTI) control system was developed and modeled to reduce tremor of the wrist.

As alluded to in Section 3.5, it was necessary to include four independent control loops; two loops for each of the two axes. One of the loops operated using an LVDT and a PID controller to maintain the position of the proof mass around an approximately centered location. The other control loop aimed to move the proof mass in response to accelerations of the wrist, in order to null tremors. One can already see a potential conflict here, in that the LVDT loops were attempting to move the proof mass to the centered location, while the accelerometer loops were attempting the move the proof mass *away* from center to nullify tremors. A scheme involving tuning the bandwidths of each of the loops was devised in order to eliminate "fighting" of the two individual loops, and is detailed in the sections that follow.

Section 4.2 describes the model used in the controller tuning, which was performed in Section 4.5. Section 4.3 details the configuration of the controller electronics.

## 4.2 Lumped-Parameter Model

An accurate model of the mechanism creating tremor and the mechanism to control tremor was developed in order to facilitate control systems modeling and tuning. This section begins by expanding the model presented in Section 2.4 to include tremor creation via resonant spring-mass

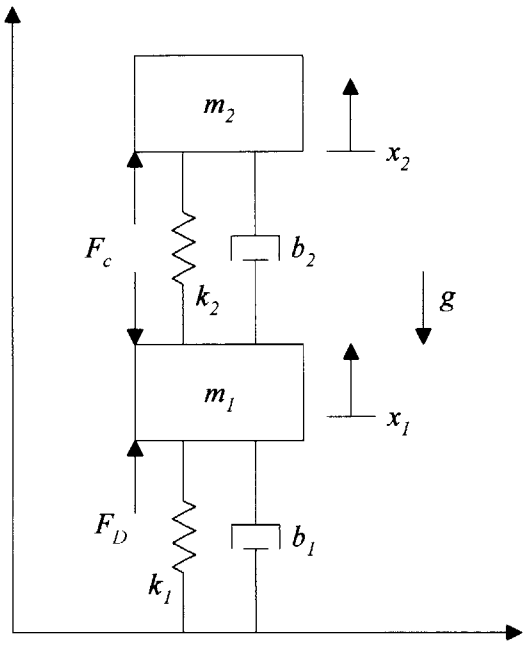


Figure 4-1: Lumped parameter model of the resonant system.

vibrations, and also a quantifiable model for the orientation of the tremor reducing device in a gravity field.

The lumped parameter model constructed for modeling purposes began with the two-mass model of Section 2.4, and added additional passive elements to the assembly. A spring and damper were added between $m_1$ and $m_2$, as well as between $m_1$ and a datum. The system was also modeled to be "standing" upright in the gravity field, with the angle $\theta$ defined to be that between gravity and the axis of motion of the masses. Figure 4-1 shows a lumped parameter diagram of the new model. Note that $\theta = 0$ in the orientation shown in Figure 4-1, so gravity is acting down the page.

The kinetic coenergy of the system is the same as Equation 2.8, but the system potential energy has new terms. The potential energy of the system is now

$$V = m_1 g x_1 + m_2 g x_2 + \frac{1}{2} k_1 x_1^2 + \frac{1}{2} k_2 x_2^2, \tag{4.1}$$

in which the gravity terms are added and defined in terms of the angle of rotation $\theta$, and an additional spring term is added. Also note that Equation 2.7 is still valid in Equation 4.1. The system Lagrangian is the same as Equation 2.10, but the Lagrangian equations are slightly changed from Equations 2.11 and 2.12. The new Lagrangian equations include the additional damping terms

as part of the generalized forces,

$$\frac{d}{dt}\left(\frac{\partial L}{\partial \dot{x}_1}\right) - \frac{\partial L}{\partial x_1} = -F_c - b_1\dot{x}_1 + b_2\dot{x}, \tag{4.2}$$

$$\frac{d}{dt}\left(\frac{\partial L}{\partial \dot{x}_2}\right) - \frac{\partial L}{\partial x_2} = F_c - b_2\dot{x}. \tag{4.3}$$

The completed equations of motion of the system are

$$\begin{aligned} m_1\ddot{x}_1 + m_1 g + b_1\dot{x}_1 - b_2(\dot{x}_2 - \dot{x}_1) + k_1 x_1 - k_2(x_2 - x_1) &= -F_c \\ m_2\ddot{x}_2 + m_2 g + b_2(\dot{x}_2 - \dot{x}_1) + k_2(x_2 - x_1) &= F_c. \end{aligned} \tag{4.4}$$

A controller consisting of a PID control on the position of the proof mass and a proportional feedback of the wrist acceleration is used in this model to simulate the controllers that were actually used in the prototype. The control law used in the simulation was

$$F_c = -K_{LP}\tilde{x} - K_{LD}\dot{\tilde{x}} - K_{LI}\int \tilde{x} - K_{AP}\ddot{x}_1. \tag{4.5}$$

In Equation 4.5, the $\tilde{x}$ terms refer to the *error* of the respective parameter. In other words,

$$\tilde{x} = \hat{x} - x, \tag{4.6}$$

in which $\hat{x}$ is the desired value of the parameter. Since the above controller consists of a PID controller for the LVDT and a proportional feedback for the accelerometer, the controller was dubbed a PIDP controller. Analyses performed in Appendix B determined that the PIDP controller was likely the best controller to use.

## 4.3 Control Electronics Layout

Development of the actual electronic hardware to provide feedback control to the tremor controller was one of the most enjoyable parts of this thesis. A digital motion controller and accessories were procured from Galil Motion Controls, Inc.[1] in order to save time and effort building custom electronics for this project. A Galil model DMC–2040 universal serial bus (USB) stand-alone controller was procured for this thesis, as well as a Galil ICM–2900 interconnect module, two Galil

[1] 3750 Atherton Road, Rocklin, CA 95765

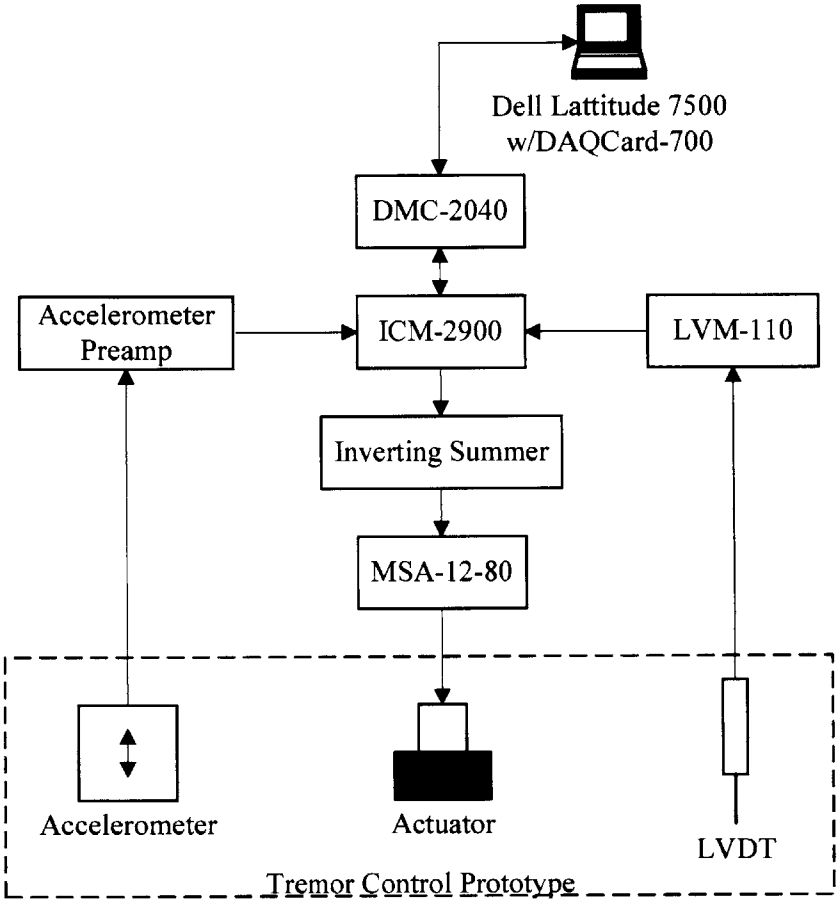


Figure 4-2: Block diagram of the control system electronics, without power supplies.

MSA–12–80 brush-type servo amplifiers, and a Galil CPS–12–24 power supply. The DMC–2040 contained a 32-bit microprocessor, digital signal processing (DSP) chips, and analog to digital (A/D) and digital to analog (D/A) converters. This unit was configured by Galil to act as a "PID in a box," which a user could easily configure by simply setting the individual gains within the unit for his/her particular plant. The DMC–2040 connected via a 100-pin cable to the ICM–2900 interconnect module. The ICM–2900 was basically a breakout box, which enabled the user to make connections to the DMC–2040 using plugs into which wires could be easily attached. Also, the ICM–2900 had custom labeling that allowed the user to easily identify what each of the 100 terminals connected to within the DMC–2040. See Figure 4-2 for a functional diagram of the layout of the controller electronics. See Table 4.1 for a record of the connections made to the ICM–2900.

The DMC–2040 is a 4-axis unit, meaning that it has provision to control four individual axes of motion. This configuration was ideal for this thesis due to the fact that the tremor controller consisted of 4 control loops—two axes, each having a position and acceleration control loop. The

| Connector Pin # | Connection To |
|---|---|
| 1 | Positive x actuator terminal |
| 2 | Positive y actuator terminal |
| 3 | Not connected |
| 4 | Brown x LVDT wire |
| 5 | Yellow x LVDT wire |
| 6 | Black x LVDT wire |
| 7 | Brown y LVDT wire |
| 8 | Yellow y LVDT wire |
| 9 | Not connected |
| 10 | x accelerometer ground |
| 11 | x accelerometer +5 Volts power |
| 12 | y accelerometer signal |
| 13 | Not connected |
| 14 | Negative x actuator terminal |
| 15 | Negative y actuator terminal |
| 16 | Not connected |
| 17 | Green/Blue x LVDT wires |
| 18 | Red x LVDT wire |
| 19 | Black y LVDT wire |
| 20 | Green/Blue y LVDT wires |
| 21 | Red y LVDT wires |
| 22 | Not connected |
| 23 | x accelerometer signal |
| 24 | y accelerometer +5 Volts power |
| 25 | y accelerometer ground |

Table 4.1: Pin assignments on the 25-pin tremor controller connector.

| Signal | Connection To | ICM–2900 Terminal Label |
|---|---|---|
| x axis accelerometer | x axis analog input | ANALOG1 |
| y axis accelerometer | y axis analog input | ANALOG2 |
| x axis LVDT | z axis analog input | ANALOG3 |
| y axis LVDT | w axis analog input | ANALOG4 |
| signal grounds | analog input grounds | ANAGND |
| x accel motor command | x axis motor command | MOCMDX |
| y accel motor command | y axis motor command | MOCMDY |
| x LVDT motor command | z axis motor command | MOCMDZ |
| y LVDT motor command | w axis motor command | MOCMDW |
| x accel amplifier enable | x axis amplifier enable | AMPENX |
| y accel amplifier enable | y axis amplifier enable | AMPENY |
| x LVDT amplifier enable | z axis amplifier enable | AMPENZ |
| y LVDT amplifier enable | w axis amplifier enable | AMPENW |

Table 4.2: Connections to ICM–2900 interconnect module.

DMC–2040 was very easily configured to act in an analog feedback mode, which accepted $\pm 10$ Volt signals from devices such as LVDTs and accelerometers, and the control loops used a user-defined analog feedback value as their desired value. For example, for an LVDT reading $\pm 10$ Volts full-scale, the user could instruct the DMC–2040 to maintain the LVDT output at 0 Volts, which would be centered. The DMC–2040 was then able to provide feedback at 1 kilohertz bandwidth.

The DMC–2040 was also very attractive due to the fact that it provided advanced options for control loop implementation. The software contained within the DMC–2040 easily allowed the user to configure low-pass filters, notch filters, feed forward control, and many other options. The default mode of operation of the DMC–2040 was such that the control loop bandwidth was 1 kilohertz. However, the controller could be programmed to operate in a "fast firmware" mode that would operate at 2 kilohertz bandwidth. Similarly, the controller could be operated at a slower bandwidth, which allowed the microprocessor to perform data collection and simple mathematical operations with the previously-occupied CPU time. The flexibility of the DMC–2040 made the construction of the control loop much more straightforward and allowed the construction of a much more capable control loop than would have normally been undertaken. Gain values were easily changed numerically in the DMC–2040, using just a couple of keystrokes to enter new gain values. See Section 4.5 for details of the process of determining and changing the DMC–2040 gains.

The DMC–2040 accepted analog inputs, and provided control output in the form of $\pm 10$ Volt DC signals. These output signals were in turn fed into MSA–12–80 brush type servo amplifiers.

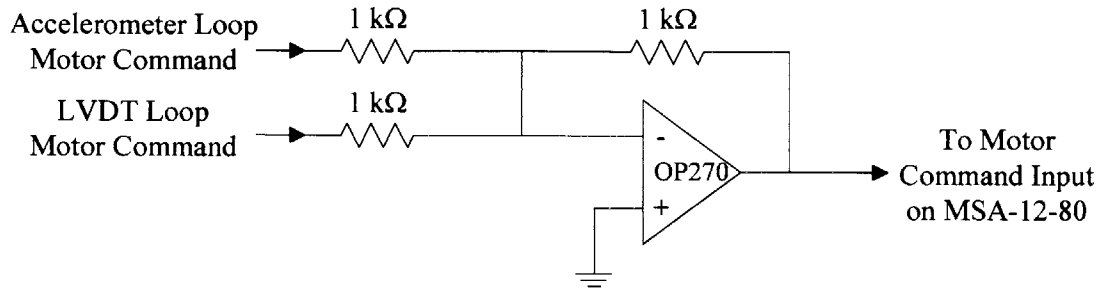


Figure 4-3: Inverting summer circuit schematic for the conversion to a MISO system.

The MSA–12–80 servo amplifiers provided a maximum of 12 Amps at 80 Volts continuous, and each actuator was powered by one of these servo amplifiers. As previously mentioned, these amplifiers were of a pulse width modulated type, and excited the actuators via a 33 kilohertz switching frequency. The MSA–12–80's were configured such that a full positive or negative 10 Volt input would provide a full positive or negative 24 Volt, high-amperage signal to the BEI actuators. The MSA–12–80 amplifiers obtained their power from the CPS–12–24 power supply. This power supply was capable of supplying 12 Amps continuous at 24 Volts, which was easily enough power to provide full force from the actuators. The actuators would conduct a current of approximately 2.4 Amperes when excited with 24 Volts, so the CPS–12–24 was easily able to fit full mode operation of the actuators within its operational range.

This system was also interesting in that the architecture of the control loops revealed that the system was a multiple input, single output (MISO) system. The DMC–2040 accepted a total of four input signals, from two LVDTs and two accelerometers, yet provided only two output signals, one to each of the two MSA–12–80's that were powering the actuators. The DMC–2040 did not allow the sensor inputs to be combined electronically, so the four outputs that were sent from the DMC–2040 were added using a simple analog summation circuit. An Analog Devices model OP270G dual, precision operational amplifier (op amp) was used to construct an inverting summer circuit. The inverting summer combined the LVDT and accelerometer control loop output of the DMC–2040, destined for each of two individual loops, into a single command for each loop. As such, the summation circuit was placed between the ICM–2900 interconnect module and the two MSA–12–80 servo amplifiers. This maintained the ease of operation of the DMC–2040 by allowing the users to individually tune each loop, and eliminated the need to build a circuit to add the power signals from what would have been four servo amplifiers. A schematic of the inverting summer appears in Figure 4-3.

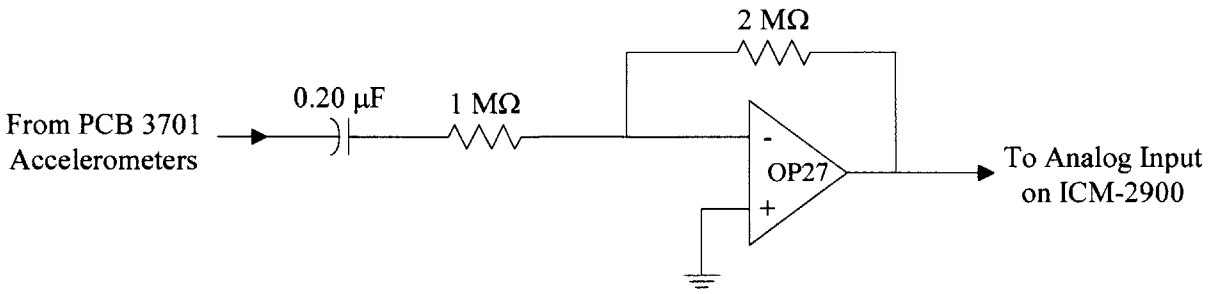


Figure 4-4: Preamplifier circuit schematic for the PCB 3701 accelerometers.

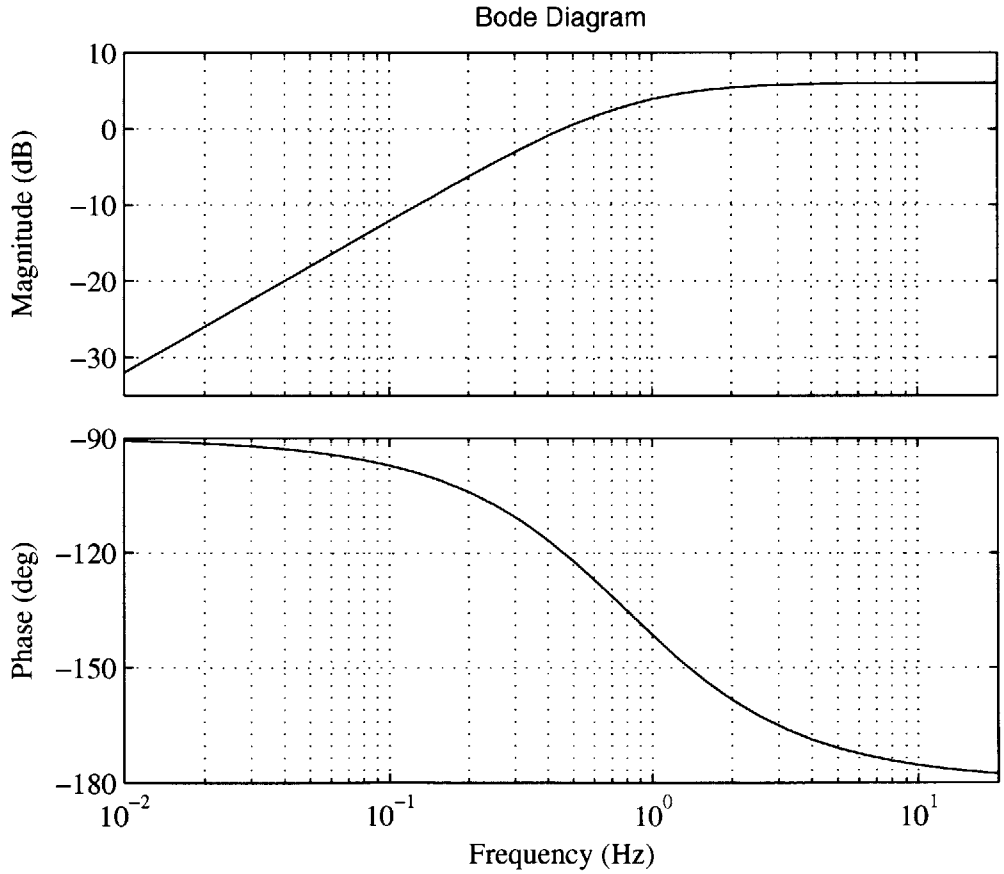


Figure 4-5: Bode plot of the response of the PCB 3701 accelerometer preamplifier circuits.

The LVDTs and accelerometers were powered by a Hewlett Packard model E3630A triple output power supply. The decision to power the sensors from a separate power supply was made in order to eliminate unnecessary loading on the DMC-2040, and also to ensure that as stable and "clean" a power supply as possible was available to the sensors.

As noted in Figure 4-2, a preamplifier stage was constructed for the accelerometer feedback loop. The presence of the preamplifier stage was meant to:

1. remove the DC component of the accelerometer output, as well as some low frequency signals from the accelerometer,

2. invert the signal from the accelerometers to provide the correct sign to the DMC–2040, and

3. amplify the signal by a factor of 2, to cause the accelerometer signals to span as much of the $\pm$ 10 Volt input range of the DMC–2040 as possible.

the DC component of the accelerometer output was blocked due to the fact that the device could easily be rotated in a gravity field. The rotation of the device with respect to gravity would lead to a bias in the accelerometer signal, that could potentially influence the operation of the control loops. The preamplifier circuit was therefore constructed with a high pass filter, which blocked DC and very low frequency signals.

A schematic of the accelerometer preamplifier circuit appears in Figure 4-4. A 0.20 $\mu$Farad capacitor, a 1 M$\Omega$ resistor, and a 2 M$\Omega$ resistor were used in the construction of this circuit. The overall preamplifier transfer function then became

$$\frac{V_f}{V_{in}} = \frac{-R_f}{R_{in} + \frac{1}{sC}}, \tag{4.7}$$

in which $V_f$ is the feedback voltage, $V_{in}$ is the input voltage, $R_f$ is the feedback resistance, $R_{in}$ is the input resistance, $C$ is the capacitance, and $s$ is the relation $s = \sigma + j\omega$. Equation 4.7 was rearranged such that it became

$$\frac{V_f}{V_{in}} = -\frac{R_f}{R_{in}} \frac{R_{in}Cs}{1 + R_{in}Cs}. \tag{4.8}$$

Substituting the proper values into Equation 4.8, the denominator becomes $1+0.20s$. If we examine the point at which the denominator is 0, we will be able to determine the frequency at which the circuit begins to allow signals to pass. If we substitute the generic relation $s = 2\pi f$, in which $f$ is the frequency, we find that the frequency above which signals will pass is approximately 0.8 Hertz.

This value is acceptable, as it is well above DC, but far enough below the lowest frequencies we expect to see that it will not block desired signals.

The interface between the human operator and the DMC–2040 was provided by a Dell Inspiron 7500 notebook computer running Microsoft Windows 2000. This computer was chosen due to the fact that experiments would require the movement of the entire test apparatus, and a notebook computer is most easily moved. Also, a National Instruments DAQ-Card 700 data acquisition card was already available for this computer, making the computer a wonderful, compact, high-performance control and data acquisition station.

## 4.4 Control Electronics Packaging

The bulky supporting electronics (power supplies, DMC–2040, ICM–2900, etc.) were bolted inside a model 1620 Pelican case. Doing this provided a wonderful structure to mount all of the hardware and wiring to, and also a means to quickly and easily move the entire experimental apparatus to a new location. All that passed from the Pelican case were three cables–one for data acquisition, one for communication between the Dell Inspiron and the DMC–2040, and one to carry signals to and from the wrist tremor prototype. See Figure 4-6 for a photograph of the equipment mounted inside of the Pelican 1620 case. The Dell Inspiron computer is visible on the top of the case, with the DMC–2040 mounted directly under the Inspiron, inside of the case. The wiring for the analog electronics and data acquisition electronics are visible on the inside of the door of the case (left side).

Figures 4-7 and 4-8 show close-up views of the Pelican 1620 case and door, respectively. The servo amplifiers and power supply are clearly visible behind the power strip in Figure 4-7, and the Hewlett Packard model E3630A DC power supply is mounted on the right side of the case. Figure 4-8 clearly shows the LVM–110 signal conditioning modules, accelerometer preamplifier and inverting summer circuits, ICM–2900, and data acquisition wiring.

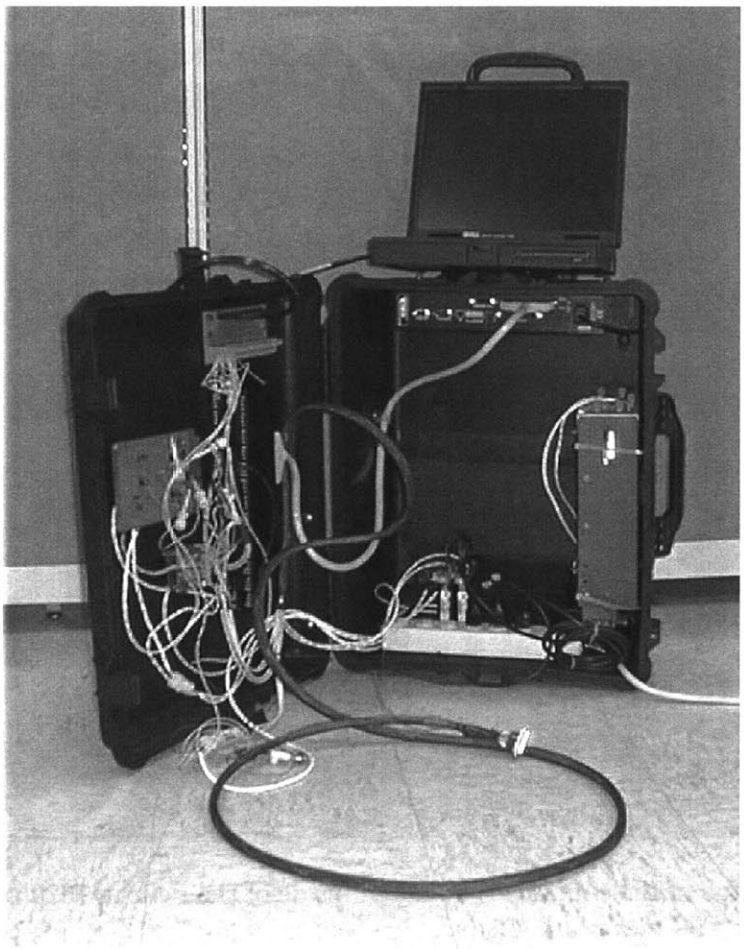

Figure 4-6: Photograph of the equipment mounted inside of the Pelican 1620 case.

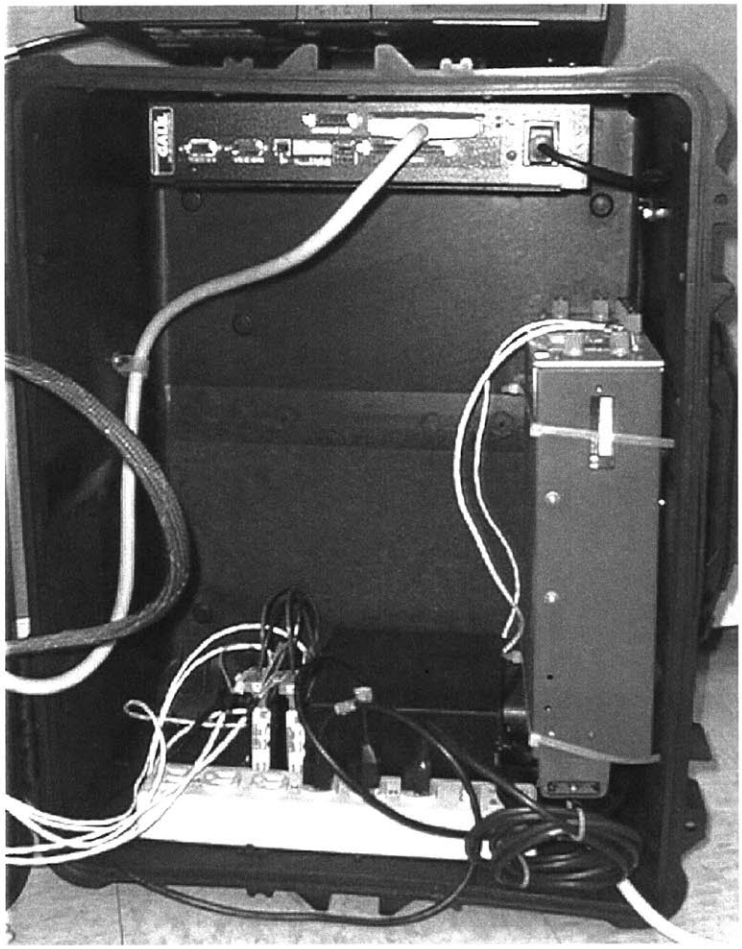

Figure 4-7: Photograph of the equipment mounted inside of the Pelican 1620 case, detailing DMC–2040, power supplies, and power amplifiers.

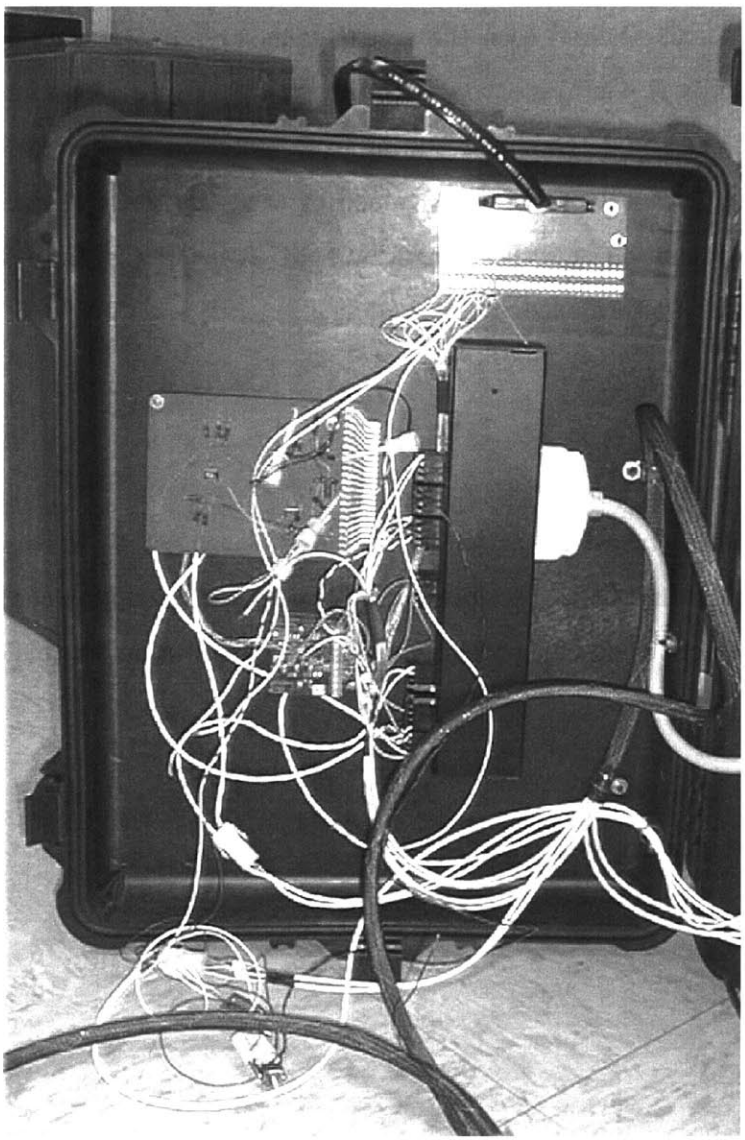

Figure 4-8: Photograph of the equipment mounted to the door of the Pelican 1620 case.

## 4.5 Control Loop Tuning

Control loop tuning was carried out experimentally by the author and Kenneth Kaiser at Draper Laboratory. Guidelines regarding what the gains should be were created using the analyses of Sections 4.2 and Appendix B, and then the actual gains were experimentally fine-tuned by the experimenters. Appendix B contains a very detailed, quantitative explanation of how the control system was modeled, and the derivations resulting in Equations 4.10 through 4.14.

Absolute controller gain values were determined by studying the influence of various physical parameters on the attenuation sensitivity function, $S_A$. Appendix B defines $S_A$ as the ratio of closed-loop to open-loop performance, or

$$\S_A \equiv \frac{\left.\frac{X_1}{D}\right|_{CL}}{\left.\frac{X_1}{D}\right|_{OL}}. \tag{4.9}$$

In Equation 4.9, $\frac{X_1}{D}$ is the transfer function of tremor displacement $X_1$ in response to disturbance dynamics $D$, and the $CL$ and $OL$ subscripts denote closed- and open-loop conditions, respectively. Carrying through the derivation of $S_A$ yields the complete expression for this equation, which is

$$S_A = \frac{1}{1+K_{AP}}\left[\frac{s^2+2\zeta_0\omega_0 s+\omega_0^2}{s^2+2\zeta_P\omega_P s+\omega_P^2}\right]. \tag{4.10}$$

In Equation 4.10, the parameters are defined as

$$\omega_0 = \sqrt{\frac{K_{LP}}{m_2}}, \tag{4.11}$$

$$\omega_P = \sqrt{\frac{K_{LP}\left(1+\frac{m_2}{m_1}\right)}{m_2\left(1+K_{AP}\right)}}, \tag{4.12}$$

$$2\zeta_0\omega_0 = \frac{K_{LD}}{m_2}, \tag{4.13}$$

and

$$2\zeta_P\omega_P = \frac{K_{LD}\left(1+\frac{m_2}{m_1}\right)}{m_2\left(1+K_{AP}\right)}. \tag{4.14}$$

This "shaping" of $S_A$ lead to the Bode plot displayed in Figure 4-9. The values of $\omega_0$, $\omega_P$, $\zeta_0$, and $\zeta_P$ were varied until a desirable Bode plot was obtained, and then the desired controller gains were computed from the above equations. The desired gains to achieve the performance displayed in

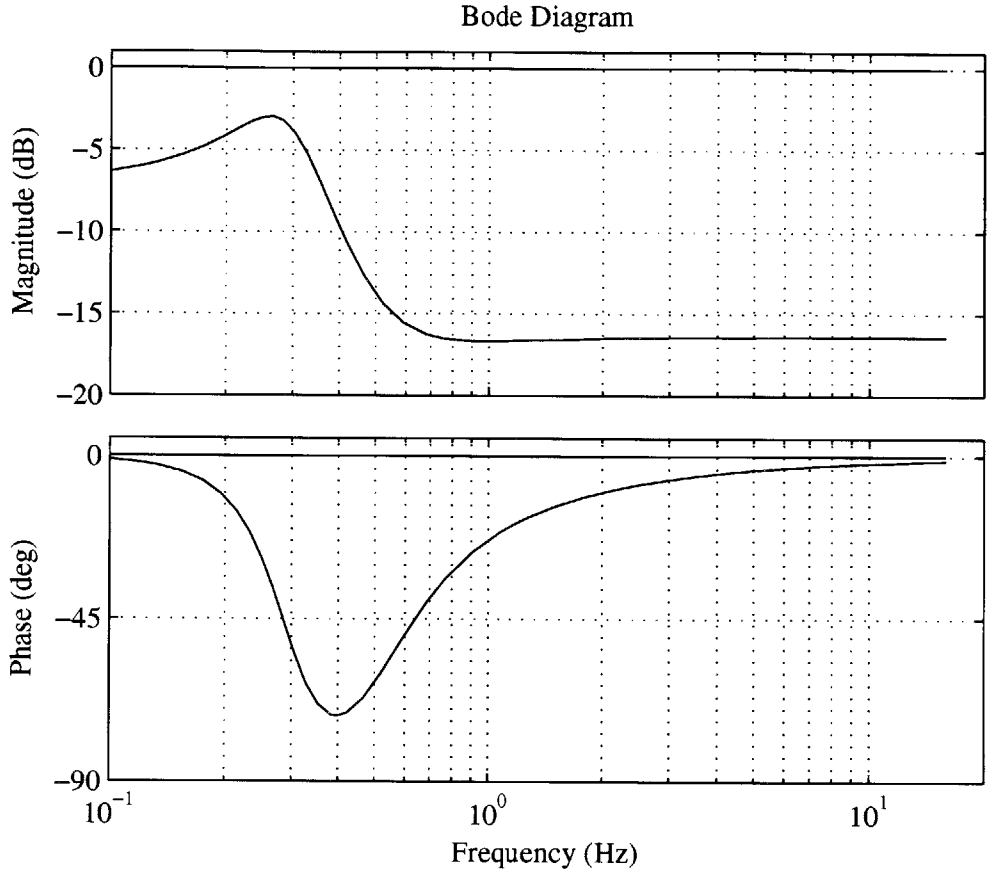


Figure 4-9: Bode plot of $S_A$ with PIDP controller.

Figure 4-9 were $K_{AP} = 12.5\left[\frac{\text{lb}}{\text{g}}\right]$, $K_{LP} = 2.04\left[\frac{\text{lb}}{\text{in}}\right]$, and $K_{LD} = 1.62 \times 10^{-3}\left[\frac{\text{lb·sec}}{\text{g}}\right]$. Obtaining these absolute controller gains was relatively straightforward. The PCB accelerometers had scale factors of 1 $\left[\frac{\text{Volt}}{\text{g}}\right]$, and acted through a 2:1 gain stage in the preamplifier circuit. The LVDTs output a full 20 Volt range over the 0.5 inch range of the Del-Tron ball slides, so their scale factors were 40 $\left[\frac{\text{Volt}}{\text{inch}}\right]$. Both the LVDT and accelerometer control loops acted through the Galil DMC–2040 controller, sending commands to the MSA–12–80 servo amplifiers. The 20 Volt input range of the MSA–12–80 amplifiers corresponded to 6 pound output ranges on the actuators, so the scale factor of the output of from the MSA–12–80 to the actuators was 0.3 $\left[\frac{\text{lb}}{\text{g}}\right]$. So, the scale factors for the signals before and after they entered the DMC–2040 were easily determined. What were not as easily determined were the absolute controller gains of the DMC–2040. Determination of these controller gains required some additional work, detailed in Subsections 4.5.1 and 4.5.2.

### 4.5.1 Determination of Absolute Controller Proportional Gain

One of the first activities to be carried out in determining the controller gains to use involved determination of the gain characteristics of the Galil DMC 2040. Due to the fact that the experimenters had access to all of the physical characteristics of the sensors and their associated signal conditioning electronics, as well as the actuators and servo amplifiers, it was possible to calculate a "physical" gain value that included units. The only gains left to be determined were those internal to the Galil DMC–2040. In other words, if the Galil unit received a certain voltage as an input, and a proportional gain was specified, what would the Galil unit provide as a command to the servo amplifier?

In order to answer this question, some simple tests were performed. The first series of tests were aimed at determining the value of a proportional gain of the Galil unit, which we will denote $K_{PG}$. The Galil DMC–2040 came with a software package known as the Galil Servo Developer Kit, or SDK. This software package provided functionality in the form of debugging tools and terminal programs to communicate more efficiently with Galil controllers. One module of the SDK, the storage scopes section, allowed the experimenter to record simple data sets for analysis in programs such as Microsoft Excel or Matlab.

The storage scopes were used to record data for conditions in which the conditions to which the sensors were subjected were known, and torque commands could be recorded. The storage scope sampling rates were recorded, as well as pertinent gain values to allow the internal Galil gains to be calculated. The storage scopes recorded raw data in the form of analog to digital (A/D) encoder counts for the sensor inputs, and voltage output values from -10 to +10 Volts for the motor commands. Unprocessed data from the Galil DMC–2040 are shown in Figure 4-10. Some things are notable about Figure 4-10.

First, the proportional relationship between the LVDT input and the motor command output is clearly visible in the plots of Figure 4-10. There is a sign difference between the two signals, which is intentional due to the fact that the LVDT motor commands are passed through the *inverting* summer circuit before being sent to the servo amplifier. Secondly, there is a bias in the output of the LVDT. The LVDT was centered by moving the Del-Tron ball slide to its centered position, and then moving the proof mass such that the ball slide moved to the end of its travel. This approach was chosen because it afforded the experimenters the opportunity to check the LVDT scale factor, since moving the ball slide through half of its range would correspond to a distance of 0.25 inches.

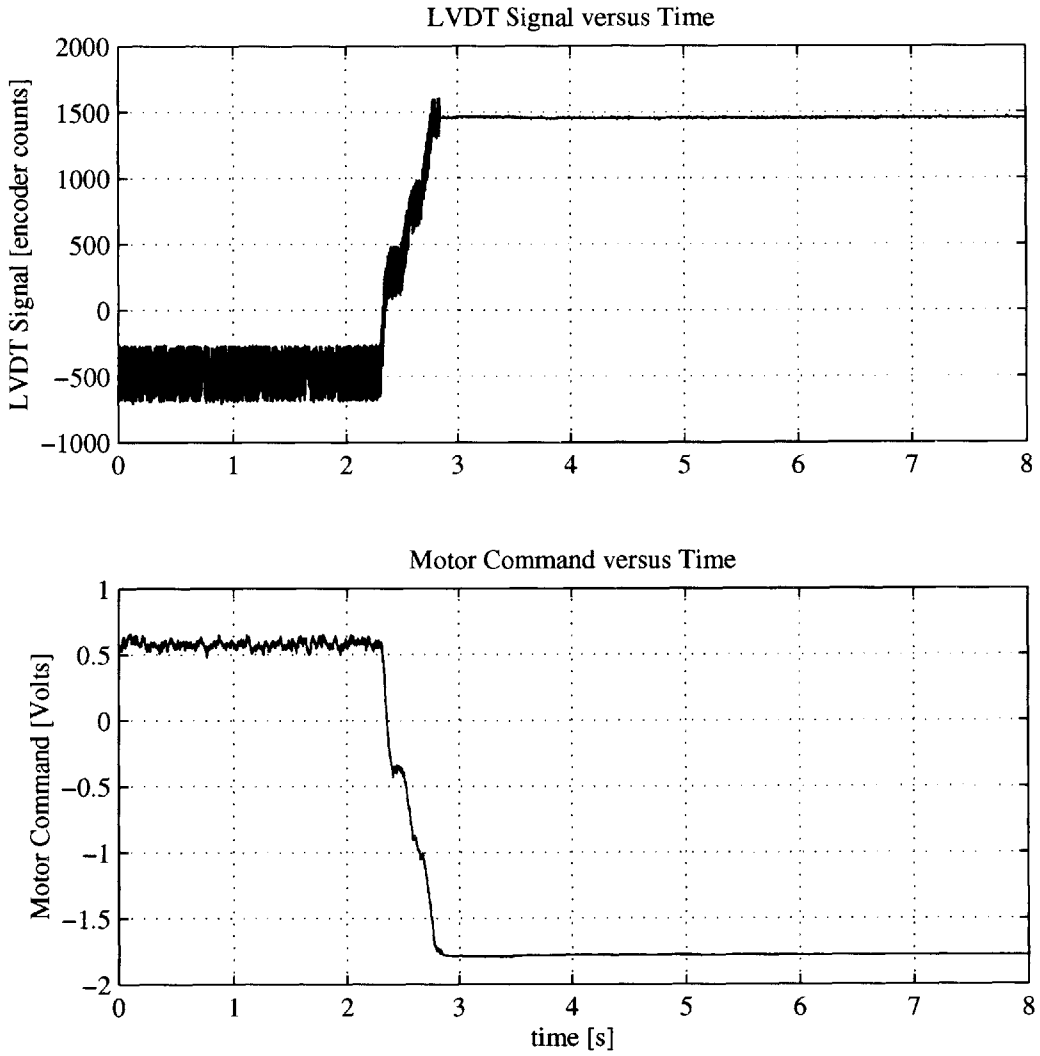


Figure 4-10: Unprocessed data output of the Galil DMC–2040.

The LVDT was in the centered position when the Galil DMC–2040 was reading approximately -500 counts on the encoder. In fact, this was acceptable due to the fact that the ball slides were stopped before reaching their full travel in one of the directions. The LVDTs were zeroed according to the ball slide range of motion *after installation in the tremor control prototype.*

In addition to LVDT signals, accelerometer signals were also recorded in a similar fashion. For these tests, the tremor control prototype was held such that the accelerometer input axis of interest was pointing approximately upward. The data recording was then started, and the prototype was then rotated so that the entire tremor control prototype was resting on the flat surface of the actuator. If the actuator of the accelerometer of interest was the one on which the tremor device rested, the resultant change of the acceleration sensed by the accelerometer would be 2 $g$.

The above trials were performed, and the data sets taken were processed to arrive at real gain values for the proportional gains of the Galil DMC–2040. The encoder inputs, which I generically refer to as $V_{in}$, were multiplied by $\left[\frac{20 \text{ Volts}}{4096 \text{ counts}}\right]$ in order to convert from encoder counts to voltages (the analog to digital converters were 12 bit; $2^{12} = 4096$ counts over a $\pm 10$ Volt range). Any value that the Galil unit may have had for a gain was then divided out of the voltage values. For example, since the accelerometer loops were studied while $K_{PA} = 5$, the resulting voltage values were divided by 5. Figure 4-11 shows the results of dividing the $V_{out}$ values (motor commands) by the $V_{in}$ values.

Ignoring the left halves of the plots in Figures 4-10 and 4-11, in which there is obvious noise, one can easily see the constant value in the left half of Figure 4-11. This constant value is $K_{GP}$, and its value in the figure is apparent as 0.25 $\left[\frac{V_{out}}{V_{in}}\right]$. The same procedure used to create Figure 4-11 was repeated on other datasets, and the mean value of $K_{GP}$ was recorded. The results are displayed in Table 4.3. Note that the mean $K_{GP}$ values in Table 4.3 are all very close to 0.25 $\left[\frac{V_{out}}{V_{in}}\right]$, regardless of which sensor system and control loop were used to record the data. In fact, the mean of the four values in the table is 0.249 $\left[\frac{V_{out}}{V_{in}}\right]$. Thus, for all calculations in this thesis, it is assumed that $K_{GP} = 0.25$ $\left[\frac{V_{out}}{V_{in}}\right]$.

### 4.5.2 Determination of Absolute Controller Derivative Gain

Section 4.5.1 detailed the methodology used to determine the absolute value of the DMC–2040 proportional gain. A similar analysis is carried out in this section, except that the absolute *derivative* gains, $K_{GD}$, are sought. Knowledge of the absolute derivative gains is beneficial so that the experimenters are able to specify system gains determined by the analyses of Appendix B.

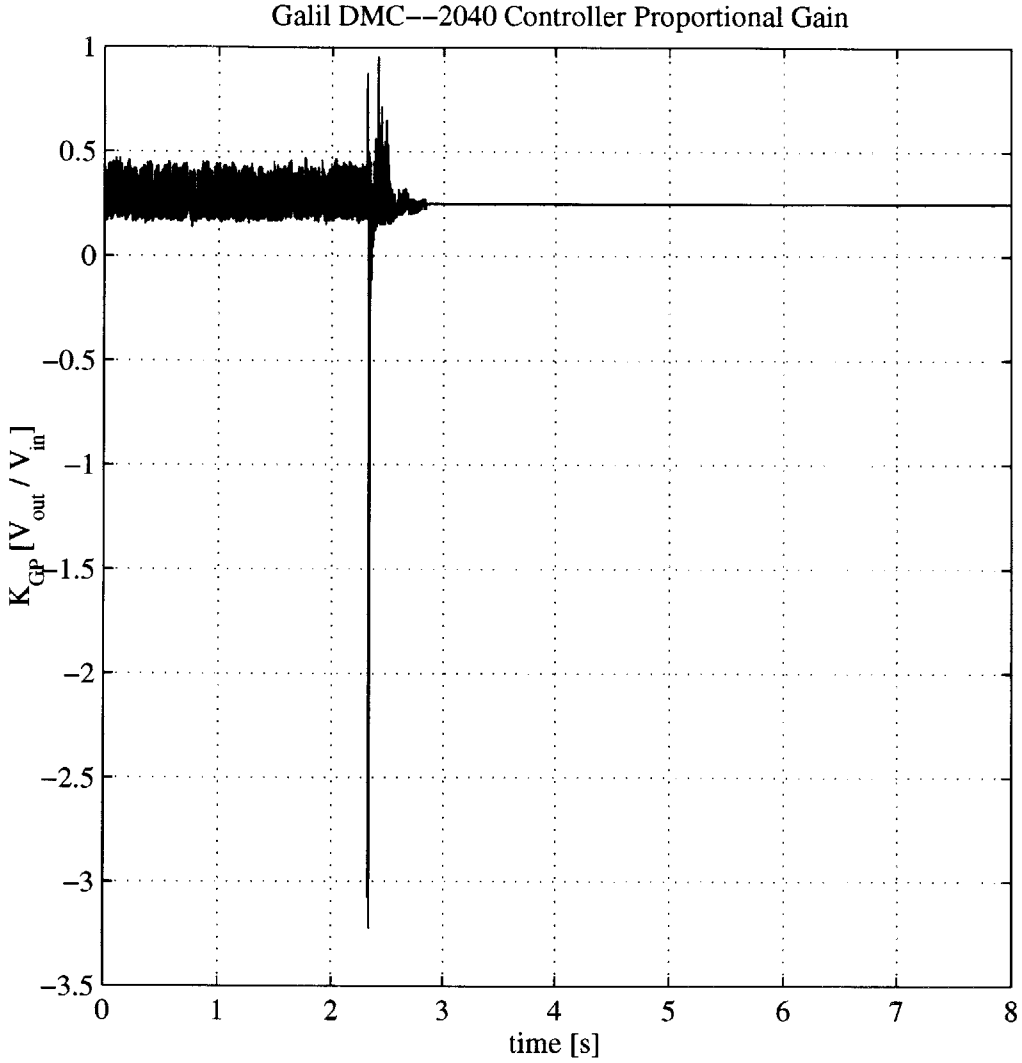


Figure 4-11: $K_{GP}$ values obtained by dividing the data from Figure 4-10.

| **Sensor Input** | **Mean** $K_{GP}$ $\left[\frac{V_{out}}{V_{in}}\right]$ |
|---|---|
| x-axis LVDT | 0.2568 |
| y-axis LVDT | 0.2491 |
| x-axis accelerometer | 0.2435 |
| y-axis accelerometer | 0.2473 |

Table 4.3: Mean $K_{GP}$ values for several different sensor inputs.

Data were again recorded using the Galil SDK, and processed using Matlab. An example of the data obtained are displayed in Figure 4-12. Notice that there are three plots in Figure 4-12, as opposed to only two plots in Figure 4-10. The top plot is the raw LVDT signal, the center plot is the LVDT signal *derivative*, and the bottom plot is the motor command. It was the author's hope that the determination of $K_{GD}$ would be as straightforward as the analysis of Section 4.5.1. Unfortunately, this was not to be the case.

Results of performing a simple division are displayed in Figure 4-13. Unlike Figure 4-11, there really is no clear trend in Figure 4-13. The value of $K_{GD}$ is very low in general—on the order of approximately $0.5 \times 10^{-6}$ $\left[\frac{V_{out} \cdot time}{V_{in}}\right]$—with "bursts" during which it assumed a value approximately 3,000 times higher. As such, taking a mean of these data was not likely to yield meaningful results. A different approach was needed.

The approach taken to determining $K_{GD}$ entailed several steps. The first step was an examination of curves such as those of Figure 4-12 to determine which portions of the data might be of interest. Portions of the LVDT signals that contained no time-varying characteristics were ignored. Portions of the LVDT signals that contained approximately constantly changing values were curve fit using $4^{\text{th}}$ order curves generated by Matlab. Curve fitting in this manner provided a function $V_{in}(t)$ that described the variation of the voltage value with time. The curve fit function was then differentiated, to arrive at an equation that described $\left[\frac{V_{in}(t)}{time}\right]$, or $\dot{V}_{in}$. The values of this curve were then divided by the motor command voltages over the same time ranges to produce vectors of $K_{GD}$ values. As with the process of straight division of the LVDT signal derivatives by the motor commands, there was some variation in the values of $K_{GD}$ obtained using this method. An example of a plot of $K_{GD}$ values appears in Figure 4-14.

Rather than experiencing 3-order of magnitude changes in the $K_{GD}$ values, there is now just a few factors of difference between the maximum and minimum values of the curve. The curve-fitting and differentiation technique were carried out over the other portions of the curve with smoothly varying LVDT signals, and the resulting mean $K_{GD}$ value resulting from this process was $2.453 \times 10^{-4}$ $\left[\frac{V_{out} \cdot sec}{V_{in}}\right]$. The value of $K_{GD}$ used throughout the rest of this thesis was taken to be $2.5 \times 10^{-4}$ $\left[\frac{V_{out} \cdot sec}{V_{in}}\right]$. It is important to note that this value of $K_{GD}$ presumably only applies to conditions in which the sample time of the DMC–2040 was operating at 1 kHz. A new determination of the value of $K_{GD}$ would need to be performed if the bandwidth of the DMC–2040 were changed.

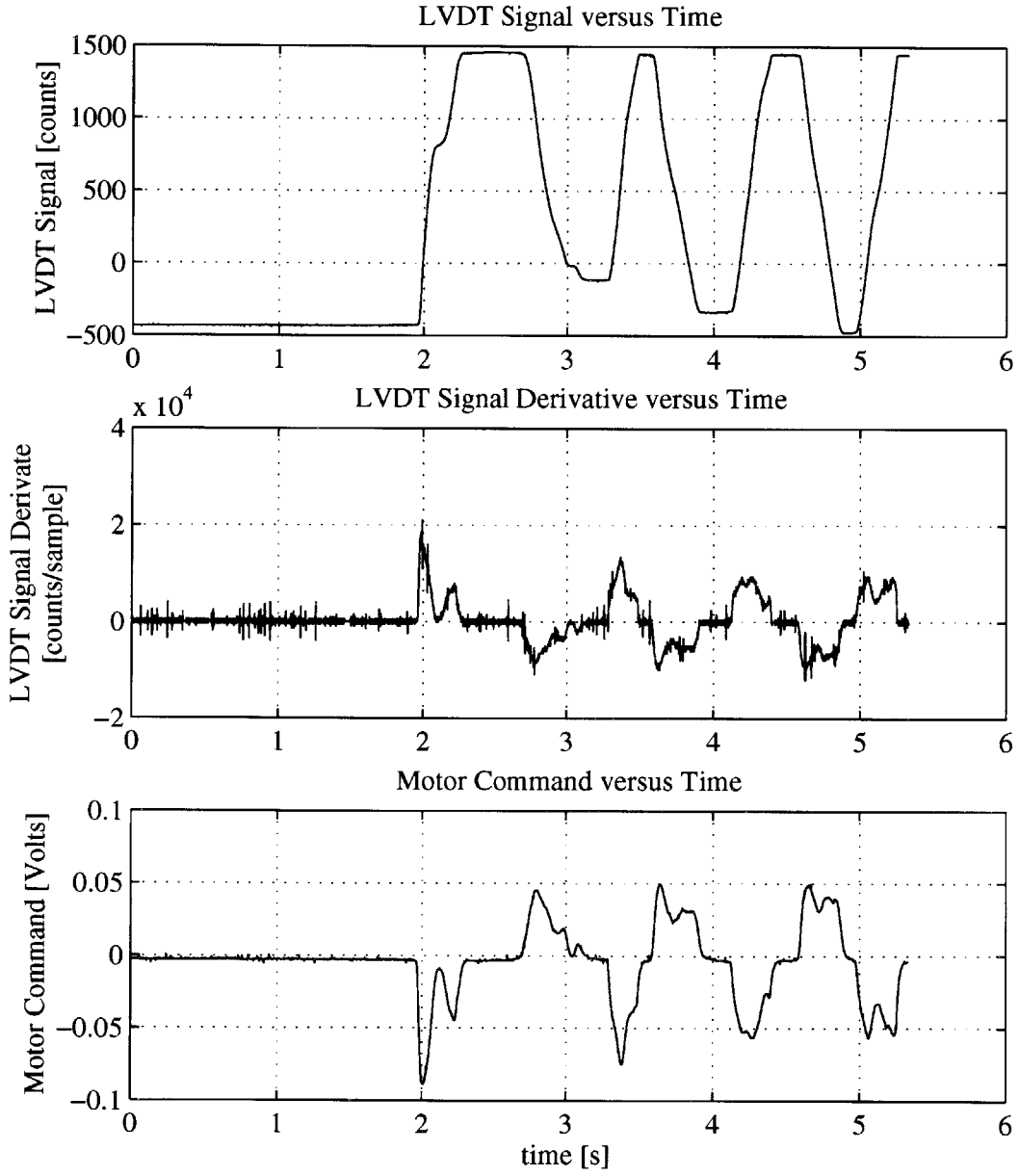


Figure 4-12: LVDT signal, LVDT signal derivative, and motor command used in the determination of $K_{GD}$.

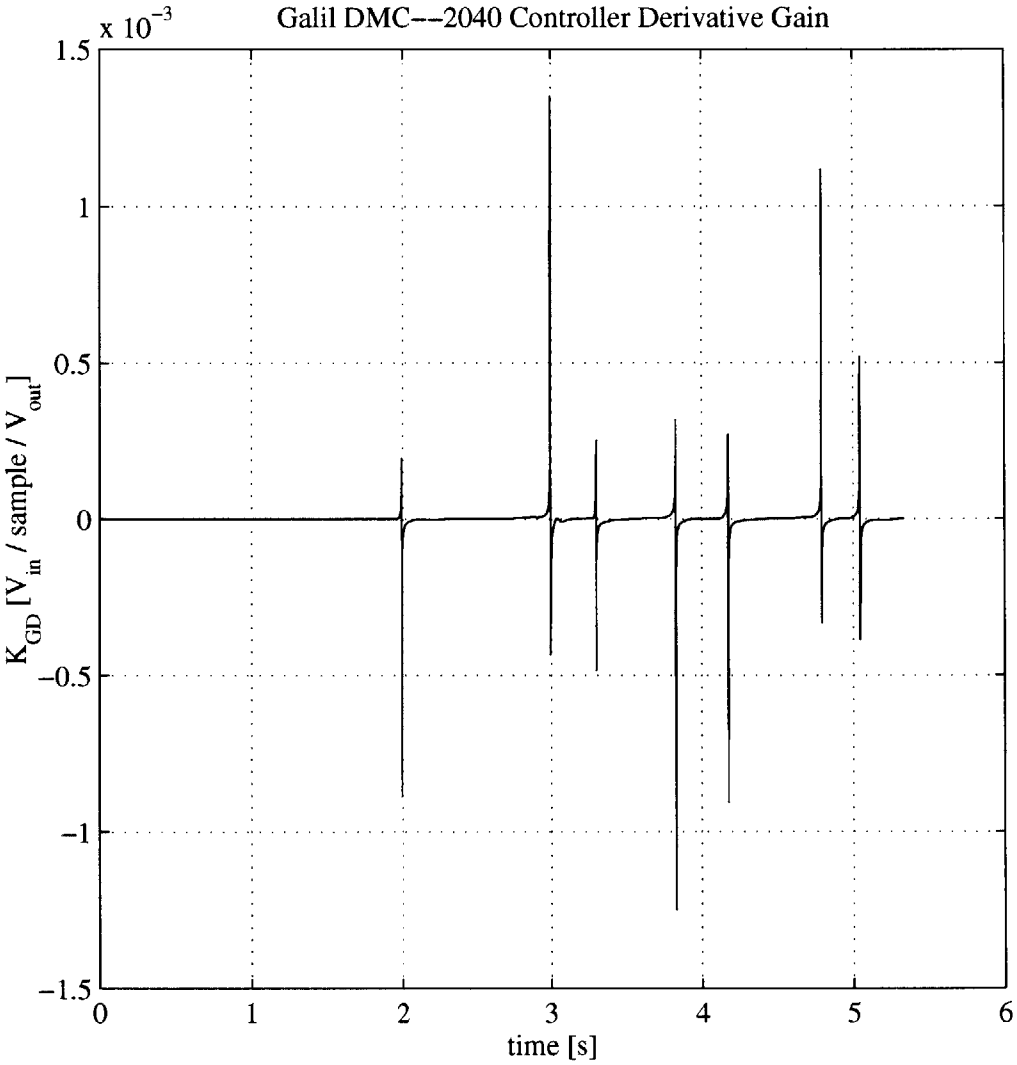


Figure 4-13: $K_{GD}$ values obtained by dividing the data from Figure 4-12.

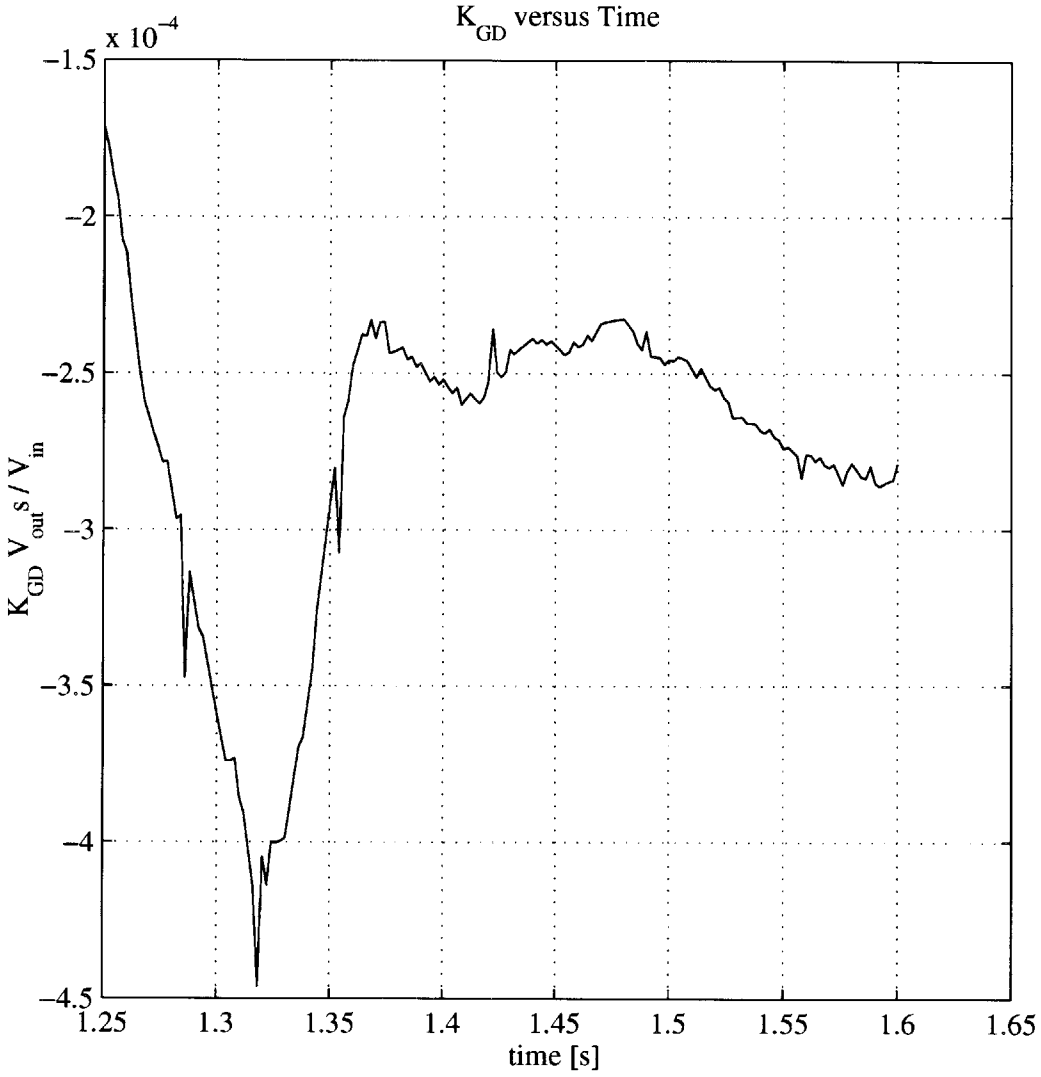


Figure 4-14: $K_{GD}$ values obtained by curve fitting method.

This page intentionally left blank.

# Chapter 5

# Experimental Results

## 5.1 Overview

With the mechanical characteristics and control systems of the tremor control prototype specified, it was time to take detailed data in an attempt to validate that the system was working. In order to do this, a National Instruments DAQCard–700 was used with the Dell Inspiron 7500 computer to record data within a Labview virtual instrument (vi). The vi file was adapted from an example file supplied with the Labview software in order to speed development of the interface.

Data were sampled at 1 kHz across 16 channels within the DAQCard–700. The sampling frequency was chosen to match that of the DMC–2040 controller. Data were written in a simple ASCII matrix file that could be easily read into Matlab. The data acquisition channels were laid out so that the configuration detailed in Table 5.1 resulted.

Thus, all of the major datasets were able to be recorded using the DAQCard–700. Both the x and y LVDT and accelerometer sensors were recorded, providing raw data regarding the position of the proof mass, and the accelerations of the wrist, respectively. The motor commands were recorded coming from each of the loops individually, and then the summed motor commands were also recorded. This allowed the experimenters to both see the motor commands resulting from different sensor systems and feedback loops, and make sure that the summed motor commands accurately reflected their constituent signals. Lastly, the voltage across the switch was recorded so that the data could be more easily analyzed, in particular with regard to comparing open loop and closed loop results.

Section 5.2 will detail the perceived effectiveness of the device. In other words, subjective descriptions of the wearer's tremor with and without the device operating will be compared. Section

| Variable | DAQCard–700 Channel | DAQCard–700 Pin Number |
|---|---|---|
| x LVDT | 0 | 3 |
| y LVDT | 1 | 5 |
| x accelerometer (PCB) | 2 | 7 |
| y accelerometer (PCB) | 3 | 9 |
| x LVDT motor command | 4 | 11 |
| y LVDT motor command | 5 | 13 |
| x accel motor command | 6 | 15 |
| y accel motor command | 7 | 17 |
| x motor command | 10 | 8 |
| y motor command | 11 | 10 |
| x accelerometer (ADXL105) | 12 | 12 |
| y accelerometer (ADXL105) | 13 | 14 |
| ground | – | 1 |

Table 5.1: Data acquisition channels.

5.3 will detail the data resulting from operation of the device. The objective data will be used to determine the performance of the device.

## 5.2 Qualitative Results: Perceived Tremor Reduction

Debugging of the device entailed a lot of guesswork by the experimenters. Initially, it was noticed that there appeared to be a sign reversal in the control loop which created a condition of positive feedback. This condition was noticed by the experimenters when the proof mass was rested on a table, and the wrist mount portion of the stabilizer was moved quickly in one direction or another. The quick movement was detected by the accelerometers, and the resulting effect was that the wrist mount felt *lighter* to the experimenters. Reversal of the algebraic sign of the accelerometer signal resulted in the wrist mount feeling *heavier* to the experimenters. In other words, the wrist mount felt as if it was more massive when the experimenters attempted to accelerate it.

Examination of the equations of motion of the device indicates that the feeling of additional mass was expected. The effect of the accelerometer feedback was such that the system felt as if it had added inertia to movement, *without added mass or weight.* So, quick accelerations by the experimenters were met with resistance from the actuators. Slow accelerations, or constant positioning of the SLA part produced no apparent change in the effective inertia of the system.

## 5.3 Quantitative Results

Quantitative results obtained with the tremor suppression device are presented in this section. Originally, it was intended to test the tremor suppression device on tremor patients, but time constraints prevented the author from doing so. It would be best to obtain permission for this testing from the proper ethical review boards, but time for this approval process was not found.

Additionally, the tremor suppression device was only partially functional. As the construction and modification of the device continued, certain performance limiting aspects of the hardware became apparent. The first was the presence of a structural resonance between the accelerometer sensing axis and the actuator force axis. This problem is detailed in earlier sections. Basically, this resonance limited the stiffness of the coupling between the sensor and the actuator, so that the gain of the control loop that controlled the actuator using the accelerometer signal could not be raised to the desired level. Another shortcoming of the tremor suppression device was that, as designed, there was far too much noise and cross-coupling between axes in the accelerometer signals. Both of these characteristics contributed to further limit the attainable gain level of the accelerometer control loop.

The resulting testing configuration accommodated the aforementioned shortcomings. The emphasis of the testing configuration was simply to show that the device was capable of performing tremor attenuation. A Micro-Mo Electronics, Inc.[1] Model 3557K024CR motor was used in order to create a condition similar to tremor. The motor had a set of screws and bolts attached to a small strip of metal on each end of the motor axle, and the screws and bolts were offset so as to create a periodic disturbance when the motor axle rotated. The screws and bolts were chosen based on their masses, and placed such that spinning the motor up to 600 rotations per minute (RPM), or 10 Hertz, would create a disturbance force of the proper magnitude predicted by Table 2.2. A frequency of 10 Hertz was chosen because it allowed the device to attenuate vibration without running into its limits of travel. When the device hit its limits of travel, the shock detected by the accelerometers often drove the accelerometer control loop unstable.

The motor and its offset weights were strapped firmly to the wrist mount portion of the tremor controller, to simulate the device being attached to a shaking wrist. The entire device was then suspended using chemistry lab stands and plastic wire wraps that were attached to the wrist mount portion of the tremor controller. The end effect was to simulate conditions of mounting the device

[1] 14881 Evergreen Avenue Clearwater, FL 33762-3008. 800-807-9166

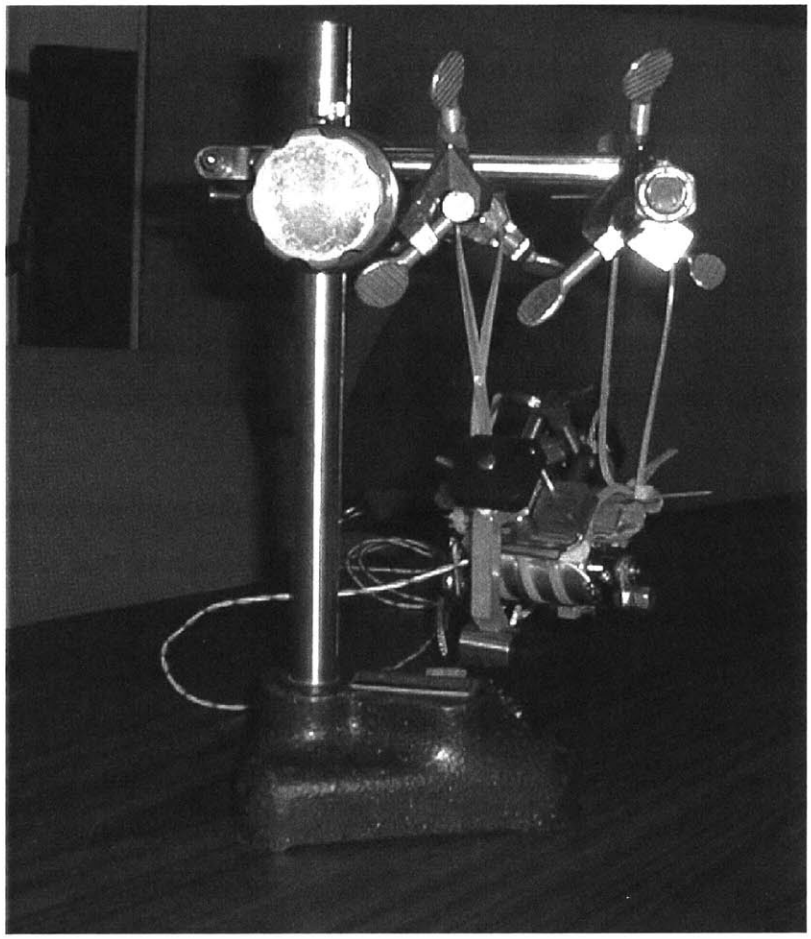

Figure 5-1: Photograph of tremor control prototype in test stand, front view.

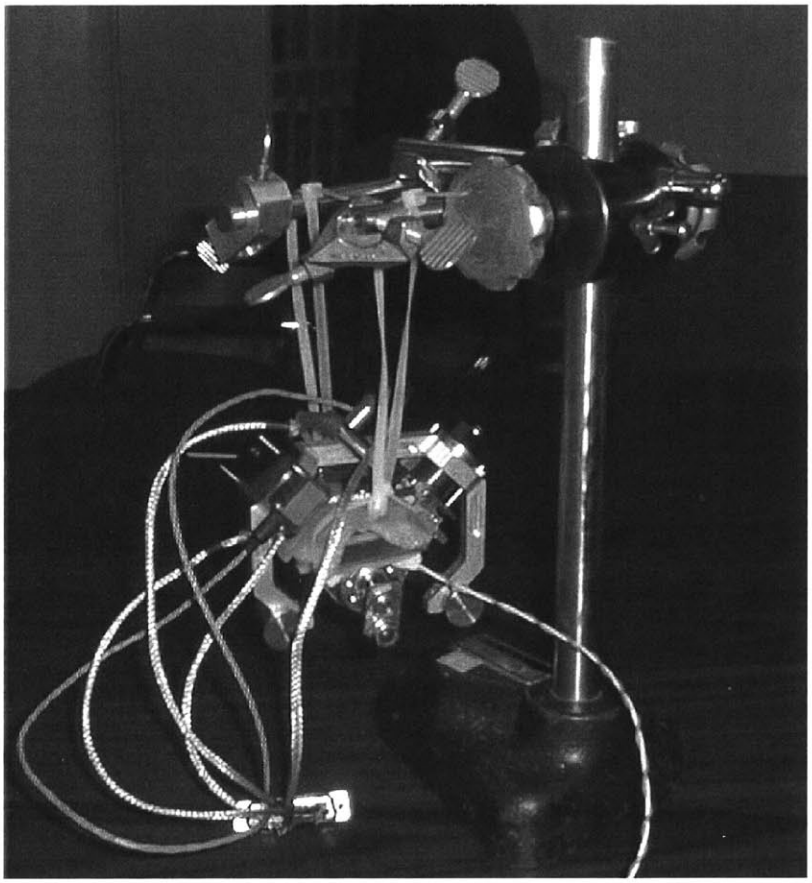

Figure 5-2: Photograph of tremor control prototype in test stand, back view.

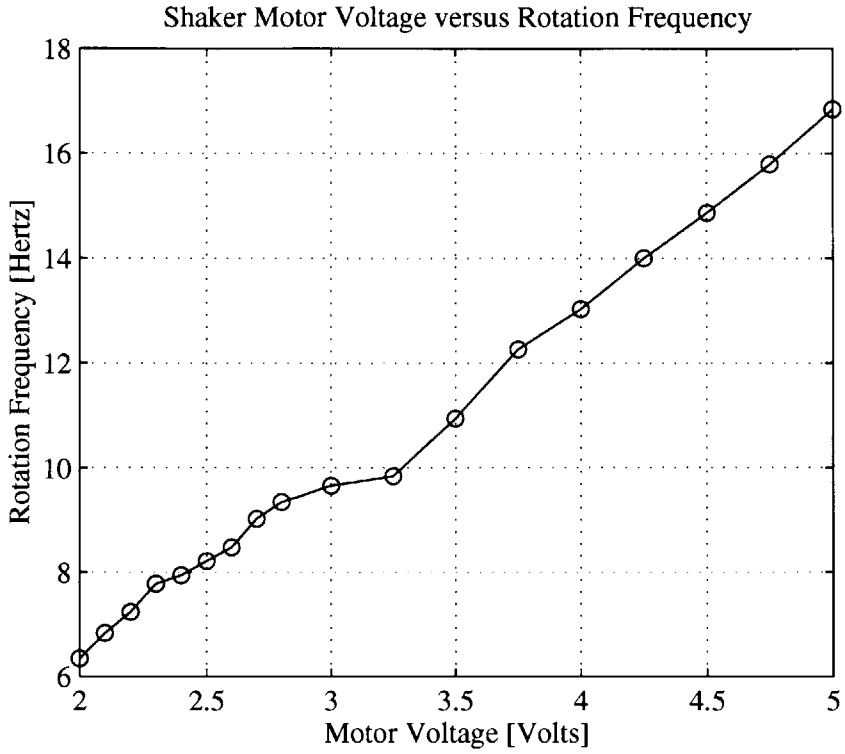


Figure 5-3: Plot of motor rotation frequencies versus excitation voltage.

to a shaking wrist, with the proof mass portion of the device suspended in free space. Figures 5-1 and 5-2 show two views of the test setup, with the tremor suppression prototype clearly suspended using plastic tie straps. The motor was activated with a 3.25 Volt power supply, which caused the motor to spin at approximately 10 revolutions per second.

The data indicated in Table 5.1 were recorded at approximately 1 kHz sampling frequency, and analyzed using Matlab. Three individual tests were performed. The first involved simply switching on the excitation motor and recording the accelerometer signals. This allowed a baseline to be established for future comparison; the vibrations of the device without any influencing movement of the proof mass was made available from this test.

### 5.3.1 Baseline Results

Figure 5-4 shows the acceleration value of the x-axis accelerometer from time 6 seconds to time 7 seconds of the baseline test. Thus, with the proof mass resting on the wrist mount bracket and no force exerted at all by the actuator, the assembly was being shaken with a force of approximately $\pm 0.25\ g$. Also note from Figure 5-4 that the tremor suppression device was being excited at slightly

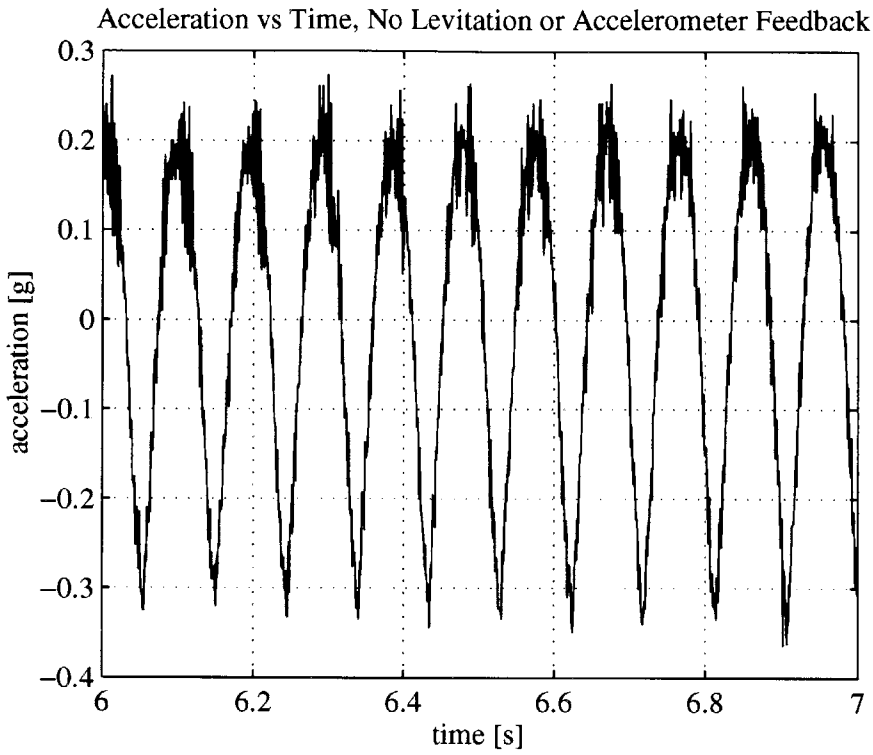


Figure 5-4: Baseline acceleration of device under influence of shaker motor.

more than 10 Hertz. In the one second period of Figure 5-4, slightly more than 11 cycles are noted. This is actually beneficial, since the device is being excited by a higher force than anticipated as a result of the faster excitation frequency. Figure 5-5 shows the power spectrum density of the acceleration signal under conditions of excitation by the shaker motor. Note that the power peaks at approximately 11 Hertz. The source of the acceleration power at approximately 22 Hertz is not known, but it is likely a harmonic resulting from the 11 Hertz excitation frequency.

### 5.3.2 Levitated Results

The next set of results display data obtained when the proof mass was simply levitated, and no acceleration feedback was present. These data were recorded in order to determine system performance with the presence of the tuned vibration absorber. Note that the absorber, as designed, was *not* expected to attenuate tremor. This is due to the fact that the tuned absorber must be designed for a particular frequency band, which was well away from the 11 Hertz excitation frequency used here. The amplitude of the power of the tremor oscillations was noticed to be approximately $3.6 \times 10^5$ for 7,500 data points when no levitation was present. The amplitude of

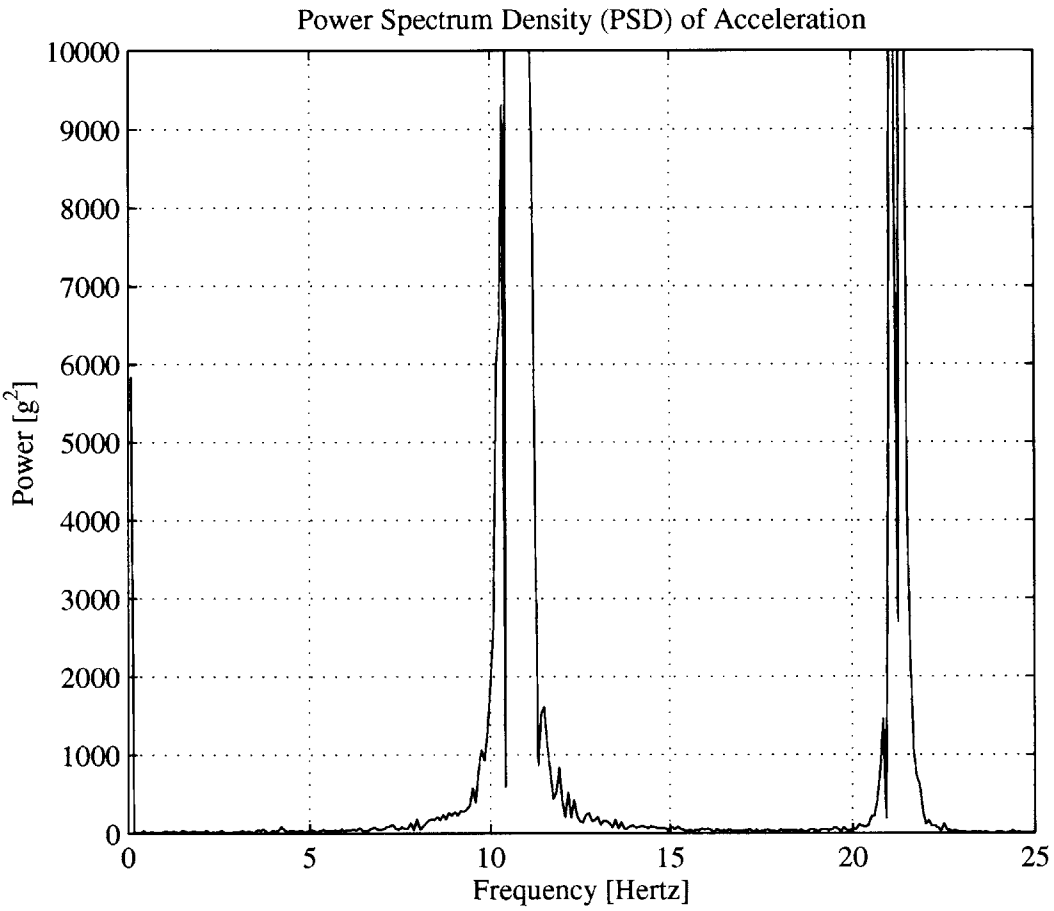


Figure 5-5: Power Spectrum Density of acceleration under influence of shaker motor.

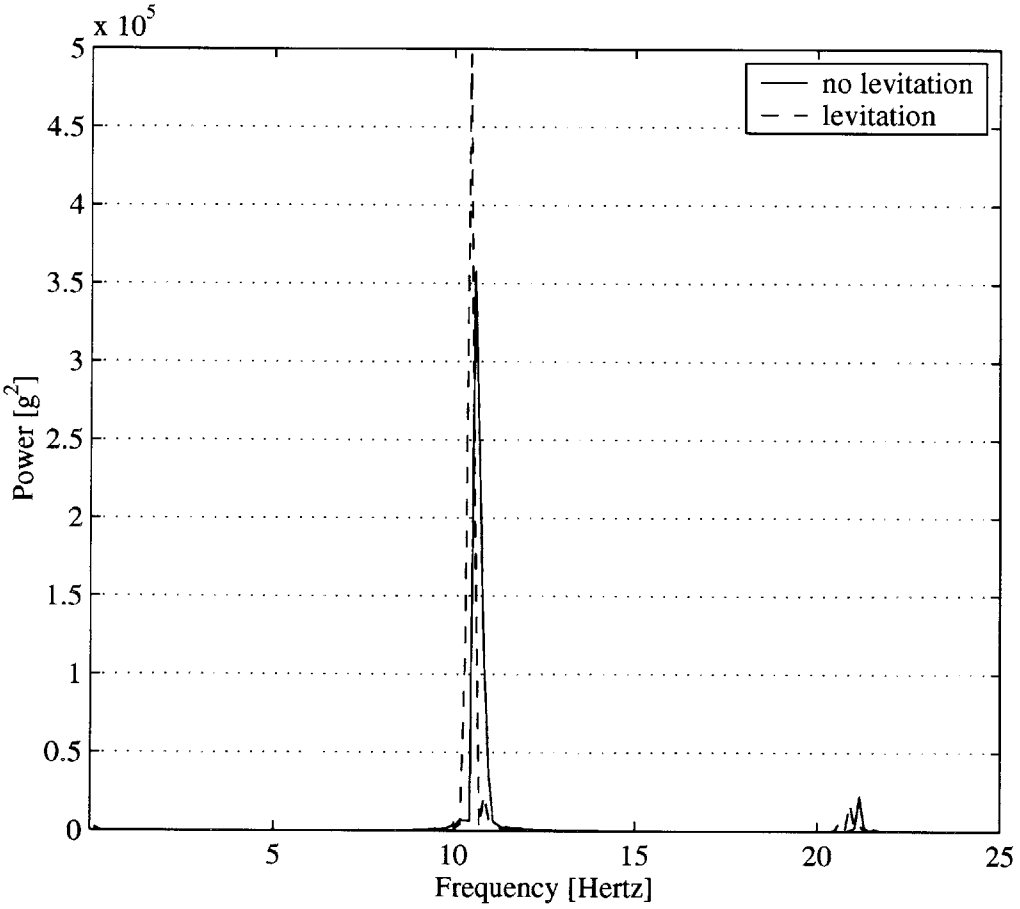


Figure 5-6: Levitated and non-levitated PSD.

the power of the tremor oscillations was noticed to be approximately $5 \times 10^5$ for 7,500 data points when levitation and the tuned absorber were active. Thus, the data claim that the tuned vibration absorber, acting by itself, is not providing appreciable tremor attenuation at 11 Hertz.

### 5.3.3 Levitated and Tremor Compensated Results

The results presented in this section are those to which the entire thesis has lead. These data were recorded under conditions of a levitated proof mass, proportional and derivative LVDT gains to create a tuned absorber, and an acceleration feedback gain of 80, as keyed into the Galil DMC–2040. The data of Figure 5-7 were obtained by toggling the accelerometer loop proportional gain between values of 0 and 80. Switching this gain in this manner would effectively switch the accelerometer feedback loop on (for values of 80) and off (for values of 0). The condition of the accelerometer feedback loop can be determined by examination of the actuator force; if the loop was enabled, there was force output by the actuator. Similarly, if the feedback loop was not enabled, there was no force output by the actuator.

Examination of 5-7 is disappointing at first glance. It appears as though the presence or absence of actuator force feedback has no effect on the acceleration of the tremor controller mount. The accelerometer feedback loop was first on, then off, then on, then off again, as shown by the actuator force plot of Figure 5-7.

However, it is easy to reveal the truth displayed in Figure 5-7 by looking at the data in better time-resolved detail. Figure 5-8 examines the data of Figure 5-7 over the time interval from 28 to 31 seconds. During this period of time, the accelerometer feedback gain was changed from 80 to 0, switching accelerometer feedback off. As can be seen in the waveform of the acceleration plot of Figure 5-8, the accelerometer feedback loop *was* functioning to reduce tremor accelerations. Although the peak accelerations "spiked" to a particular value, regardless of the condition of the accelerometer feedback loop, the underlying sinusoid experienced a great change in amplitude. It was only the acceleration peaks that were visible in Figure 5-7, which lead to the initially disappointing appearance.

In order to test the hypothesis that the underlying tremor sinusoid was of lower magnitude for closed-loop operation of the accelerometer feedback, the Power Spectrum Densities of the closed- and open-loop waveforms were examined. Figure 5-9 shows both PSD results plotted on one set of axes. Note that the power of the tremor oscillations for open- versus closed-loop operation vary by a ratio of approximately 1:4. This shows conclusively that power was removed from the tremor

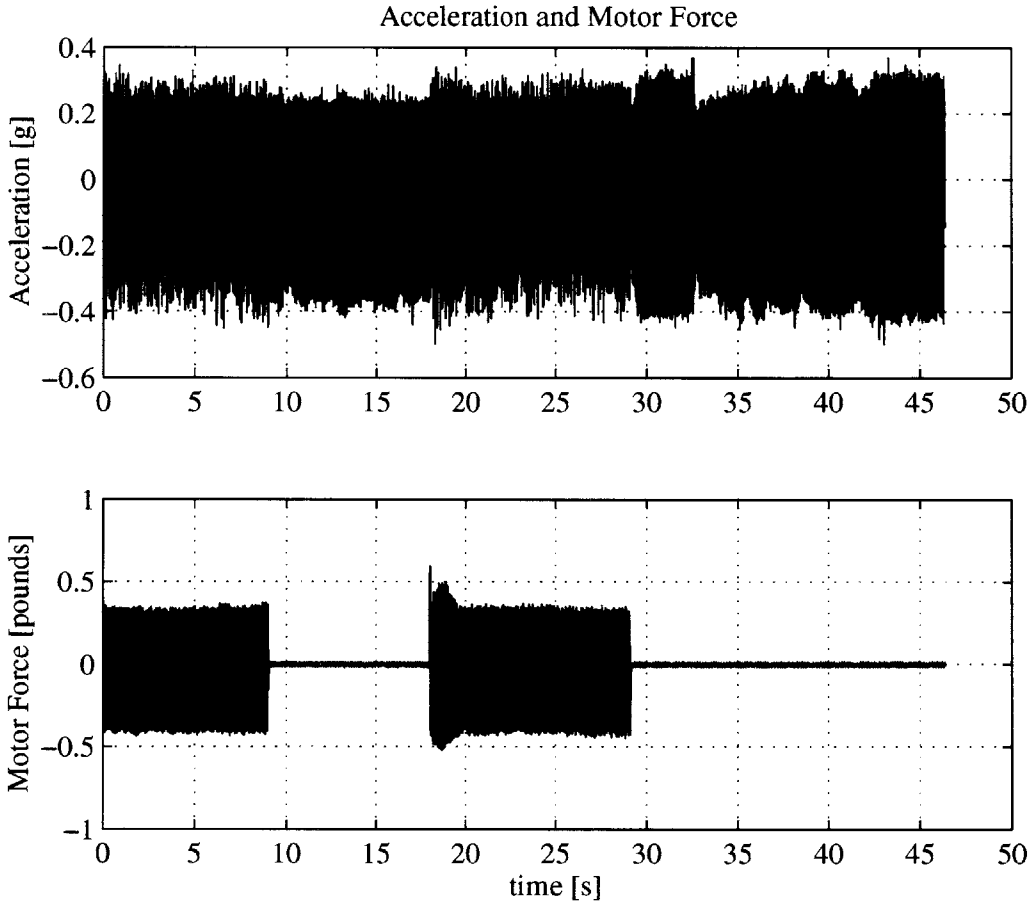


Figure 5-7: Acceleration and actuator force of x-axis control loop.

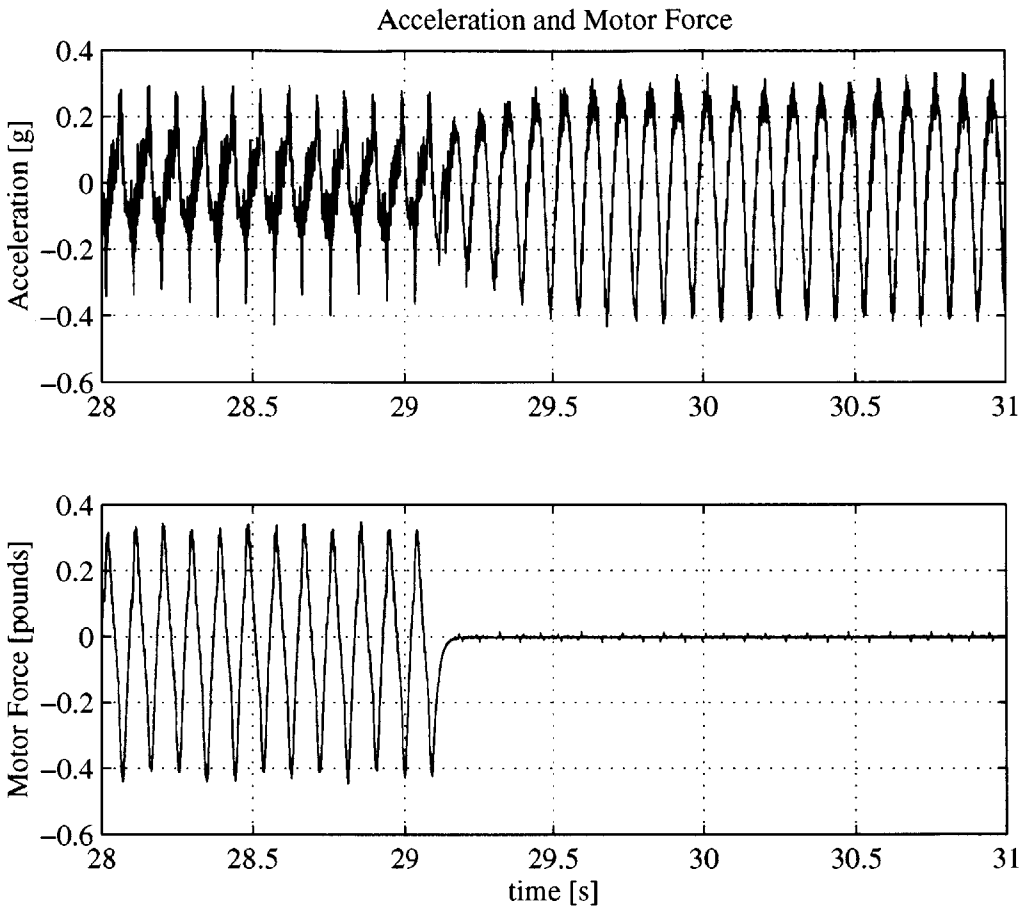


Figure 5-8: Acceleration and actuator force of x-axis control loop, in detail.

oscillations by the operation of the accelerometer feedback loop.

A more intuitive measure of the effectiveness of the tremor suppression device is a display of open- and closed- loop displacement due to tremor. Figure 5-10 shows open- and closed- loop displacement of the accelerometers obtained by numerically integrating the acceleration data presented in Figures 5-7 and 5-8. Note that there is some low-frequency content to the waveforms of Figure 5-10, which distorts the data slightly. Nonetheless, it is easy to see the difference in the vibration amplitudes of the waveforms in Figure 5-10. The closed-loop tremor displacement is approximately 1/2 of the open-loop tremor displacement. These results are good given that the tremor amplitudes were slightly higher than expected.

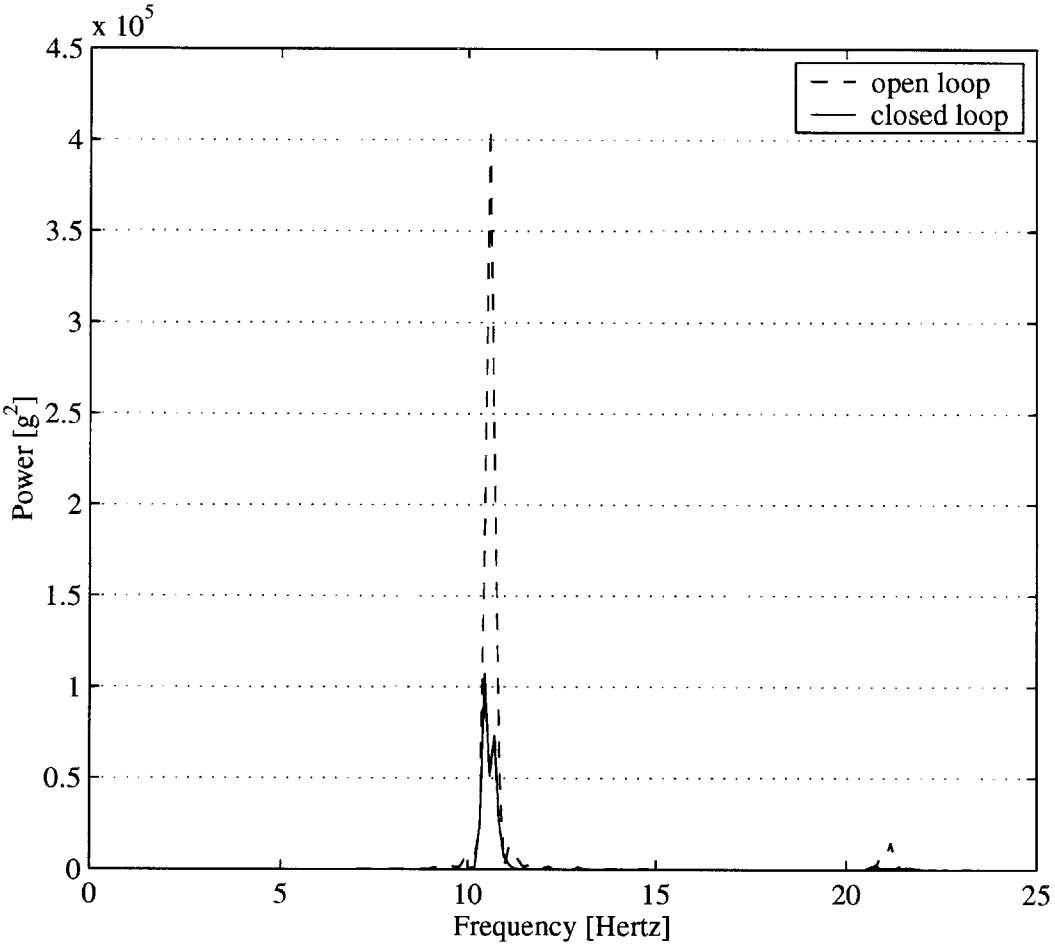


Figure 5-9: Open- and closed-loop PSD results.

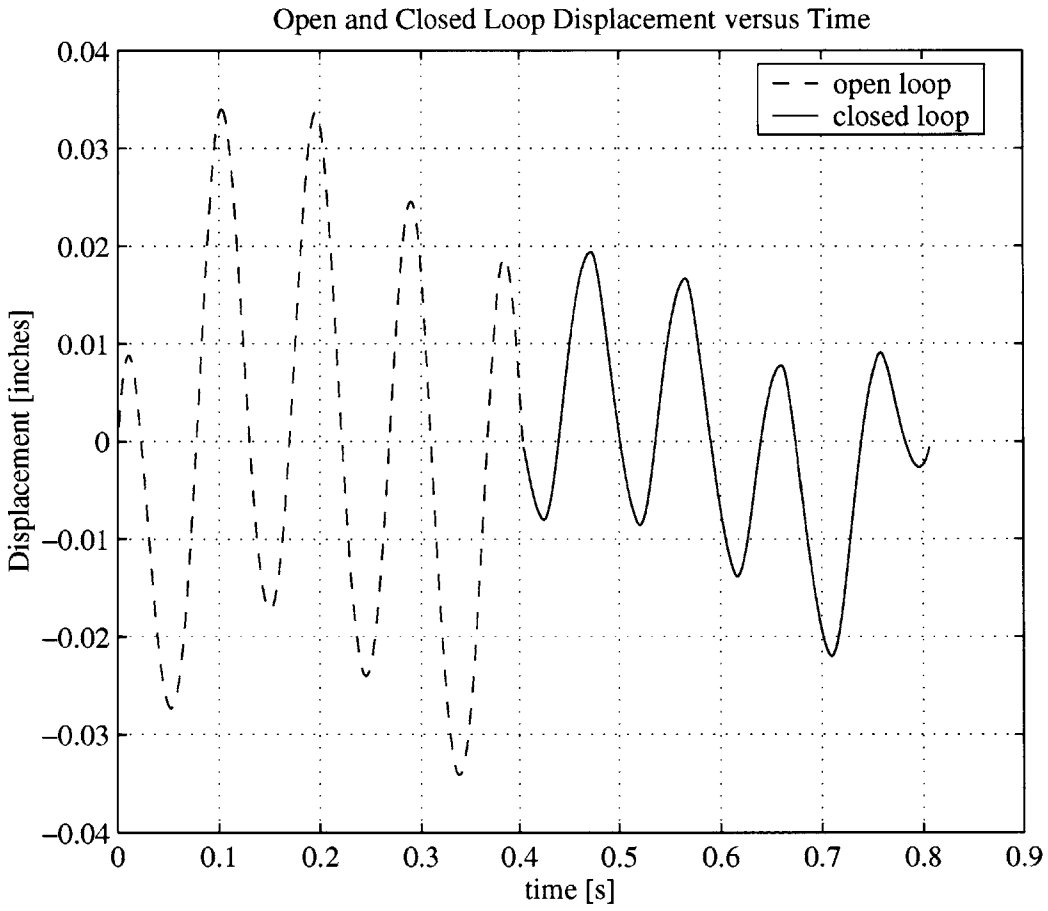


Figure 5-10: Open- and closed-loop displacement.

# Chapter 6

# Conclusions and Suggestions for Future Work

## 6.1 Conclusions

This thesis is concluded on the positive outcome of the attempt to build an active tremor suppression device. The tremor suppression device was able to center the proof mass using the LVDT control loops. Addition of accelerometer feedback gain and the tuned vibration absorber provided considerable vibration attenuation. The device was limited to single-axis operation due to higher than anticipated levels of friction in sliding guide interfaces.

The device constructed had a mass of approximately 640 grams, of which 572 grams was moving mass. The ratio of moving mass to total mass is a measure of the efficiency of the design. Since a proof mass actuation scheme was used, sufficient mass had to be added to allow the stabilizer to function properly. On the other hand, the system should add as little mass as possible to the wrist of the individual wearing the device. The ideal situation would be for the device to be composed entirely of moving mass, which would be a moving mass to total mass ratio of 100%. Realistically, though, the system must have some stationary mass. The design introduced in this thesis was roughly 89% moving mass, which is very efficient compared to the ideal of 100% moving mass.

Design of the device and packaging of the various subsystems within the device were aimed at increasing user acceptance. It was desired to build a system that would be practical for a potential patient to use—in other words, the system should comfortably mount to the wrist yet provide tremor attenuation with the lowest possible mass. The device was successfully designed with a

system to share a common proof mass, which resulted in the weight of the device being roughly halved with respect to a system making use of a distinct proof mass for each axis of operation.

The control system used for the tremor attenuation was a proportional- integral-derivate (PID) controller for the position of the proof mass, and a simple proportional controller for the acceleration feedback. The proportional and derivative terms of the position control loop were used to specify the parameters of the tuned vibration absorber, while the integral term was used to center the proof mass against gravity. The proportional gain of the accelerometer feedback loop was used simply to counteract tremor accelerations. Absolute controller gains of the Galil DMC–2040 were determined to be $K_{GP} = 0.25 \left[\frac{V_{out}}{V_{in}}\right]$ for the proportional gain of the device, and $K_{GD} = 0.25 \times 10^{-}3 \left[\frac{V_{out} \cdot sec}{V_{in}}\right]$ for the derivative gain of the device. Modeling of the dynamics of the device suggested that absolute controller gains should take values of $K_{AP} = 12.5 \left[\frac{\text{lb}}{\text{g}}\right]$, $K_{LP} = 2.04 \left[\frac{\text{lb}}{\text{in}}\right]$, and $K_{LD} = 1.62 \times 10^{-}3 \left[\frac{\text{lb} \cdot \text{sec}}{\text{g}}\right]$. The position loop integral gain, $K_{LI}$, was made just large enough to center the mass but not influence the dynamics of the device. These gains were actually used during experiments, and were capable of adequately attenuating tremor.

A shaker motor with a mass of 22 grams at 0.5 inches offset was used to excite the device at approximately 11 Hertz. Based on analyses performed in Chapter 2, the excitation force was slightly higher than actually required, and less offset mass could have been used. Nonetheless, the device demonstrated a 4:1 reduction in single-axis tremor vibration power from open- to closed-loop operation. Furthermore, the device demonstrated a 2:1 reduction in single-axis tremor vibration amplitude from open- to closed- loop operation. The tremor vibration power amplitudes in open- and closed-loop operation were approximately $4 \times 10^5$ $[g^2]$ and $1 \times 10^5$ $[g^2]$, respectively. Similarly, the tremor vibration amplitude was reduced from approximately 0.06 inches to slightly less than 0.03 inches from open- to closed-loop operation. A harmonic that appeared at approximately 22 Hertz during open-loop operation was almost completely eliminated during closed-loop operation.

Dr. Alice Flaherty, of the MGH Neurology Department has suggested that the observed 2:1 reduction in tremor vibration amplitude would be of use in treating tremor patients. Thus, this thesis seems to have produced more than enough information and data to warrant further study along the path begun. The proof mass actuation scheme, used in conjunction with tuned vibration absorption and acceleration feedback, shows promise in resulting in a new treatment for tremor.

Additional testing showed that the tuned vibration absorber, without acceleration feedback, was not effective in reducing tremor vibration amplitudes. This was to be expected, since a tuned vibration absorber has to be tuned to operate at a given frequency. The tuned absorber in this

thesis was designed to be used in conjunction with the acceleration feedback, and was tuned to operate at a lower frequency than the 11 Hertz excitation frequency utilized. Tremor vibration amplitudes with and without the tuned vibration absorber actually increased slightly, from $3.6 \times 10^5$ $[g^2]$ to $5.0 \times 10^5$ $[g^2]$.

## 6.2 Suggestions for Future Work

It is hoped that this thesis will serve as the starting point for a vast array of tremor control projects. As such, the suggestions for future work will be rather extensive, in order to aid future researchers in the realm of tremor control for some time.

It would be beneficial to perform a review and a mechanical redesign of the tremor control hardware. Better packaging could be achieved through a variety of strategies. The LVDT signals proved to contain very little noise, so the wiring for them could perhaps be left unshielded and better integrated into the mounting structure of the device. The PCB accelerometers could also be moved such that they would become an integral part of the adapter plate between the ball slides and the BEI actuators. This would eliminate the structural resonance problems that were seen between the actuator and PCB accelerometers. Another method for reducing the severity of that particular structural resonance would be a different method of guiding the movement of the proof mass with respect to the mount. Instead of using the sliding guide pins, the author is intrigued by the idea of adapting the proof mass and stainless steel adapter plates to hold the Del-Tron ball slides. The movement of the PCB accelerometer between the actuator and the stainless steel adapter plate would free the flat surface on the adapter plate for this purpose.

The results presented in Chapter 5 make me wonder whether or not the device might in fact be over designed. The vibrations imparted to the device were quite a bit above the magnitude of tremors expected at that frequency, yet the device performed quite admirably. Perhaps the device could be redesigned with a lower proof mass, or perhaps the good performance of the device was due simply to the high frequencies of the tremor oscillations. Future work will have to answer this question. In any event, I would like to propose the idea of eliminating the coupled proof mass, and halving the effective proof mass used by each axis. In other words, used two separate proof masses that each move along only one axis, with each mass weighing approximately 1/2 pound. This approach would eliminate the structural resonance problems encountered in this thesis, which resulted from the delicate mechanism to allow the shared proof mass. The splitting of the proof

mass into two masses would be only for experimental purposes, with the possibility of reverting to the shared proof mass once more is learned regarding the control of tremor. Thus, we would leverage off the idea that the device could be over designed in terms of the weight of the proof mass in order to gain a lot of knowledge regarding potential system performance.

Another important design change to be made would be the remanufacture of the SLA mount using aluminum, or ABS plastic. The SLA process enabled the part to be made very quickly (a couple of days), but the experimenters paid dearly for this speed in the form of flexibility of this mounting base. The SLA mount was easily rocked back and forth while the proof mass was held stationary, which exhibited the inadequate stiffness of the assembly. Indeed, an aluminum wrist mount was ordered by the author, but not delivered in time for testing to be accomplished. As it was, the design was modified to include steel sheet metal washers between the screw heads and the SLA mount to enhance the stiffness of the device. Attempting to tighten the screws onto the SLA mount resulted in cracking of the SLA part. The addition of the metal washers did allow for tighter screws, and increased stiffness, but the desired level of stiffness was still not achieved.

Changes to the control system architecture would also benefit the device. The DC component of the accelerometer signals could be used to determine the attitude of the prototype with respect to gravity. This would be helpful for centering the mass, since a proportional force could be derived from this signal, minimizing the work that must be performed by the LVDT loops. Additionally, it is plausible that cross-axis coupling could be reduced by building a simple summation circuit that would subtract a low percentage (3% or so, as listed in the PCB specification sheets) of the opposing axis's accelerometer signal. These are really minor changes, though. The author was very happy with the level of performance and features available through the Galil control electronics.

Better shielding for the accelerometer wiring of the device would also be welcome. The author did as much as possible to shield all exposed wiring, but the practical considerations in routing wiring through the device resulted in spans of unshielded wire. I believe that these rather small spans of wire introduced almost all of the electrical noise to the system. With a system having gains as high as those of the accelerometer control loops, it is critical to reduce noise as much as possible. This included shielding noise sources as well as noise sinks. Indeed, removing the grounds from the shields showed that the Galil MSA–12–80 servo amplifiers were a significant source of noise.

# Appendix A

# Mechanical Drawings of Parts Used

The drawings on the pages that follow were those that were sent to the machine shop at Draper Laboratory for the production of parts used in the tremor control prototype. Mitchell Hansberry, of Draper Laboratory, expertly prepared these drawings and performed a good deal of the specification of precision mechanical design and overall system design of the parts used in this thesis. I am indebted to him for his efforts in making this thesis a reality. I don't remember the last time I worked on a design project in which every single component functioned perfectly the first time around. Mitch also was able to quickly and competently dispatch the minor design revisions I sent his way after the first batch of parts were produced. These drawings and the corresponding solid model parts were created using SolidWorks Corporation[1] SolidWorks software.

[1] 300 Baker Avenue, Concord, MA 01742. 800–693–9000

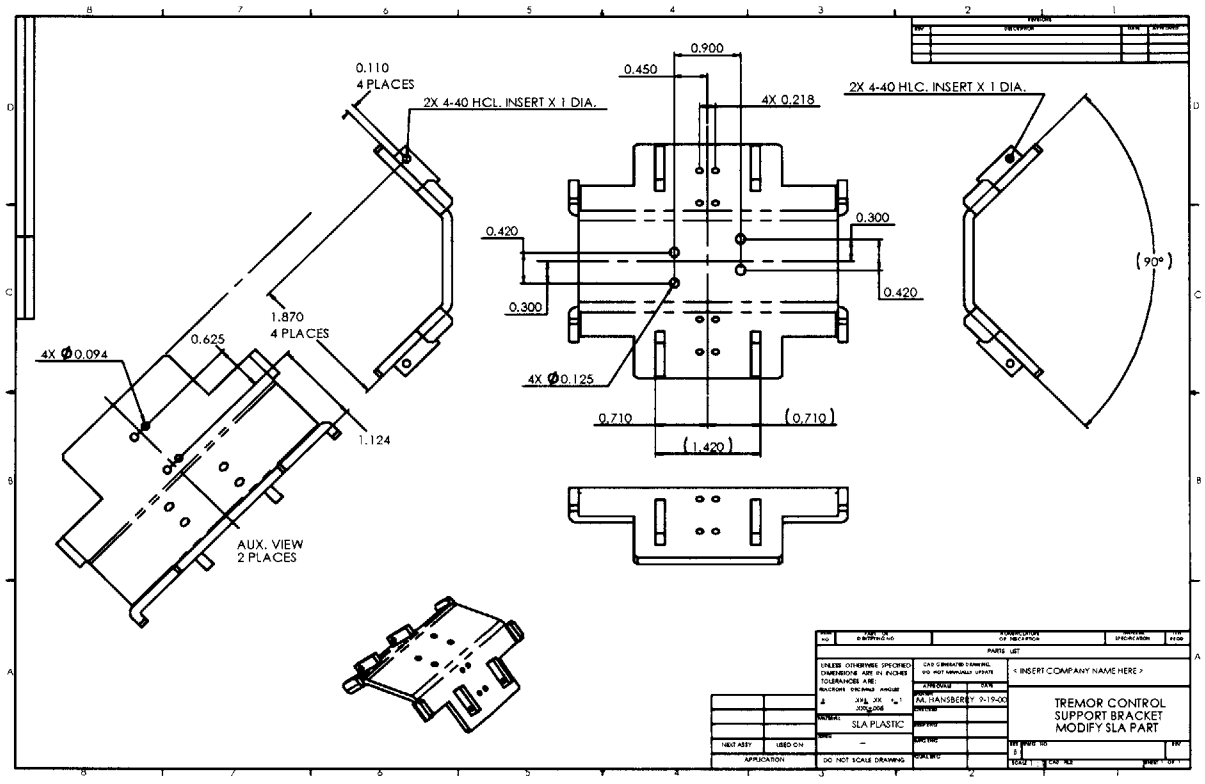


Figure A-1: Mechanical drawing of the SLA wrist mount.

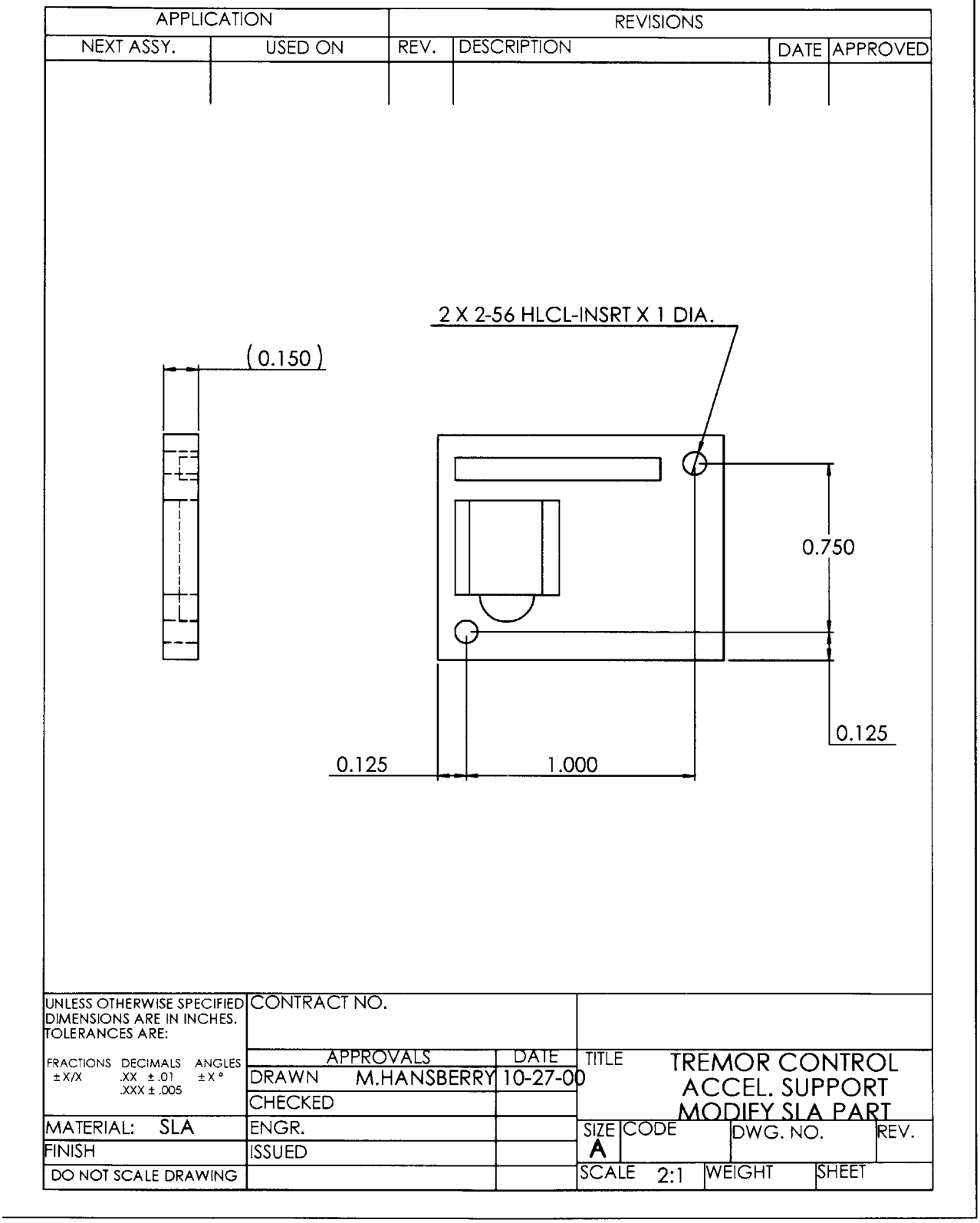


Figure A-2: Mechanical drawing of the accelerometer standoff.

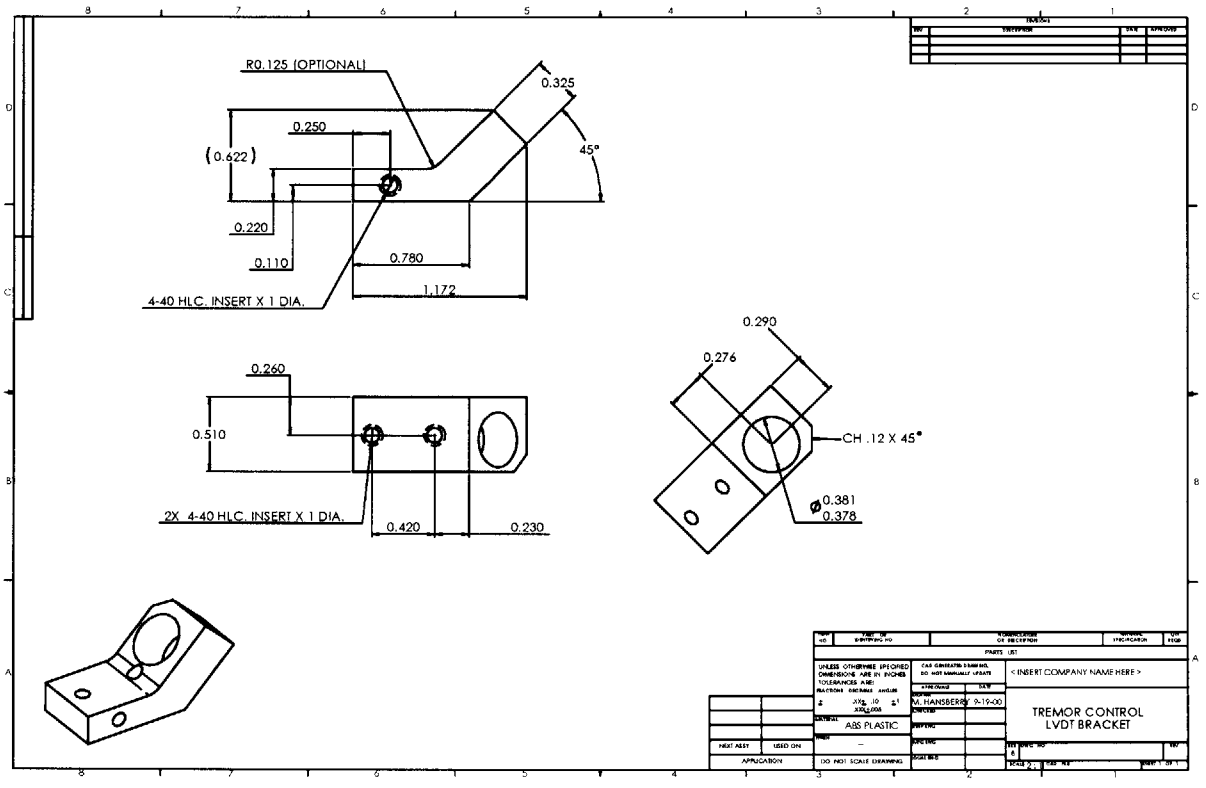


Figure A-3: Mechanical drawing of the LVDT mounting bracket.

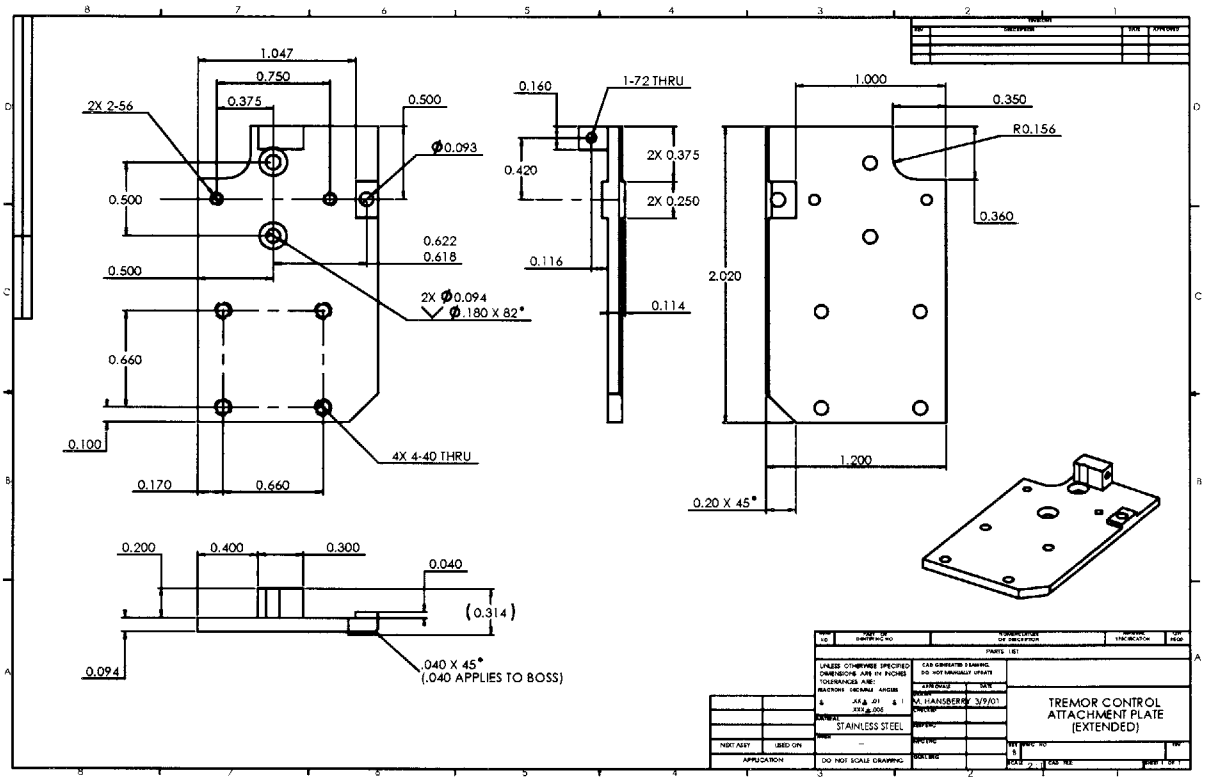


Figure A-4: Mechanical drawing of the adapter plate between the actuator and ball slide.

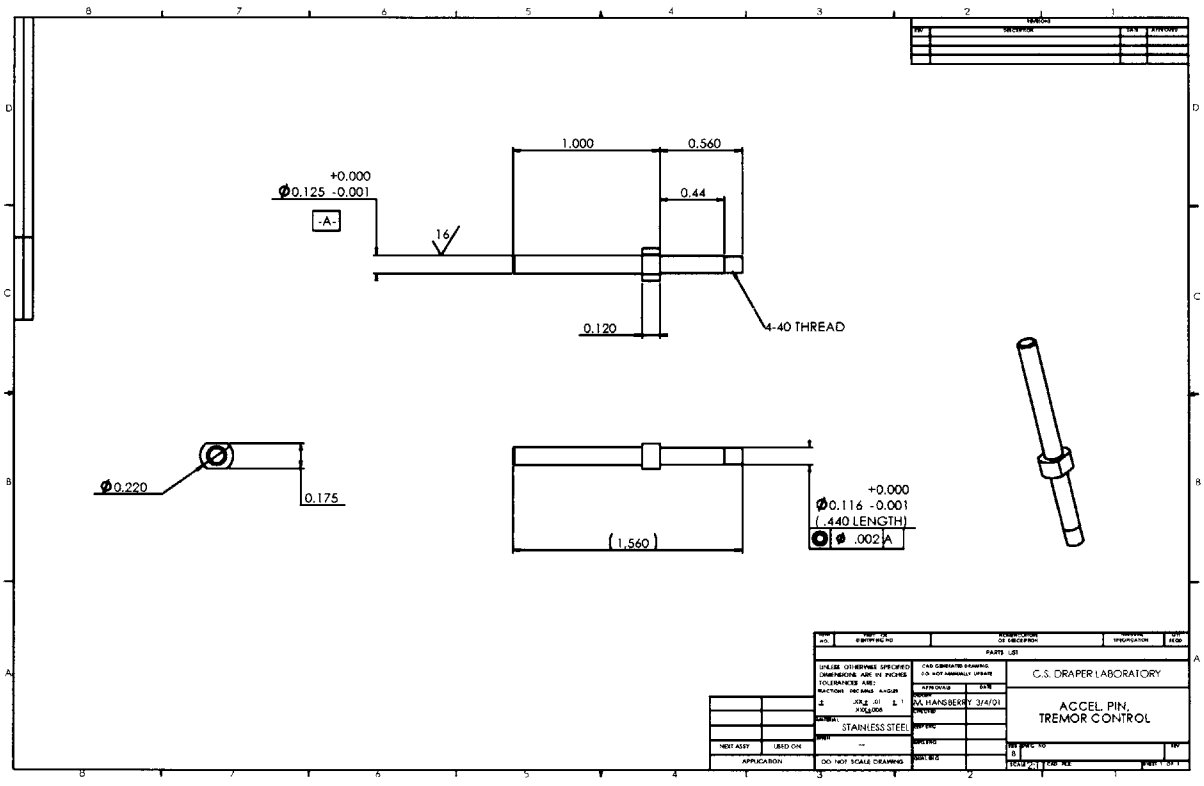


Figure A-5: Mechanical drawing of the proof mass guide pin mounting through the accelerometer.

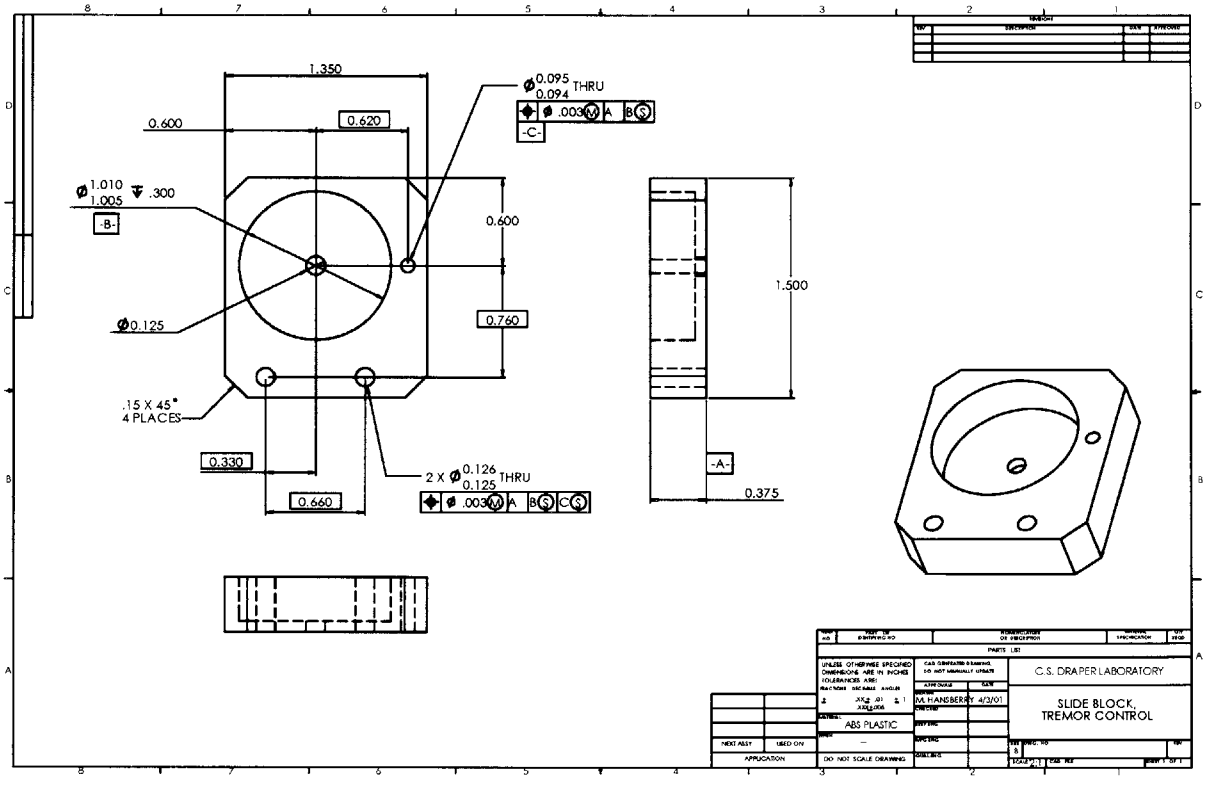


Figure A-6: Mechanical drawing of the slide block.

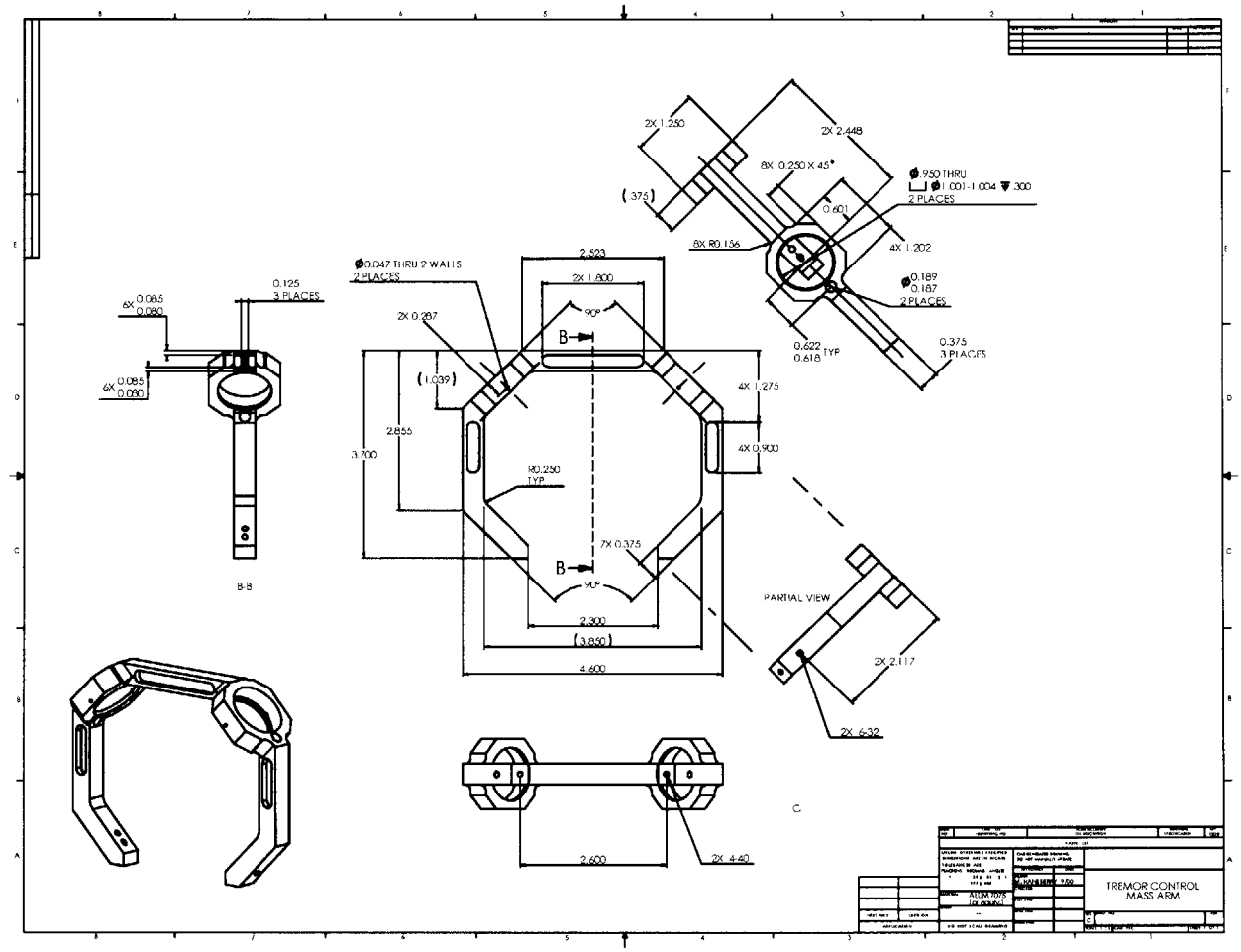


Figure A-7: Mechanical drawing of the proof mass frame.

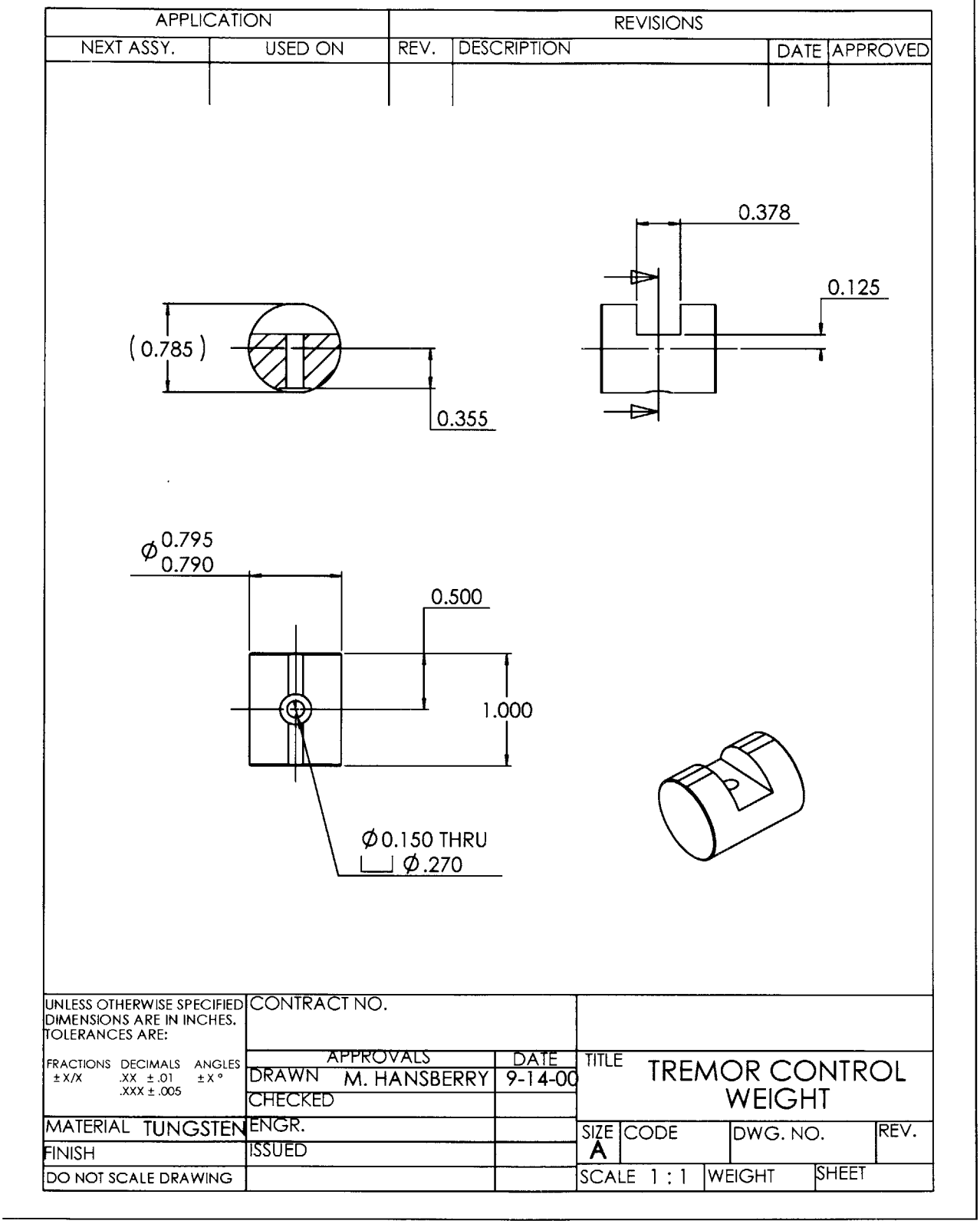


Figure A-8: Mechanical drawing of tungsten weight.

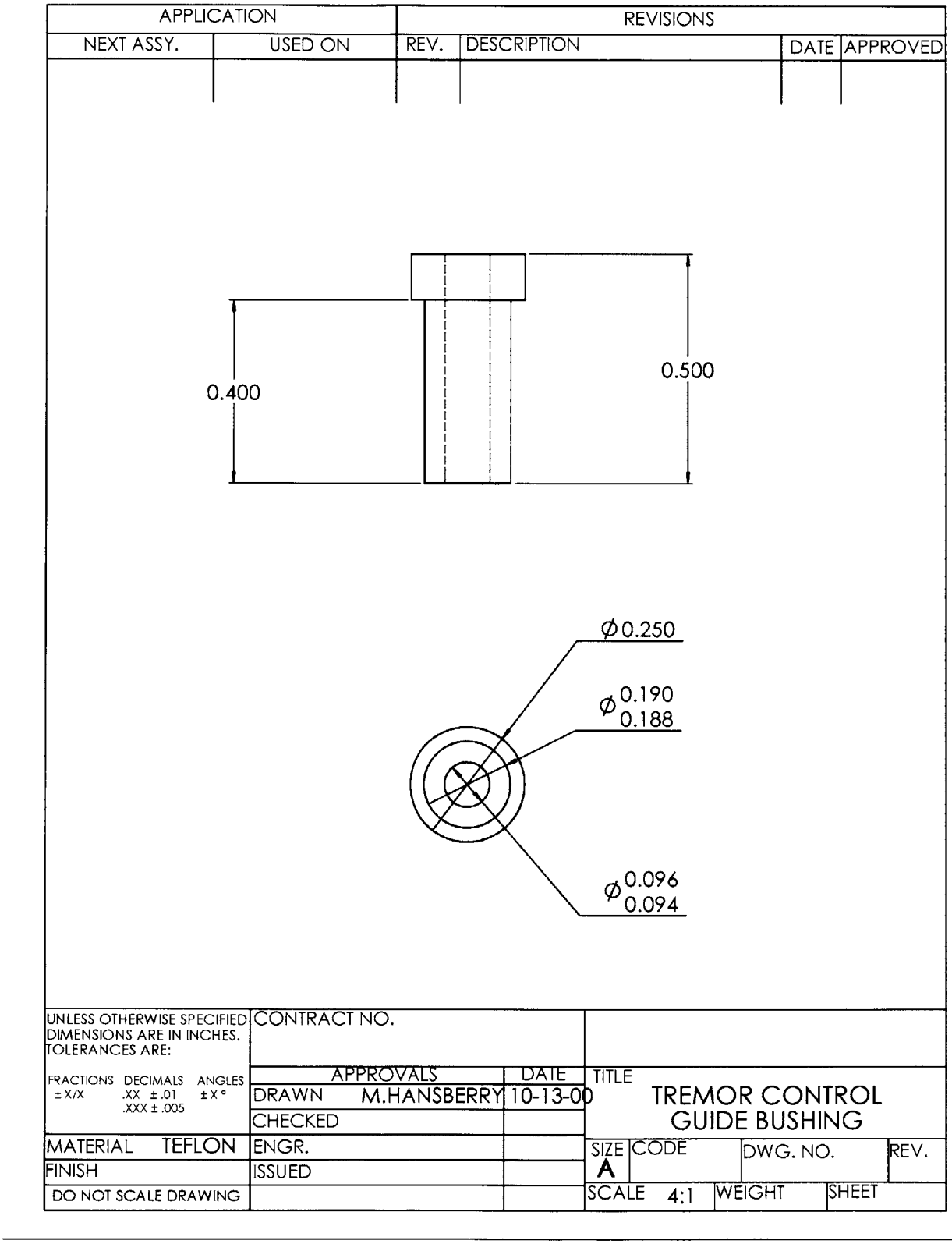


Figure A-9: Mechanical drawing of Teflon bushing.

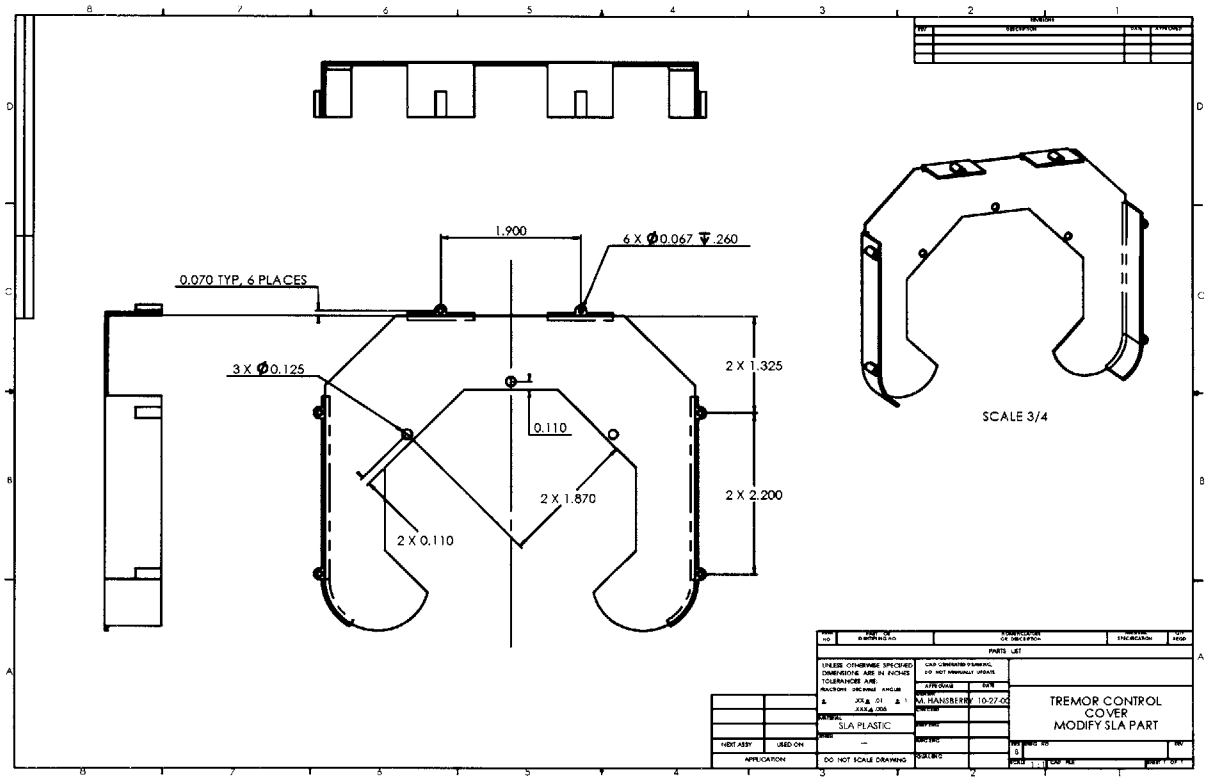


Figure A-10: Mechanical drawing of the shield.

This page intentionally left blank.

# Appendix B

# Analyses Utilized in Controller Tuning

## B.1 Overview

This appendix details analyses performed by Kenneth Kaiser to determine the best combinations and values of gains for the controller and plant at hand. Even though these analyses were not created by the author, they are included because they were instrumental in leading the author to the assumed best set of controller values and gains. The plant used is the same one detailed in Chapter 4, as is the controller.

## B.2 System Description

Figure B-1 is a block diagram representing the system analyzed in this appendix. Note that the main transfer function of interest is that from the disturbance, $D$, to wrist motion, $x_1$, since we are interested in the effect of the tremor motion on wrist motion. The system transfer function from the disturbance to the displacement of the wrist is

$$\frac{X_1}{D} = \frac{(G_D G_{P1})(1 + G_{P2} G_L)}{(1 + G_{P2} G_L) + (G_A + G_{P1} G_L)}. \tag{B.1}$$

The transfer function of $m_1$ is

$$G_{P1} = \frac{1}{m_1 s^2}, \tag{B.2}$$

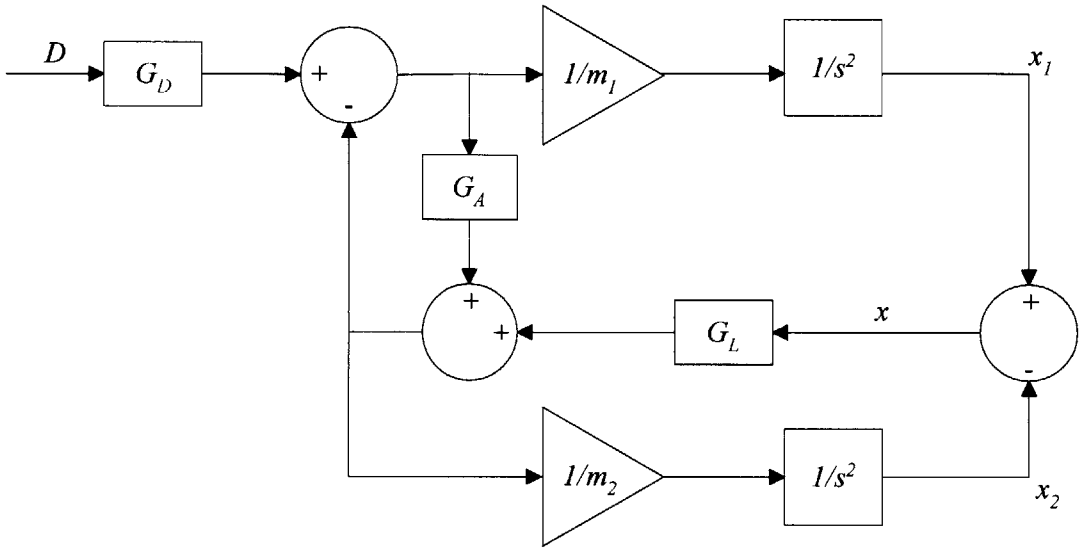


Figure B-1: Block diagram of the system analyzed using classical controls techniques.

the transfer function of $m_2$ is

$$G_{P2} = \frac{1}{m_2 s^2}, \tag{B.3}$$

and the controller transfer functions are generically defined as

$$G_L = K_{LP} + \frac{K_{LI}}{s} + K_{LD}s \tag{B.4}$$

for the LVDT control loops, and

$$G_A = K_{AP} + \frac{K_{AI}}{s} + K_{AD}s \tag{B.5}$$

for the accelerometer control loops. Thus, generally speaking, we will be assuming that both the accelerometer and LVDT control loops are operating with PID controllers. Additionally, the plant dynamics under influence of a sinusoidal disturbance force of frequency $\omega$ are symbolized by $G_D$, which is defined as

$$G_D = \frac{\omega_0}{s^2 + 2\zeta\omega_0 s + \omega_0^2}. \tag{B.6}$$

These plant dynamics represent a simple resonant, spring-mass system.

## B.3 Special Cases

The first order of business is to look for "gross" characteristics within the system that we may want to either ensure or avoid. For example, we should ask questions such as, "do we really need LVDT control loops?" I refer to these as the special cases. Special case I is $G_{P1} = G_{P2}$ and $G_A = 1$. This corresponds to a case in which $m_1 = m_2$ and, the accelerometer feedback consists of a simple proportional gain of value 1. The transfer function given in Equation B.1 simplifies to

$$\frac{X_1}{D} = \frac{G_D G_{P1}}{2} \tag{B.7}$$

for any $G_L$. This situation basically means that, for any LVDT gains, the system will be completely uncontrollable since the LVDT controller transfer function does not appear anywhere in the transfer function of Equation B.7. Therefore, it may be beneficial to stay away from a case in which $m_1 \cong m_2$ and the accelerometer gains are low.

Special Case II is $G_L = 0$, which corresponds to having no LVDT feedback. The absence of LVDT feedback would cause Equation B.1 to simplify to

$$\frac{X_1}{D} = \frac{G_D G_{P1}}{1 + G_A}. \tag{B.8}$$

Defining the acceleration control loop to have a PID controller, as in Equation B.5, and maintaining the same relationship for the transfer function of $m_1$ as in Equation B.2, Equation B.8 becomes

$$\frac{X_1}{D} = \frac{\frac{1}{m_1 s^2} G_D}{1 + K_{AP} + \frac{K_{AI}}{s} + K_{AD} s}. \tag{B.9}$$

Multiplying the numerator and denominator of Equation B.9 by $m_1 s^2$, the new form of Equation B.9 is

$$\frac{X_1}{D} = \frac{G_D}{m_1} \cdot \frac{1}{\left(K_{AD} s^3 + \left(1 + K_{AP}\right) s^2 + K_{AI} s\right)}. \tag{B.10}$$

The final form of Equation B.10 is presented as

$$\frac{X_1}{D} = \frac{G_D}{m_1 s} \cdot \frac{1}{\left(K_{AD} s^2 + \left(1 + K_{AP}\right) s + K_{AI}\right)}, \tag{B.11}$$

which is not bad. A transfer function like Equation B.11 could lead to system performance as displayed in Figure B-2. The "moral" of this particular portion of analysis is that the system

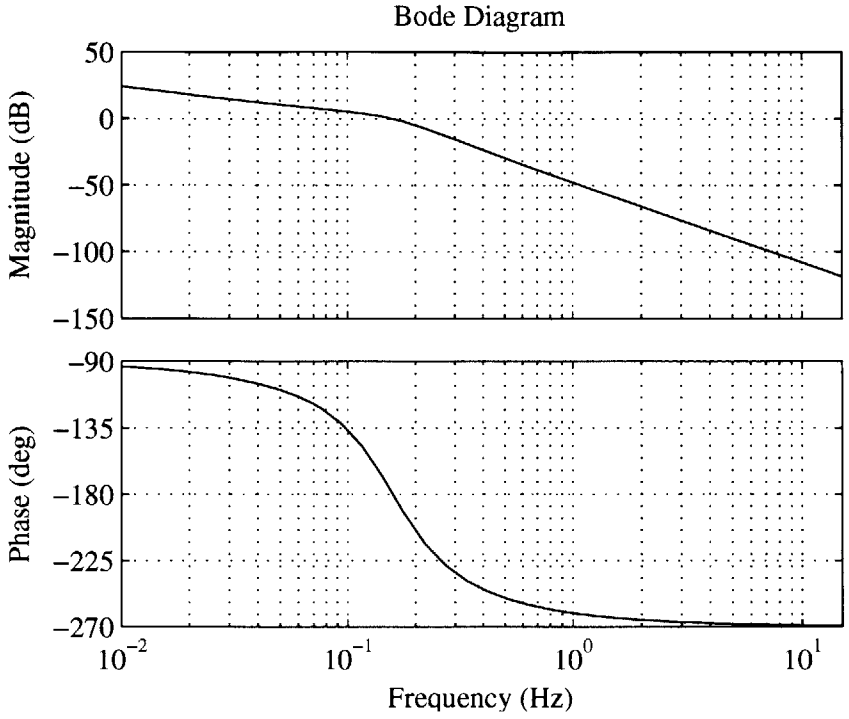


Figure B-2: Possible system performance with a transfer function similar to Equation B.11.

benefits by the presence of some form of feedback on the accelerometers; $G_A \neq 0$. Additionally, it seems to indicate that the influence of the LVDT loops can be limited to simply centering the proof mass. The LVDT control loops may not necessarily need to perform any sort of compensation to reduce tremor motion.

Special Case III is $G_A = K_{AP}$, or a proportional gain on the accelerometer, and $G_L = K_{LP}$, a proportional gain on the LVDT. The benefits of a controller such as this would be the inherent simplicity in having only two gains to adjust per loop. The transfer function given in Equation B.1 becomes

$$\frac{X_1}{D} = \frac{G_D G_{P1}\left(1 + K_{LP} G_{P2}\right)}{1 + K_{AP} + K_{LP}\left(G_{P1} + G_{P2}\right)}. \tag{B.12}$$

Substituting Equations B.2 and B.3 into Equation B.12 produces

$$\frac{X_1}{D} = G_D \left[ \frac{\frac{1}{m_1 s^2}\left(1 + K_{LP}\frac{1}{m_2 s^2}\right)}{1 + K_{AP} + \frac{K_{LP}}{m_1 s^2} + \frac{K_{LP}}{m_2 s^2}} \right]. \tag{B.13}$$

Multiplying the numerator and denominator of Equation B.13 by $m_1 s^2 m_2 s^2$ yields

$$\frac{X_1}{D} = \left[\frac{G_D}{m_1 m_2 s^2}\right] \left[ \frac{m_2 s^2 + K_{LP}}{s^2(1 + K_{AP}) + K_{LP}\left(\frac{1}{m_1} + \frac{1}{m_2}\right)} \right]. \tag{B.14}$$

Note that Equation B.14 has no damping terms (no terms are multiplied by $s$), which is a suggestion that the system may not perform that well. Additionally, we can find conditions for $K_{AP}$ such that the system will be completely uncontrollable, regardless of the value of $K_{LP}$. In order to do this, take the term in brackets in Equation B.14,

$$\left[\frac{\frac{m_2 s^2}{K_{LP}}+1}{\frac{(1+K_{AP})s^2}{K_{LP}}+\left(\frac{1}{m_1}+\frac{1}{m_2}\right)}\right], \tag{B.15}$$

and factor out the $\left(\frac{1}{m_1}+\frac{1}{m_2}\right)$ term so that the denominator can be more clearly seen,

$$\frac{1}{\left(\frac{1}{m_1}+\frac{1}{m_2}\right)}\left[\frac{\frac{m_2 s^2}{K_{LP}}+1}{\frac{(1+K_{AP})s^2}{K_{LP}\left(\frac{1}{m_1}+\frac{1}{m_2}\right)}+1}\right]. \tag{B.16}$$

Then if

$$\frac{m_2}{K_{LP}}=\frac{(1+K_{AP})}{K_{LP}\left(\frac{1}{m_1}+\frac{1}{m_2}\right)} \tag{B.17}$$

the term in brackets in Equation B.16 would become 1. Continuing with algebra,

$$1+\frac{m_2}{m_1}=1+K_{AP}, \tag{B.18}$$

or

$$K_{AP}=\frac{m_2}{m_1}. \tag{B.19}$$

For this condition of $K_{AP}$, $K_{LP}$ can be anything and the system will not see influence of the LVDT loop. Substituting Equation B.19 into Equation B.14, the transfer function becomes

$$\frac{X_1}{D}=\frac{G_D}{m_1 m_2 s^2\left(\frac{1}{m_1}+\frac{1}{m_2}\right)}, \tag{B.20}$$

or

$$\frac{X_1}{D}=\frac{G_D}{(m_1+m_2)\,s^2}. \tag{B.21}$$

As can be seen in Equation B.21, there is no influence of the LVDT control loop in the system transfer function. Also note that this is a generalization of case I in which $G_{P1} \neq G_{P2}$, or the masses $m_1$ and $m_2$ are not equal. Some conclusions can be drawn based on the three special cases

presented.

1. The controller will very likely need control in the form of acceleration feedback. In other words, $G_A \neq 0$. Special case II shows the potential benefits of using acceleration feedback.

2. The effect of $G_L$ tends to cancel. This was apparent in special cases I and III, in which it was relatively easy to find conditions for $G_A$ that cancelled any effect of the LVDT controller, $G_L$.

3. The system will need more than gains $K_{AP}$ and $K_{LP}$, or no damping will be present in the system. Special case III shows this in Equation B.21.

## B.4 Determination of Controller Types

It is time to take the lessons learned in previous sections and decide what types of controllers to use for each of the loops. We wish to manipulate Equation B.1 such that the influence of the plant and controller dynamics are as clear as possible. We begin by substituting Equations B.2 and B.3 for $G_{P1}$ and $G_{P2}$ into Equation B.1, so that Equation B.1 becomes

$$\frac{X_1}{D} = G_D \left[ \frac{\left(\frac{1}{m_1 s^2}\right)\left(1 + \frac{G_L}{m_2 s^2}\right)}{\left(1 + \frac{G_L}{m_2 s^2}\right) + \left(G_A + \frac{G_L}{m_1 s^2}\right)} \right]. \tag{B.22}$$

Multiplying the numerator and denominator of Equation B.22 by $m_1 s^2$ results in

$$\frac{X_1}{D} = G_D \left[ \frac{\left(1 + \frac{G_L}{m_2 s^2}\right)}{m_1 s^2 + \frac{m_1}{m_2} G_L + m_1 s^2 G_A + G_L} \right]. \tag{B.23}$$

Bringing a factor of $\frac{1}{m_2 s^2}$ out of the numerator results in

$$\frac{X_1}{D} = \frac{G_D}{m_2 s^2} \left[ \frac{(m_2 s^2 + G_L)}{m_1 s^2 (1 + G_A) + \left(1 + \frac{m_1}{m_2}\right) G_L} \right]. \tag{B.24}$$

Equation B.24 is the system transfer function containing only transfer functions for the plant, LVDT loop controller, and accelerometer controller. This equation will be studied extensively to determine whether or not a particular gain value is needed, and what the value of the gain should be.

First, let $G_A = K_{AP}$ only, which would be a simple proportional feedback of the accelerometer signal. Equation B.24 becomes

$$\frac{X_1}{D} = \frac{G_D}{m_2 s^2}\left[\frac{(m_2 s^2 + G_L)}{m_1 (1 + K_{AP}) s^2 + \left(1 + \frac{m_1}{m_2}\right) G_L}\right]. \tag{B.25}$$

As $s \to \infty$, Equation B.25 becomes

$$\frac{X_1}{D} \to \frac{G_D}{m_1 (1 + K_{AP}) s^2} \to 0. \tag{B.26}$$

The transfer function of Equation B.26 gives good attenuation in $K_{AP}$. This is rather expected, given the result of Equation B.11 presented within special case II.

Next let the LVDT loops act as proportional-derivative controllers, and let the accelerometer loops act as proportional loops. In other words, we remove terms from Equations B.4 and B.5 so that the controller transfer functions become

$$\begin{aligned} G_L &= K_{LP} + K_{LD} s \\ G_A &= K_{AP}. \end{aligned} \tag{B.27}$$

Substituting Equations B.27 into Equation B.24 produces the transfer function

$$\frac{X_1}{D} = \frac{G_D}{m_2 s^2}\left[\frac{m_2 s^2 + K_{LP} + K_{LD} s}{m_1 (1 + K_{AP}) s^2 + K_{LD} s \left(1 + \frac{m_1}{m_2}\right) + K_{LP}\left(1 + \frac{m_1}{m_2}\right)}\right]. \tag{B.28}$$

For $s \to 0$,

$$\frac{X_1}{D} \to \frac{G_D}{(m_1 + m_2) s^2}, \tag{B.29}$$

and for $s \to \infty$,

$$\frac{X_1}{D} \to \frac{G_D}{m_1 (1 + K_{AP}) s^2} \to 0. \tag{B.30}$$

What conclusions and observations can be drawn from Equations B.29 and B.30?

1. One complex zero pair, and one complex pole pair.

2. Can we cancel $G_D$ in Equation B.30 with the zero and put the pole pair in a better place?

3. A $\frac{K_{LI}}{s}$ term is needed to keep the LVDT centered.

4. We don't want a $\frac{K_{AI}}{s}$ term or it will ramp off.

5. Do we want a $K_{AD}s$ term?

6. The two quadratics should next be normalized so that we can get a better idea of the level of attenuation.

To summarize, we are working with three transfer functions, $G_D$, $G_L$, and $G_A$, which are defined by Equations B.6 and B.27, respectively. Normalization of the two quadratics follows. Starting from Equation B.28, and factoring a $m_1(1+K_{AP})$ term out of the denominator and a $m_2$ term out of the numerator, we have

$$\frac{X_1}{D} = \frac{G_D m_2 \left(s^2 + \left(\frac{K_{LD}}{m_2}\right)s + \frac{K_{LP}}{m_2}\right)}{m_2 s^2 m_1 (1+K_{AP}) \left(s^2 + \frac{\left(1+\frac{m_1}{m_2}\right)K_{LD}s}{m_1(1+K_{AP})} + \frac{\left(1+\frac{m_1}{m_2}\right)K_{LP}}{m_1(1+K_{AP})}\right)}. \tag{B.31}$$

Rearranging terms, we arrive at the normalized form of Equation B.28

$$\frac{X_1}{D} = \frac{G_D}{m_1(1+K_{AP})s^2}\left[\frac{s^2 + \left(\frac{K_{LD}}{m_2}\right)s + \frac{K_{LP}}{m_2}}{s^2 + \left(\frac{1}{m_1}+\frac{1}{m_2}\right)\left(\frac{K_{LD}}{1+K_{AP}}\right)s + \left(\frac{1}{m_1}+\frac{1}{m_2}\right)\frac{K_{LP}}{(1+K_{AP})}}\right]. \tag{B.32}$$

The resulting system equation has three degrees of freedom, $K_{LP}$, $K_{LD}$, and $K_{AP}$, which are the controller gains of a PD controller for the LVDT, and a proportional controller for the accelerometer. What can be done to the system dynamics using these gains? Try canceling $G_D$ using the gains, which would correspond to canceling the plant dynamics using the controller gains. The most straightforward way to cancel $G_D$ would be to find terms such that the numerator of Equation B.32 would be equivalent to the denominator of Equation B.6. The end result of this condition, when Equation B.6 is substituted into Equation B.32 would be

$$\frac{X_1}{D} = \frac{\omega_0^2}{m_1(1+K_{AP})s^2}\left[\frac{1}{s^2 + \left(\frac{1}{m_1}+\frac{1}{m_2}\right)\left(\frac{K_{LD}}{1+K_{AP}}\right)s + \left(\frac{1}{m_1}+\frac{1}{m_2}\right)\frac{K_{LP}}{(1+K_{AP})}}\right] \tag{B.33}$$

with

$$2\zeta\omega_0 = \frac{K_{LD}}{m_2} \text{ and } \omega_0^2 = \frac{K_{LP}}{m_2}. \tag{B.34}$$

Rearranging the equations within B.34 reveals that $K_{LD}$ and $K_{LP}$ are

$$K_{LD} = 2\zeta\omega_0 m_2 \tag{B.35}$$

and

$$K_{LP} = \omega_0^2 m_2. \tag{B.36}$$

Equations B.35 and B.36 will be used throughout the rest of this chapter as the relations for $K_{LD}$ and $K_{LD}$.

Now it is instructive to see what poles remain following cancellation of $G_D$, and what degrees of freedom remain from $K_{AP}$. Beginning from Equation B.33 and substituting the results displayed in Equations B.35 and B.36,

$$\frac{X_1}{D} = \frac{\omega_0^2}{m_1\left(1+K_{AP}\right)s^2}\left[\frac{1}{s^2+\left(\frac{1}{m_1}+\frac{1}{m_2}\right)\left(\frac{2\zeta\omega_0 m_2}{1+K_{AP}}\right)s+\left(\frac{1}{m_1}+\frac{1}{m_2}\right)\frac{\omega_0^2 m_2}{(1+K_{AP})}}\right]. \tag{B.37}$$

Rearranging terms slightly,

$$\frac{X_1}{D} = \frac{\omega_0^2}{m_1\left(1+K_{AP}\right)s^2}\left[\frac{1}{s^2+\frac{1+\frac{m_2}{m_1}}{1+K_{AP}}2\zeta\omega_0 s+\frac{1+\frac{m_2}{m_1}}{1+K_{AP}}\omega_0^2}\right]. \tag{B.38}$$

Assume a solution of the form

$$s^2+\left(2\zeta_A\omega_A\right)s+\omega_A^2 \tag{B.39}$$

for the bracketed denominator of Equation B.38. If we equate the coefficient of $s$ in the denominator of Equation B.38 with the coefficient of the $s$ in Equation B.9, we arrive at the relation

$$\left(\frac{1+\frac{m_2}{m_1}}{1+K_{AP}}\right)2\zeta\omega_0 = 2\zeta_A\omega_A, \tag{B.40}$$

or

$$\zeta_A = \zeta\sqrt{\frac{1+\frac{m_2}{m_1}}{1+K_{AP}}}. \tag{B.41}$$

Similarly, equating the coefficient without an $s$ term in the denominator of Equation B.38 with the coefficient without an $s$ term in Equation B.39, we arrive at the relation

$$\omega_A = \omega_0\sqrt{\frac{1+\frac{m_2}{m_1}}{1+K_{AP}}}. \tag{B.42}$$

Note that if $K_{AP}$ is large then both $\zeta_A$ and $\omega_A$ decrease. This is important because it means that a high proportional accelerometer loop gain decreases the system damping. Finishing the

normalization is accomplished by simply substituting the results of Equations B.41 and B.42 into Equation B.38 to yield

$$\frac{X_1}{D} = \frac{\omega_0^2}{m_1\left(1+K_{AP}\right)s^2}\left[\frac{\omega_A^2}{s^2+2\zeta_A\omega_A s+\omega_A^2}\right]\frac{1}{\omega_A^2}. \tag{B.43}$$

Substituting Equation B.42 into Equation B.43 gives us

$$\frac{X_1}{D} = \frac{\omega_0^2}{m_1\left(1+K_{AP}\right)s^2}\left[\frac{\omega_A^2}{s^2+2\zeta_A\omega_A s+\omega_A^2}\right]\left[\frac{1+K_{AP}}{\left(1+\frac{m_2}{m_1}\right)\omega_0^2}\right]. \tag{B.44}$$

Lastly, canceling and rearranging terms in Equation B.44 yields the result

$$\frac{X_1}{D} = \frac{1}{\left(m_1+m_2\right)s^2}\left[\frac{\omega_A^2}{s^2+2\zeta_A\omega_A s+\omega_A^2}\right]. \tag{B.45}$$

We now use the results presented in Equations B.41, B.42, and B.45 as trial solutions into which real numbers can be substituted. For example try the following numbers in the formulae; $\omega_D = \omega_0 = 2\pi 5$ and $\zeta = 0.1$, $m_2 = 32.2/1.0$, $m_1 = 32.2/1.25$, $m_1 + m_2 = 32.2/0.56$, and $1 + \frac{m_2}{m_1} = 2.25$. These numbers correspond to, respectively, a plant and disturbance frequency of 5 Hz, a proof mass weighing 1 pound, an assumed wrist inertia of 1.25 pounds, and some low damping coefficient. Substituting these values in Equations B.41, B.42, and B.45 yields

$$\omega_A = \frac{2\pi 5 \times 1.5}{\sqrt{1+K_{AP}}} = \frac{15\pi}{\sqrt{1+K_{AP}}} \tag{B.46}$$

and

$$\zeta_A = 0.1\frac{1.5}{\sqrt{1+K_{AP}}} = \frac{0.15}{\sqrt{1+K_{AP}}} \tag{B.47}$$

These numbers don't look particularly promising, due to two reasons. First, the relationship between $\omega_A$ and $\zeta_A$ is such that the frequency of the system is over two orders of magnitude higher than the damping constant of the system. This is potentially problematic, since it translates into a lightly damped system oscillating at high frequencies. Secondly, the absolute value of the $\zeta_A$ term is low, even for high $K_{AP}$. So, regardless of the value of $\omega_A$ and $K_{AP}$, the system will be lightly damped. Hence, it is not likely this system will perform well.

## B.5 Attenuation Sensitivity Function

It would be helpful to have some way to easily determine the relative effectiveness of a particular system configuration, in terms of its closed loop behavior. In order to do this, we define the attenuation sensitivity function, $S_A$, such that

$$S_A \equiv \frac{\left.\frac{X_1}{D}\right|_{CL}}{\left.\frac{X_1}{D}\right|_{OL}}, \tag{B.48}$$

Equation B.48 is simply a ratio of closed to open loop performance. It will be easy to measure the effectiveness of a particular system configuration by examining the value of $S_A$. We can say that, for any given value of $S_A$ corresponding to some system configuration,

$$\begin{aligned} &S_A > 1 \text{ performance is worse than open loop,} \\ &S_A < 1 \text{ performance is better than open loop.} \end{aligned} \tag{B.49}$$

We seek a closed-form description of $S_A$, which is obtained by substituting the open and closed loop versions of Equation B.32 into Equation B.48. The open loop version of Equation B.32 is

$$\left.\frac{X_1}{D}\right|_{OL} = \frac{G_D}{m_1 s^2}, \tag{B.50}$$

which is obtained by simply zeroing out the transfer functions of the controllers. As expected, we have the transfer function of the plant dynamics, $G_D$, interacting with the mass of the wrist, $m_1$. The closed loop version of Equation B.32 is

$$\left.\frac{X_1}{D}\right|_{CL} = \frac{G_D}{m_1 \left(1 + K_{AP}\right) s^2} \left[ \frac{s^2 + \left(\frac{K_{LD}}{m_2}\right) s + \left(\frac{K_{LP}}{m_2}\right)}{s^2 + \left(\frac{1}{m_1} + \frac{1}{m_2}\right)\left(\frac{K_{LD}}{1+K_{AP}}\right) s + \left(\frac{1}{m_1} + \frac{1}{m_2}\right)\frac{K_{LP}}{1+K_{AP}}} \right]. \tag{B.51}$$

Substituting Equations B.50 and B.51 into Equation B.48 reveals that $S_A$ is

$$S_A = \frac{1}{1 + K_{AP}} \left[ \frac{s^2 + \left(\frac{K_{LD}}{m_2}\right) s + \left(\frac{K_{LP}}{m_2}\right)}{s^2 + \left(\frac{1}{m_1} + \frac{1}{m_2}\right)\left(\frac{K_{LD}}{1+K_{AP}}\right) s + \left(\frac{1}{m_1} + \frac{1}{m_2}\right)\frac{K_{LP}}{1+K_{AP}}} \right]. \tag{B.52}$$

Equivalently,

$$S_A = \frac{s^2 + \left(\frac{K_{LD}}{m_2}\right) s + \frac{K_{LP}}{m_2}}{\left(1 + K_{AP}\right) s^2 + \left(\frac{1}{m_1} + \frac{1}{m_2}\right) K_{LD} + \left(\frac{1}{m_1} + \frac{1}{m_2}\right) K_{LP}}. \tag{B.53}$$

Our ultimate goal is to make the attenuation sensitivity function have a value of 0. A $S_A$ value of 0 would mean that the amplitude of tremor motions in closed loop operation would be 0. Can we make $S_A = 0$ at $s = j\omega_D$? Substitute into Equation B.53 and find out

$$S_A|_{\omega_D} = \frac{-\omega_0^2 + \frac{K_{LD}}{m_2}(j\omega_D) + \frac{K_{LP}}{m_2}}{-(1+K_{AP})\omega_D^2 + \left(\frac{1}{m_1}+\frac{1}{m_2}\right)K_{LD} + \left(\frac{1}{m_1}+\frac{1}{m_2}\right)K_{LP}}. \tag{B.54}$$

Rearranging the terms in Equation B.54 into real and imaginary parts,

$$S_A|_{\omega_D} = \frac{\left(\frac{K_{LP}}{m_2} - \omega_D^2\right) + j\left(\frac{K_{LD}}{m_2}\omega_D\right)}{\left[\left(\frac{1}{m_1}+\frac{1}{m_2}\right)K_{LP} - (1+K_{AP})\omega_D^2\right] + j\left[\left(\frac{1}{m_1}+\frac{1}{m_2}\right)K_{LD}\omega_D\right]}. \tag{B.55}$$

We pause here to perform some analysis on Equation B.55. Note the following items:

1. If the real parts are tuned to zero then,

$$S_A|_{\omega_D} = \frac{j\frac{K_{LD}}{m_2}\omega_D}{j\left(\frac{1}{m_1}+\frac{1}{m_2}\right)K_{LD}\omega_D} = \frac{1}{1+\frac{m_2}{m_1}} = 0.444 \tag{B.56}$$

   Substituting into Equation 2.16, we find $20\log_{10}(0.444) = -7$ db, which is the tremor attenuation from open loop to closed loop. This is not particularly good attenuation.

2. What if $K_{AP}$ is very large? This would be the case in which we were trying our best to attenuate the tremor. Then

$$S_A|_{\omega_D} \to \frac{\left(\frac{K_{LP}}{m_2} - \omega_D^2\right) + j\left(\frac{K_{LD}}{m_2}\omega_D\right)}{-(1+K_{AP})\omega_D^2} \tag{B.57}$$

   Now we tune such that

$$\left(\frac{K_{LP}}{m_2} - \omega_D^2\right) = 0, \tag{B.58}$$

   which leads to the result

$$K_{LP} = m_2\omega_D^2, \tag{B.59}$$

   as in Equation B.36. Substituting Equation B.59 into Equation B.57 shows that the attenuation sensitivity function is

$$S_A|_{\omega_D} = -j\frac{\frac{K_{LD}}{m_2}\omega_D}{(1+K_{AP})\omega_D^2}. \tag{B.60}$$

3. We also substitute Equation B.59 directly into Equation B.55 so that we can perform some

approximations. The result is

$$S_A|_{\omega_D} = \frac{j\left(\frac{K_{LD}}{m_2}\omega_D\right)}{\left(\frac{m_2}{m_1} - K_{AP}\right)\omega_D^2 + \left(\frac{1}{m_1} + \frac{1}{m_2}\right)K_{LD}\omega_D}. \tag{B.61}$$

If we set $K_{LD} = 0$, then

$$S_A|_{\omega_D} = \frac{0}{\left(1 + \frac{m_2}{m_1}\right)\omega_D^2 - (1 + K_{AP})\omega_D^2} = \frac{0}{\left(\frac{m_2}{m_1} - K_{AP}\right)\omega_D^2} \tag{B.62}$$

Therefore, we could notch out $\omega_D$. Would the system be stable if $K_{AP} = 0$? That is, would Equation B.62 lend itself to stability if there were no accelerometer feedback? If $K_{AP} = 0$, the resulting transfer function would be

$$S_A|_{\omega_D} = \frac{0}{\frac{m_2}{m_1}\omega_D^2}, \tag{B.63}$$

which would be stable as long as the denominator were not small.

## B.6 "Shaping" of the Attenuation Sensitivity Function

We now work on "shaping" $S_A$ so that it will have the attenuation characteristics that we desire. We begin by recounting the result displayed in Equation B.53

$$S_A = \frac{s^2 + \left(\frac{K_{LD}}{m_2}\right)s + \left(\frac{K_{LP}}{m_2}\right)}{(1 + K_{AP})s^2 + \left(\frac{1}{m_1} + \frac{1}{m_2}\right)K_{LD} + \left(\frac{1}{m_1} + \frac{1}{m_2}\right)K_{LP}}. \tag{B.64}$$

Factoring the $\frac{1}{1+K_{AP}}$ from the denominator of Equation B.64, we find

$$S_A = \frac{1}{1 + K_{AP}}\left[\frac{s^2 + \left(\frac{K_{LD}}{m_2}\right)s + \left(\frac{K_{LP}}{m_2}\right)}{s^2 + \frac{\left(\frac{1}{m_1}+\frac{1}{m_2}\right)K_{LD}}{1+K_{AP}} + \frac{\left(\frac{1}{m_1}+\frac{1}{m_2}\right)K_{LP}}{1+K_{AP}}}\right]. \tag{B.65}$$

We also substitute the results displayed in Equations B.35 and B.36 into Equation B.65, after which the result is

$$S_A = \frac{1}{1 + \frac{m_2}{m_1}}\left[\frac{s^2 + 2\zeta_0\omega_0 s + \omega_0^2}{\omega_0^2}\right]\left[\frac{\omega_P^2}{s^2 + 2\zeta_P\omega_P s + \omega_P^2}\right]. \tag{B.66}$$

Additionally, $\omega_P^2 = \left(\frac{1}{m_1} + \frac{1}{m_2}\right)\left(\frac{K_{LP}}{1+K_{AP}}\right)$ and $2\zeta_P\omega_P = \left(\frac{1}{m_1} + \frac{1}{m_2}\right)K_{LD}$. Starting from Equation B.36,

$$K_{LP} = \omega_0^2 m_2, \tag{B.67}$$

or

$$\omega_0 = \sqrt{\frac{K_{LP}}{m_2}}. \tag{B.68}$$

Assuming $\omega_0 = \omega_P$, and setting Equations B.68

$$2\zeta_0\sqrt{\frac{K_{LP}}{m_2}} = \frac{K_{LD}}{m_2} \tag{B.69}$$

$$\zeta_0 = \frac{1}{2}\frac{K_{LD}}{m_2}\sqrt{\frac{m_2}{K_{LP}}} = \frac{1}{2}\frac{K_{LD}}{\sqrt{m_2}}\frac{1}{\sqrt{K_{LP}}} \tag{B.70}$$

Substituting Equation B.68 into Equation B.70, we arrive at

$$\zeta_0 = \frac{1}{2}\frac{K_{LD}}{\sqrt{m_2}}\frac{1}{\omega_0\sqrt{m_2}} = \frac{1}{2}\frac{K_{LD}}{m_2\omega_0}. \tag{B.71}$$

Rearranging, the definition of $K_{LD}$ becomes

$$K_{LD} = 2\zeta_0\omega_0 m_2. \tag{B.72}$$

Substituting Equation B.72 into Equation B.42 gives us

$$\omega_P^2 = \left(\frac{1}{m_1} + \frac{1}{m_2}\right)\frac{\omega_0^2 m_2}{1+K_{AP}} = \left(1 + \frac{m_2}{m_1}\right)\frac{\omega_0^2}{1+K_{AP}} \tag{B.73}$$

$$\omega_P = \sqrt{1 + \frac{m_2}{m_1}}\frac{\omega_0}{\sqrt{1+K_{AP}}} \tag{B.74}$$

Combining Equations B.73, B.41 and B.42, we arrive at

$$2\zeta_P\omega_P = \left(\frac{1}{m_1} + \frac{1}{m_2}\right)2\zeta_0\omega_0 m_2 \tag{B.75}$$

$$\zeta_P\omega_P = \left(1 + \frac{m_2}{m_1}\right)\zeta_0\omega_0 \tag{B.76}$$

How does $\zeta_P$ vary with $K_{AP}$? Substitute Equation B.73 in Equation B.75, we have

$$\zeta_P \left[ \omega_0 \frac{\sqrt{1+\frac{m_2}{m_1}}}{\sqrt{1+K_{AP}}} \right] = \left(1+\frac{m_2}{m_1}\right) \zeta_0 \omega_0. \tag{B.77}$$

Rearranging terms,

$$\zeta_P = \zeta_0 \sqrt{1+\frac{m_2}{m_1}} \sqrt{1+K_{AP}}. \tag{B.78}$$

We have relations for $K_{LP}$ and $K_{LD}$, but how do we pick $K_{AP}$?

$$S_A = \frac{1}{1+\frac{m_1}{m_2}} \left[ \frac{s^2+2\zeta_0\omega_0 s+\omega_0^2}{\omega_0^2} \right] \left[ \frac{\omega_0^2 \frac{1+\frac{m_2}{m_1}}{1+K_{AP}}}{s^2+2\zeta_0\omega_0\left(1+\frac{m_2}{m_1}\right)s+\frac{1+\frac{m_2}{m_1}}{1+K_{AP}}\omega_0^2} \right] \tag{B.79}$$

Rederive $S_A$. Starting back at Equations B.50 and B.51, the definitions of the transfer closed loop and open loop transfer functions are

$$\left.\frac{X_1}{D}\right|_{CL} = \frac{G_D G_{P1}\left(1+G_{P2}G_L\right)}{\left(1+G_{P2}G_L\right)+\left(G_A+G_{P1}G_L\right)}. \tag{B.80}$$

and

$$\left.\frac{X_1}{D}\right|_{OL} = G_D G_{P1}, \tag{B.81}$$

respectively. Substituting Equations B.80 and B.81 into Equation B.48,

$$S_A = \frac{1+G_{P2}G_L}{\left(1+G_{P2}G_L\right)+\left(G_A+G_{P1}G_L\right)}. \tag{B.82}$$

For $G_L = G_A = 0$, which is the open loop condition, $S_A = 1$. With respect to a reference line of open loop attenuation, we can define performance better than or worse than open loop for conditions of $S_A$

Now we try a proportional-derivative controller for both the accelerometer loop and LVDT loop. In other words,

$$\begin{aligned} G_L &= K_{LP} + K_{LD}s \\ G_A &= K_{AP} + K_{AD}s \end{aligned} \tag{B.83}$$

Additionally, $G_{P1} = \frac{1}{m_1 s^2}$ and $G_{P2} = \frac{1}{m_2 s^2}$, as given in Equations B.2 and B.3. Substituting the

definitions of $G_{P1}$ and $G_{P2}$ into Equation B.82, $S_A$ becomes

$$S_A = \frac{1 + \frac{K_{LP}+K_{LD}s}{m_2 s^2}}{1 + \frac{K_{LP}+K_{LD}s}{m_2 s^2} + K_{AP} + K_{AD}s + \frac{K_{LP}+K_{LD}s}{m_1 s^2}}. \tag{B.84}$$

Multiplying both the numerator and denominator of Equation B.84 by $m_2 s^2$ yields

$$S_A = \frac{m_2 s^2 + K_{LD}s + K_{LP}}{m_2 K_{AD} s^3 + m_2 (1 + K_{AP}) s^2 + K_{LD}\left(1 + \frac{m_2}{m_1}\right) s + K_{LP}\left(1 + \frac{m_2}{m_1}\right)}. \tag{B.85}$$

Let's try a special case—let $K_{AD} = 0$ (no derivative feedback on the accelerometer), $G_L = K_{LP} + K_{LD}s$ (a proportional-derivative controller on the LVDT), and $G_A = K_{AP}$ (a simple proportional gain on the accelerometer). Making the appropriate substitutions, Equation B.85 becomes

$$S_A = \frac{m_2 s^2 + K_{LD}s + K_{LP}}{m_2 (1 + K_{AP}) s^2 + K_{LD}\left(1 + \frac{m_2}{m_1}\right) s + K_{LP}\left(1 + \frac{m_2}{m_1}\right)}. \tag{B.86}$$

We normalize Equation B.86 to find

$$S_A = \frac{m_2 \left[s^2 + \frac{K_{LP}}{m_2} s + \frac{K_{LP}}{m_2}\right]}{m_2 (1 + K_{AP}) \left[s^2 + \frac{K_{LD}\left(1+\frac{m_2}{m_1}\right)}{m_2(1+K_{AP})} s + \frac{K_{LP}\left(1+\frac{m_2}{m_1}\right)}{m_2(1+K_{AP})}\right]}. \tag{B.87}$$

Now normalize through the substitution of Equations B.67 and B.72 into Equation B.87 so we can perform frequency shaping,

$$S_A = \frac{1}{1 + K_{AP}} \left[\frac{s^2 + 2\zeta_0\omega_0 s + \omega_0^2}{s^2 + 2\zeta_P\omega_P s + \omega_P^2}\right]. \tag{B.88}$$

subject to the conditions $2\zeta_0\omega_0 = \frac{K_{LD}}{m_2}$, $\omega_0^2 = \frac{K_{LP}}{m_2}$, $2\zeta_P\omega_P = \frac{K_{LD}\left(1+\frac{m_2}{m_1}\right)}{m_2(1+K_{AP})}$, and $\omega_P^2 = \frac{K_{LP}\left(1+\frac{m_2}{m_1}\right)}{m_2(1+K_{AP})}$. We have three degrees of freedom in Equation B.88, which are $K_{AP}$, $K_{LP}$, and $K_{LD}$. With the four variables that we have—$\zeta_0$, $\omega_0$, $\zeta_P$, and $\omega_P$—what shaping can be done? Given $\zeta_0$, $\omega_0$, $m_1$, and $m_2$

$$S_A = \frac{1}{1 + K_{AP}} \left[\frac{s^2 + 2\zeta_0\omega_0 s + \omega_0^2}{s^2 + 2\zeta_P\omega_P s + \omega_P^2}\right] \tag{B.89}$$

$$K_{LP} = m_2\omega_0^2 \tag{B.90}$$

$$K_{LD} = 2\zeta_0\omega_0 m_2 \tag{B.91}$$

$$\omega_P = \omega_0 \frac{\sqrt{1+\frac{m_2}{m_1}}}{\sqrt{1+K_{AP}}} \tag{B.92}$$

$$\zeta_P = \zeta_0 \frac{\sqrt{1+\frac{m_2}{m_1}}}{\sqrt{1+K_{AP}}}. \tag{B.93}$$

For $s \to \infty$,

$$S_A \to \frac{1}{1+K_{AP}}. \tag{B.94}$$

For $s \to 0$,

$$S_A \to \frac{\omega_0^2}{(1+K_{AP})\,\omega_P^2}. \tag{B.95}$$

In addition, substituting Equation B.92 into Equation B.95,

$$S_A(0) = \frac{1}{1+\frac{m_2}{m_1}} \tag{B.96}$$

Summary for frequency plots. Given $m_1$, $m_2$, $\zeta_0$, $\omega_0$, then one degree of freedom remains, $K_{AP}$. Define $\gamma$ such that

$$\gamma = \frac{\sqrt{1+\frac{m_2}{m_1}}}{\sqrt{1+K_{AP}}} \tag{B.97}$$

Then $\omega_P = \gamma\omega_0$ and $\zeta_P = \gamma\zeta_0$, with the $S_A$ reference line at 1. This changes Equation B.89 according to

$$S_A = \frac{1}{1+K_{AP}} \left[ \frac{s^2 + 2\zeta_0\omega_0 s + \omega_0^2}{s^2 + 2\zeta_0\omega_0\gamma s + \omega_0^2\gamma} \right]. \tag{B.98}$$

Our best bet is to set $\zeta_0$, $\omega_0$, $\frac{m_2}{m_1}$, $K_{AP}$ to $\gamma$, $\omega_P$, $\zeta_P$ and plot it. Setting the respective equations equal to one another

$$\frac{\zeta_P}{\omega_P} = \frac{\zeta_0}{\omega_0} \tag{B.99}$$

$$\frac{K_{LD}}{K_{LP}} = \frac{2\zeta_0\omega_0 m_2}{\omega_0^2 m_2} = 2\frac{\zeta_0}{\omega_0} \tag{B.100}$$

$$\frac{\zeta_0}{\omega_0} = \frac{K_{LD}}{2K_{LP}} = \frac{\zeta_P}{\omega_P} \tag{B.101}$$

For $s \to \infty$,

$$S_A \to \frac{1}{1+K_{AP}}. \tag{B.102}$$

For $s \to 0$,

$$S_A \to \frac{1}{1+K_{AP}} \frac{\frac{K_{LP}}{m_2}}{\frac{K_{LP}}{1+K_{AP}}\left[\frac{1}{m_1}+\frac{1}{m_2}\right]} = \frac{1}{1+\frac{m_2}{m_1}}, \tag{B.103}$$

as in Equation B.96.

From Bode plots of $S_A$ (see Figure B-3), we see $\gamma_0 = 0.1$, $\zeta_0 = 3.0$, $K_{AP} = 10.0$, $\frac{\zeta_0}{\omega_0} = 4.78$, $\gamma = 0.4523$, $\omega_0 = 0.6283$, $\zeta_P = 1.3568$ and $\omega_P = 0.2842$. At 1.0 Hz we have

$$S_A = \frac{1}{1 + K_{AP}} \left[ \frac{-(2\pi)^2 + 2\zeta_0\omega_0 (2\pi j) + \omega_0^2}{-(2\pi)^2 + s\zeta_0\omega_0\gamma^2 (2\pi j) + \omega_0^2\gamma_0^2} \right]. \tag{B.104}$$

Substituting

$$\omega_0 = (2\pi 0.1)^2 \tag{B.105}$$

into Equation B.104,

$$S_A = \frac{1}{1 + K_{AP}} \left[ \frac{2\zeta_0 2\pi (0.1)(2\pi j) - (2\pi)^2}{2\zeta_0 2\pi (0.1)(2\pi j)\gamma^2 - (2\pi)^2} \right]. \tag{B.106}$$

Lastly, canceling like terms in Equation B.106, we arrive at

$$S_A = \frac{1}{1 + K_{AP}} \left[ \frac{1 - 2\zeta_0 (0.1) j}{1 - 2\zeta_0 (0.1) j\gamma^2} \right] \approx \frac{1}{1 + K_{AP}}. \tag{B.107}$$

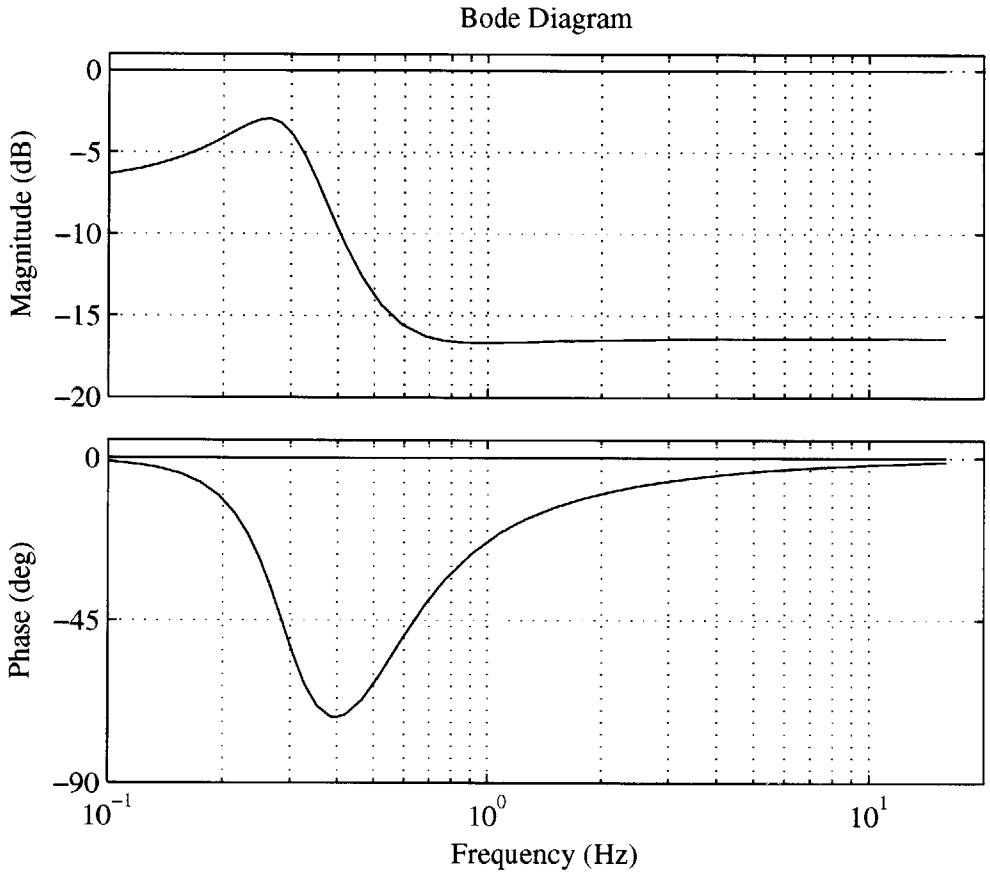


Figure B-3: Bode plot of $S_A$ with PIDP controller.

This page intentionally left blank.

# Bibliography


[1] Anonymous, *i*MEMS Accelerometer specification sheets, Analog Devices, Inc., 1999.

[2] Anonymous, BEI Sensors & Systems Company, Kimco Magnetics Division, Voice Coil Actuator product specification sheets, 1999.

[3] Anonymous, Image Stabilizer product specification sheets, Canon USA, Inc., 1997.

[4] Anonymous, Del-Tron product specification sheets, Del-Tron Precision, Inc., 2000.

[5] Anonymous, PCB Piezotronics Corporation, capacitive accelerometer specification sheets, 2001.

[6] Anonymous, M-40 product specification sheets, Saco Maine Corporation, 2000.

[7] Cleeves L., Findley L.J., "Propranolol and propranolol-LA in essential tremor: a double-blind comparative study," *Journal of Neurology, Neurosurgery, and Psychiatry* 1988; 51:379–384.

[8] Crandall S.H., Karnopp D.C., Kurtz Jr. EF, Pridmore-Brown DC, "Dynamics of Mechanical and Electromechanical Systems,"Krieger Publishing Company, 1982.

[9] Den Hartog J.P., "Mechanical Vibrations," 4$^{th}$ ed., McGraw-Hill, 1956.

[10] Elble R.J., Koller W.C., "Tremor," The Johns Hopkins University Press, 1990.

[11] Findley L.J., Koller W.C., "Handbook of Tremor Disorders," Marcel Dekker, Inc., 1995.

[12] Hall W.D., "Hand-held Gyroscopic Device," U.S. Patent Number 5,058,571, 1991.

[13] Hallett M., "Overview of Human Tremor," *Movement Disorders* 1998; 13 Suppl 3:43–48.

[14] Halliday D., Resnick R., Walker J., "Fundamentals of Physics," 4$^{th}$ ed., John Wiley & Sons, Inc., 1993.

[15] Johnson D.E., Hilburn J.L., Johnson J.R., Scott P.D., "Basic Electric Circuit Analysis," 5th ed., Prentice-Hall, Inc., 1995.

[16] Koller W.C., "Unified rating scale for parkinsonism," In: Koller WC, ed. *Handbook of Parkinson's Disease*, Marcel Dekker, Inc., 1987.

[17] Koller W.C., "Dose-response relationship of propranolol in the treatment of essential tremor," *Archives of Neurology* 1986; 43:42–43.

[18] Lee R.G., Stein R.B., "Resetting of tremor by mechanical perturbations: a comparison of essential tremor and parkinsonian tremor," *Annals of Neurology* 1981; 10:523–531.

[19] MacKay W.A., "Resonance properties of the human elbow," *Canadian Journal of Physiology and Pharmacology* 1984; 62(7):802–808.

[20] Norman K.E., Edwards R., Beuter A., "The measurement of tremor using a velocity transducer: comparison to simultaneous recordings using transducers of displacement, acceleration, muscle activity," *Journal of Neuroscience Methods* 1999; 92(1–2):41–54.

[21] Riviere C.N., Rader R.S., Thakor N.V., "Adaptive canceling of physiological tremor for improved precision in microsurgery," *IEEE Transactions on Biomedical Engineering* 1998; 45(7):839–846.

[22] Riviere C.N., Khosla P.K., Sulzmann Armin ed, "Active hand-held instrument for error compensation in microsurgery," *Conference: Microrobotics and microsystem fabrication* 1998;3202:86–95.

[23] Rosen M.J., Kotovsky J., "A wearable tremor-suppression orthosis," *Journal of Rehabilitation Research and Development* 1998; 35(4):373–387.

[24] Walsh E.G., Wright G.W., "Inertia, resonant frequency, stiffness and kinetic energy of the human forearm," *Quarterly Journal of Experimental Physiology* 1987; 72(2):161–170.

[25] Webster D.O., "Critical analysis of the disability of Parkinson's disease," *Modern Trends* 1968; 5:257–282.